Republic of Iraq
Ministry of Higher Education and Scientific Research
University of Babylon
College of Education for Pure Sciences
Department of Physics

Impact of Green and Black Nickle Oxide Nanoparticles on Structural and some Physical Properties of Polymeric Blend Poly (vinyl alcohol)- Poly (ethylene glycol)

A Thesis
Submitted to the Council of the College of Education for Pure Sciences of University of Babylon in Partial Fulfillment of the Requirements for the Degree of master's in education / Physics

by

Marwa Mazen Naeem Abdul Amir

B. Sc. in Physics
(University of Babylon, 2009 A.D)

Supervised by

Prof. Dr. Fouad Shakir Hashim **Prof. Dr. Shurooq Sabah Abed Al-Abbas**

2023 A.D **1445 A.H.**

بسم الله الرحمن الرحيم

قَالُوا۟ سُبْحَٰنَكَ لَا عِلْمَ لَنَآ إِلَّا مَا عَلَّمْتَنَآ ۖ إِنَّكَ أَنتَ ٱلْعَلِيمُ ٱلْحَكِيمُ

صدق الله العظيم

(سورة البقرة: آية ٣٢)

Supervisor's Certificate

We certify that this thesis entitled " **Impact of Green and Black Nickle Oxide Nanoparticles on Structural and some Physical Properties of Polymeric Blend Poly (vinyl alcohol)- Poly (ethylene glycol)**" wrote by Marwa Mazen Naeem has been prepared under our supervision at the College of Education for Pure Sciences, University of Babylon, in partial fulfillment of the requirements for the degree of Master in College of Education for Pure Sciences, University of Babylon, in part.

Signature:

Supervisor:

Prof. Dr. Fouad Shakir Hashim

Date: / / 2023

Signature:

Supervisor :

Prof. Dr. Shurooq Sabah Abed Al-Abbas

Date: / / 2023

In view of the available recommendations, I forward this dissertation for debate by the examining committee.

Signature:

Head of Physics Department:

Prof. Dr. Khalid Haneen Abbas

Date: / / 2023

Linguistic Supervisor's Certification

This is certified that I have read thesis entitled **" Impact of Green and Black Nickle Oxide Nanoparticles on Structural and some Physical Properties of Polymeric Blend Poly (vinyl alcohol)- Poly (ethylene glycol)**" and I found that this thesis is linguistic qualified for debate.

Signature:

Name:

Title:

Address:

Date: / / 2023

Scientific Supervisor's Certification

This is certified that I have read this thesis entitled **" Impact of Green and Black Nickle Oxide Nanoparticles on Structural and some Physical Properties of Polymeric Blend Poly (vinyl alcohol)- Poly (ethylene glycol)"** and I found that this thesis is scientific qualified for debate.

Signature:

Name:

Title:

Address:

Date: / / 2023

Dedication

In the name of (Allah) the Almighty, to whom I carry his name with pride, my dear father, may God have mercy on him.

To the meaning of love and tenderness, to whose supplication was the secret of my success, my dear mother, may God prolong her life.

To the companion of my life, support and giving, the closest people to myself, the symbol of sincerity and loyalty, and my beating heart, my dear husband, may God protect and preserve him.

To everyone who extended a helping hand to accomplish this humble work, with sincere love, I offer my dedication to you.

Marwa

Acknowledgments

First of all, we would like to thank Allah who helped us finish this research, and graduate with a master's degree.

I would like to thank the professors **Dr. Fouad Shaker Hashem and Dr. Shorouq Sabah Abdel Abbas** for supporting and giving me advice, and I would like to thank the deanship of department of physics/ college of education for pure science.

Marwa

Summary

Nanocomposite films based on polymeric blend poly (vinyl alcohol) (PVA) and poly (ethylene glycol) (PEG) with (90:10) wt.% PEG in PVA and NiO or Ni_2O_3 at five different weight like 0.03, 0.045, 0.06, 0.075 and 0.09 g was fabricated using casting method. The spectral properties include X-ray diffraction (XRD), optical microscope (OM), field emission scanning electron microscope (FESEM) and Fourier transformation infrared ray (FTIR) were investigated. According to XRD analysis, the polymeric blend is shown to have a semi-crystalline nature whose peak in accordance with the plane (101) reflection, and the incorporated of NiO and Ni_2O_3 nanoparticles into blended polymers act noticeable change in the crystallinity of the film. The optical microscope images denote a good distribution of NiO and form a network of paths charge transfer within the polymeric blend. FESEM images showed an increase in the number of aggregations on the surface of the polymeric matrix as a result of adding different amount of NiO and Ni_2O_3 nanoparticles. The analysis of FTIR spectra confirms the presence of functional groups belonging to the polymer systems. From the optical properties, the absorbance, absorption coefficient, refractive index, polarizability, extinction coefficient, real and imaginary dielectric constant increase with increasing concentration of NiO and Ni_2O_3 NPs respectively, while the transmittance and indirect energy gap decrease with increasing concentration of NiO and Ni_2O_3 NPs respectively. these results can be used as solar collectors, UV shielding and wrapper for storing medicines. The AC electrical properties exhibit that the dielectric constant and dielectric loss for (PVA-PEG/NiO) and (PVA-PEG/Ni_2O_3) films are increased with the increase in the amount of nano-additives and decreasing with the increase of frequency of the applied electric field, on the other hand, the A.C electrical conductivity increased with the increase in the amount of nano-additives and decreasing with the increase of frequency of the applied electric

field. The antibacterial susceptibility examined of (PVA-PEG/9wt.%NiO) and (PVA-PEG/9wt.% Ni_2O_3) films was made by Agar disk method against two isolates of bacteria: gram- negative bacteria *Escherichia coli* and gram-positive bacteria *Staphylococcus aureus* and exhibited that the best growth inhibition zone was observed with ratio 9wt.% of Ni_2O_3 (24 mm) against *Staphylococcus aureus*.

List of Contents

List of Figure

List of Tables

List of symbols		
Symbol	**Physical Meanings**	**Unites**
ε_1	**Real part of the dielectric constant**	**-**
α	**Absorption Coefficient**	**cm^{-1}**
δ	**Dielectric loss angle**	**-**
A	**Absorbance**	**%**
A_r	**Area**	**A^o**
C	**Capacitance**	**F**
c	**Velocity of Light**	**m/s**
C_o	**Capacitance Vacuum**	**F**
C_P	**Capacitor containing an insulator material**	**F**
D	**Electrical displacement**	**C/m^2**
E	**Electrical field intensity**	**V/m**
E	**Energy**	**eV**
E_g^{opt}	**Optical energy gap**	**eV**
E_i	**Internal field of a molecule**	**V/m**
E_{ph}	**Energy of Phonon**	**eV**
ε	**Complex dielectric constant**	**-**
ε'	**Dielectric constant**	**-**
ε''	**Dielectric loss**	**F/cm**
ε_o	**Vacuum permittivity**	**F/cm**
h	**Planck Constant**	**J.s**
I	**Electrical current**	**A**
i	**Imaginary number**	**-**
I_o	**the intensity of incident rays**	**Lumen**
I_p	**Conduction current**	**A**

I_q	**Capacitate current**	**A**
I_T	**The intensity of transmitted rays**	**Lumen**
k_o	**Extinction Coefficient**	**-**
N	**Complex refractive index**	**-**
n	**Exponential Constant**	**-**
n	**Refractive Index**	**-**
P	**Polarization**	**-**
R	**Reflectance**	**%**
R_p	**Parallel with a resistance**	**-**
t	**Thickness of the film**	**µm**
T	**Transmittance**	**%**
T_g	**Glass Transition Temperature**	**^oC**
T_m	**Melting Temperature**	**^oC**
V_m	**Maximum voltage**	**V**
w	**Angular frequency**	**$rad.s^{-1}$**
Z	**Impedance**	**-**
ε_2	**Imaginary part of the dielectric constant**	**-**
σ_{opt}	**Optical conductivity**	**S^{-1}**

List of Abbreviations

Abbreviation	Meaning
PVA	**Poly (vinyl alcohol)**
WPVA	**Plasticized PVA**
PEG	**Poly (ethylene glycol)**
PEO	**Polyethylene oxide**
POE	**polyoxymethylene**
HEp-2	**Human airway epithelial**
MCF-7	**Human breast cancer**
NPs	**Nanoparticles**
RT	**Room temperature**
IR	**Infrared**
PLT	**Positron Lifetime Technique**
MW	**Molecular weights**
FTIR	**Fourier transform infrared spectroscopy**
XRD	**X-Ray diffraction**
XRF	**X-Ray-fluorescence**
FWHM	**Full width at the half of the maximum intensity**
FESEM	**Field Emission Scanning Electron Microscope**
SCF	**Subsequent supercritical fluid**
HRTEM	**High Resolution Transmission Electron Microscope**
S. aureus	***Staphylococcus aureus***
E. coli	***Escherichia coli***
NCs	**Nanocomposites**
OM	**Optical microscope**
CCD	**Charge coupled device**

CHAPTER ONE

Introduction and Literature Review

1.1 Introduction

Nanotechnology is one of the most popular topics for current research and development across a wide range of technological fields. This encompasses polymer science and technology, and research in this. include a wide range of fields [1]. Nanotechnology will enable the development of novel materials providing the basis for the design and development of new properties and structures which will result in increased performance, reduced cost of maintenance and enhanced functionality [2].

There is a significant feature of nanotechnology which is the reduction instruments, sensors, and computers, both old and modern, that will have a significant effect on the planet computers of exponentially great strength that generate algorithms to mimic human brains, examples of future miniaturization include biosensors that warn us at the earliest stage of disease initiation, preferably at the molecular level, and medicines that target particular diseases [3].

Nanorobots capable of repairing internal damage and removing toxic pollutants from human bodies, as well as nano scaled sensors capable of continuously monitoring our local world, are both possibilities. Nanotechnology has a broad variety of possible uses, ranging from nanoscale circuitry and optics to nano biological structures and nanomedicine [4,5].

Polymer science was born in the great industrial laboratories of the world of the need to make and understand new kinds of plastics, rubber, adhesives, fibers, and coatings. Only much later did polymer science come to academic life perhaps because of its origins, polymer science tends to be more interdisciplinary than most sciences, combining chemistry, chemical engineering, materials, and other fields as well [6].

The polymers are classified into three categories: natural, industrial, and modified. Proteins, cellulose, starches, and rubber are examples of natural polymers; industrial polymers include poly (vinyl chloride), polyvinyl alcohol, nylons polyethylene, polypropylene, polyesters polycarbonate, …. etc. [7].

Today, their remarkable combination of properties, low weight and processability is responsible for the vast use of polymer materials. The polymer matrix and shaped polymer matrix composite were supplied with a large number of additives. The combination of two or more substances with various physical and chemical properties and distinct interface are known as a composite. Composite products have a wide range of uses. In recent years, it has been discovered that adding nanoparticles to polymers causes significant changes in the polymer's structural, optical, and electrical characteristics [8]. Because of it is unique characteristics such as environmental friendliness, nontoxicity, water solubility, biodegradability, outstanding electrical and optical properties, chemical stability, excellent dielectric strength, and charge storage capacity.

Polyvinyl alcohol (PVA) is classified as a basic polymer. It has a hydroxyl group that, through hydrogen bonding, can aid in the formation of an interpenetrating link in a polymer composite [9]. PVA a common type of thermoplastic polymer having the chemical formula $(C_2H_4O)_n$, is a semi-crystalline polymer [10]. PVA has some special qualities, like being environmentally friendly, non-toxic, water soluble, providing excellent optical characteristics, being chemically stable, getting excellent dielectric strength, and being able to store charges. Due to its outstanding thermo-stability, solubility in water, in height mechanical asset, chemical resistance, in height insulator asset, and superior film-forming capacity via solution casting, it makes a desirable hosting material for inorganic additions [11]. The thermoplastic polymer type poly (ethylene glycol) (PEG) has a flexible bond structure which this chemical formula $H{-}(O{-}CH_2{-}CH_2)_n{-}OH$. Additionally, PEG is acknowledged to be have

mobility, is soluble in water, and is utilized as a binder in the creation of ceramic materials due to its well-known features, including its flexibility and lack of toxicity [12].

Metal oxides are used in a number of fields, including technology, environmental remediation, photocatalysis, solar energy transfer, and electronics [13]. Nickel (II) oxide (NiO), a p-type semiconductor and energy gap (3.6-4)eV [14], is a promising candidate for gas sensors, magnetism, catalysis, supercapacitors, and batteries, due to its low cost, natural abundance, non-toxic nature, good electrochemical stability in alkaline solutions, and high theoretical capacitance [15]. Also, NiO exhibits a typical battery-type charge storage mechanism, which is preferred to develop new-age high-performance supercapacitor (HSCs). However, NiO suffers from poor rate capability due to slow ion diffusion and poor electrical conductivity [16]. Nickel(III) oxide (Ni_2O_3) is a transition metal oxide that has a rock salt structure which submits the characteristic of p- type semiconducting material with energy band gap nearly 2.2 - 3.4eV [17]. Ni_2O_3 is chemically stable and has high electrical conductivity also exceptional (optical, electronical, and magnetically) characteristics. Furthermore, it has ultra-fine structure with a uniform size and well dispersion. It has attracted a great attention because of its wide applications such as in manufacturing magnetic materials, gas sensors photovoltaic devices, fuel cell, and catalytic materials [18] . It is possible to convert NiO to Ni_2O_3 or vice versa by using gamma irradiation of the metal oxide according to the work mentioned in the reference [17].

Given the importance of metal oxide nanomaterials and their application in many fields and they can be used with polymers to improve the physical properties of these polymers and their use in wide areas, the purpose of this research is preparation and investigation structural, optical, and electrical

properties of (PVA-PEG/NiO) and (PVA-PEG/Ni_2O_3) nanocomposite and apply it as an antibacterial.

1.2 Polymer Blends

The fate of polymer blends is derived from the compatibility and or miscibility of their components. Most experimental studies have been carried out by casting from solution, though most commercial polymer blends are prepared by melt mixing by twin-screw extruders. The miscibility of two polymers is `depending on the specific interactions between polymer chains. This can be explained by the factor of entropy in the following equation, which represents the second law of thermodynamics [19].

$$\Delta G_{mix} = \Delta H_{mix} - T\,\Delta S_{mix} \qquad (1.1)$$

where, ΔG = change in free energy, ΔH = change in enthalpy, ΔS = change in entropy, T = absolute temperature.

For a homogeneous miscible blend, the Gibbs free energy of mixing requires a negative value. For high molecular weight polymer blends, the gain in entropy is negligible. Hence, the free energy of mixing can only be negative if the heat of mixing is negative. This means that the mixing must be exothermic, which usually requires specific interactions between the blend components. These interactions may range from strongly ionic to weak and non-bonding, including hydrogen bonding, ion-dipole, dipole-dipole, and donor-acceptor interactions. Based on the miscibility, three types of blends can be distinguished: (i) completely miscible blends, (ii) partially miscible blends (iii), and fully immiscible blends. Completely miscible blends consist of one homogeneous phase. This type of blend exhibits only one glass transition temperature (T_g), which is between the T_g of both blend components with a close relation to the blend composition. Partially miscible blends, in which a part of one blend component is dissolved in the other, exhibits normally good compatibility and fine phase morphologies. However, fully immiscible blends exhibit a coarse

phase morphology having a sharp interface and a poor adhesion between both blend phases. This is the reason for often observed poor properties of immiscible blends, which strongly depend on the size and distribution of the phases [20].

Forming polymer blends is a traditional method for making new materials with enhanced properties. Unfortunately, because of the large unfavorable enthalpy, most polymer blends tend to phase separate, which results in poor mechanical properties. Therefore, controlling the phase behavior and morphology becomes a key factor in determining the performance of polymer blends, which mainly rely on the interface between polymer components. Traditionally, block and graft copolymers are used to strengthen the interface and stabilize the morphology. However, they are system specific, relatively expensive to engineer, and very difficult to produce for systems with more than two components [21].

1.3 Nanomaterials

Nanomaterials describe, in principle, materials of which a single unit small sized (in at least one dimension) between (1-100) nm the usual definition of nanoscale and nanoscale defined as the "length range approximately from 1 nm to 100 nm". This includes both nanoobjects [22].

Nanomaterials research takes a materials science-based approach to nanotechnology, leveraging advances in materials metrology and synthesis which have been developed in support of microfabrication research. Materials with structure at the nanoscale often have unique optical, electronic, thermo-physical or mechanical properties [23-25]. The classification of nanomaterials is based on the number of dimensions, which are in nano range (≤ 100 nm) [26], as shown in Figure (1.1) [27].

1- 0D nanomaterials have all the dimension within nanoscale, i.e., no dimension is larger than 100 nm. The most common example of 0D- dimensional

nanomaterials is the nanoparticle. These nanoparticles can be crystalline or amorphous, metallic, ceramic, or polymeric.

2- 1D nanomaterials have two dimensions in nano range. This leads to needle like shaped materials having one dimension at nanoscale. 1D nanomaterials include nanoplatelets, nanorods, nano clays and nanosheets.

3- 2D nanomaterials have one dimensions in nano range. 2D nanomaterials include nanofibers, nanotubes, nanorods and whiskers. Carbon nanotubes are good example of 2D nanomaterials.

4- 3D nanomaterials have all three dimensions is not nano range. 3D nanomaterials include nanogranules, nano clays and equiaxed nanoparticles.

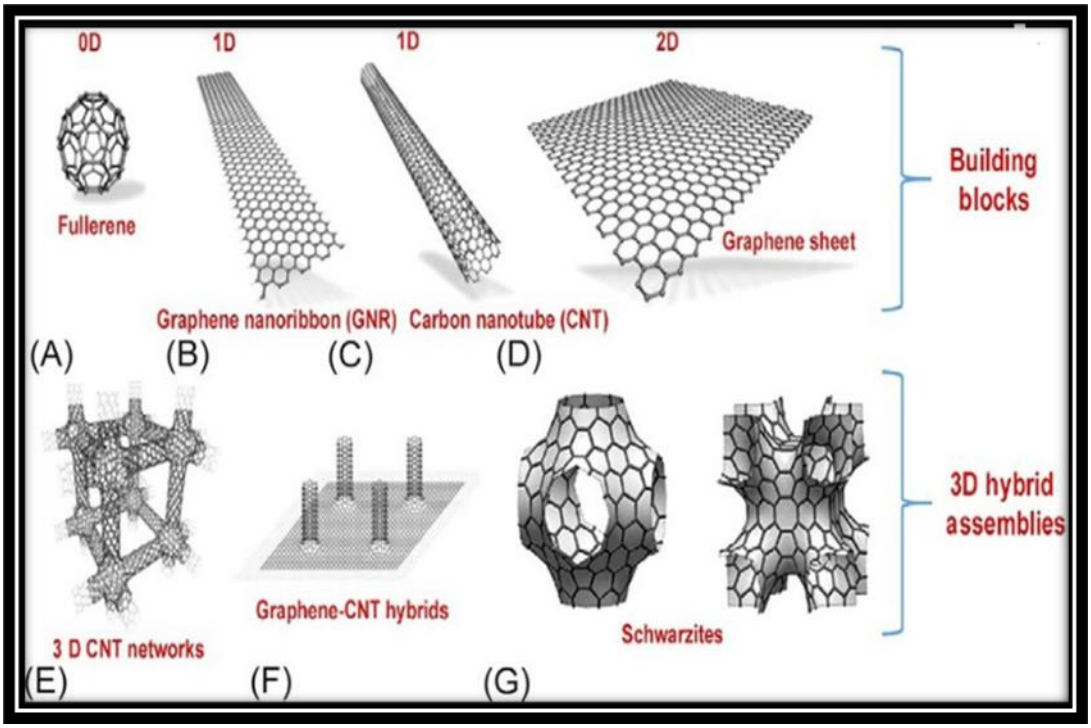

Fig.(1.1): Classification of nanomaterials (a) 0D (b) 1D (c) 2D (d) 3D [27].

1.4 Nanocomposite

Nanocomposites are a major factor in the formation of novel advanced materials suitable for a variety of different applications, such as electrical engineering , nanocomposites have attracted considerable interest in both

academia and industry [28]. Composite materials can be defined as a material system composed of a combination of two or more materials that differ in form or material composition; the properties of a composite are different from those materials. The compound consists of two major components: the matrix (the basic material) and the additives. The matrix surrounds other constituents and makes them more cohesive to form a "compact system" [29]. Additives are constituents added to polymers to provide them with specific properties and improve basic properties. These constituents are added in a granular form or as small particles. Nanocomposites can be defined as a composite material in which at least one of the phases (mostly the filler) shows dimensions in the nanometer range, as the filler, size reaches the nanometer level, the interactions at the interfaces become considerably large with respect to the size of the inclusion and thus the final properties show significant changes. A nanocomposite has two parts, filler and the matrix, a traditional composite typically uses a fiber such as carbon fiber or fiberglass as the filler. The properties of nanocomposites are highly dependent on: properties of the filler (geometry, size, filler type etc.), host matrix: (crystallinity, polymer chemistry, nature thermoplastic or thermosetting etc.), surface treatment, interfacial properties, fill grade, degree of dispersion and agglomeration, Relative arrangements and subsequent synergy between constituents and Synthesis methods [29]. The properties of polymer nanocomposites are affected by: the nature of the polymer matrix and filler, dispersion state of the particles, filler-matrix interaction, filler size and surface modification of the filler [30].

1.5 Materials Used in the Study

1.5.1 Polyvinyl alcohol (PVA)

Poly-vinyl alcohol (PVA) is synthetic polymer employed since the early 1930s in a wide range of industrial, commercial, medical and food applications including resins , surgical threads, lacquers and food-contact applications [31]. Poly (vinyl alcohol) is a synthetic polymer that comes in the form of a granular powder that is odorless, transparent, tasteless, white, or cream-colored [32]. Polycarbonate (vinyl alcohol), which may be combined in water, has the benefit of being resistant to solvents and oils, as well as having outstanding characteristics [33].

PVA polymer has high tensile and compressive strengths, tensile modulus, and abrasion resistance due to its highest crystalline lattice modulus. Many researchers have looked at using PVA as a filler or in cross-linked products, additionally, it has been widely employed as a thermoplastic polymer to make nontoxic, harmless, and living tissues, among other things [34,35] . It has been used in a wide range of applications and is also widely used in semiconductor applications [36]. Figure (1.2) shows the chemical structure of PVA [36]. Table (1.1) explain the physical properties of PVA [37].

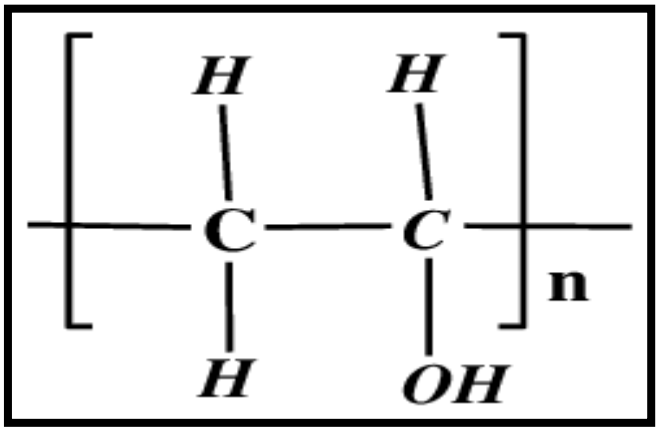

Fig. (1.2) The chemical structure of PVA [36]**.**

Table (1.1): Physical and chemical properties of poly(vinyl alcohol) (PVA) [37].

Property	Description
Appearance	White to an ivory white granular powder
Molecular formula	$(C_2H_4O)_n$
Solution PH	5- 6.5
Density g/cm^3	1.3 g/cm^3
Refractive index	1.55
Glass transition Temperature T_g ºC	85 ºC
Melting point	200 ºC

1.5.2 Polyethylene glycol (PEG)

Polyethylene glycol (PEG) is a polyether compound derived from petroleum with many applications, from industrial manufacturing to medicine. PEG is also known as polyethylene oxide (PEO) or polyoxymethylene , depending on its molecular weight [38] . PEG is a water-soluble synthetic polymer widely used in pharmaceutical and cosmetic industries [39]. PEG has many attractive properties such as wide range of molecular weight, biocompatibility, low toxicity, and chain flexibility, and it has been used frequently in the production of polymer blends as it can improve the flexibility and ductility of rigid polymers. Figure (1.3) shows the chemical structure of PEG [40]. Table (1.2) explain some physical properties of PEG [41].

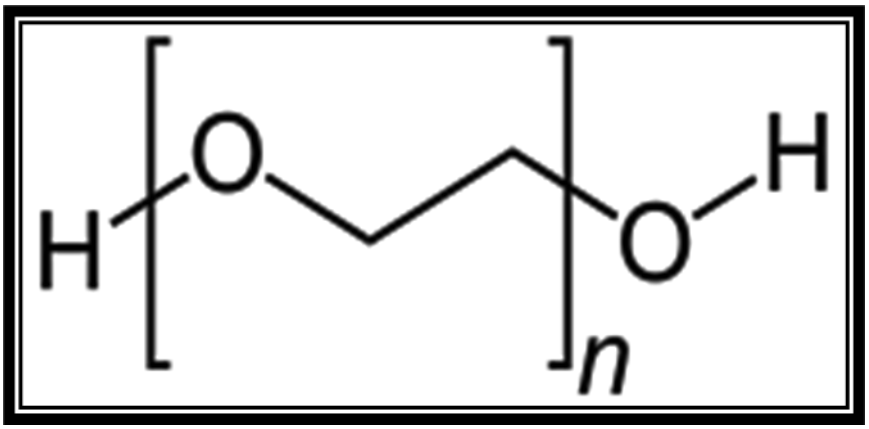

Fig.(1.3): The chemical structure of PEG [40].

Table (1.2): Physical properties of polyethylene glycol (PEG) [41].

Property	Description
Appearance	White to very pale yellow
Molecular formula	$C_{2n}H_{4n+2}O_{n+1}$
Solution PH	5.5-7
Density	1.27 g/cm^3 at 25 °C
Refractive index	1.469
Glass transition temperature T_g ºC	55 ºC
Melting point	250 °C

1.5.3 Nickel Oxide

Nickel (II) oxide (NiO) is a p-type semiconductor metal oxide possessing a band gap from 3.6 to 4.0 eV that has great importance and has received enormous consideration in research owing to its peculiar properties like large surface area, high chemical stability, good electronic conductivity, and super conductance characteristics [42]. Its ecofriendly nature and high reactivity makes it a potential candidate for applications in the field of magnetism, electronics, energy technology gas sensors, electrochemical super capacitors, catalysis, battery cathodes, magnetic materials, fuel cells, optical fibers, and biomedicines [43]. NiO nanoparticle is known for its antimicrobial activity against various.

Bacterial pathogens and as an effective photocatalyst in the removal of dyes and organic pollutants from wastewater. It is also good in imparting cytotoxic activity over various cells like human airway epithelial (HEp-2) and human breast cancer (MCF-7) cells [44].Various techniques have been adopted for the synthesis of NiO nanostructures such as sol-gel, co-precipitation, hydrothermal, solvothermal, anodic arc plasma, Sono chemical, pyrolysis by

microwave, thermal decomposition, micro-emulsion and chemical precipitation [44], [45]. Figure (1.4) obtains the structure of NiO NPs [46]. Table (1.3) explain the physical properties of NiO NPs [47].

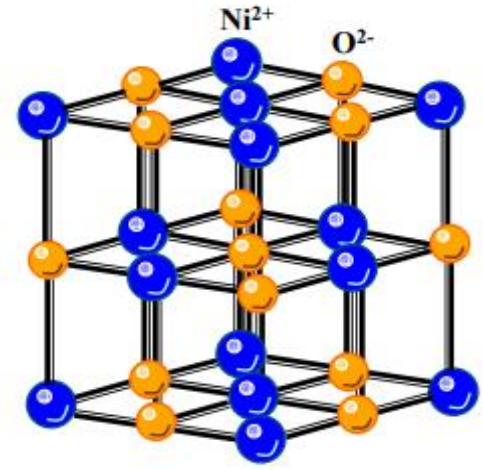

Fig. (1.4): The crystal structure of NiO NPs [46].

Table (1.3): Physical properties of Nickle oxide nanoparticle [47]

Property	Description
Structure	**Face center cubic**
Appearance	**Green Powder**
Compound formula	**NiO**
Molar mass	**74.71 g/mol**
Density	**6.67 g/cm^3**
Melting point	**1955 °C**

Nickel (III) Oxide (Ni_2O_3) is a p- type semiconducting material with energy band gap range 2.2 to 3.4 eV. Ni_2O_3 is one of the promising metal oxides that can be synthesized by various methods such as sol-gel, solvent thermal technique, Hydrothermal technique and solution combustion method etc. Among all these methods, low temperature solution combustion synthesis has received considerable attention due to the existence of its applications and properties in gas sensor devices, catalysis, ferrofluids and magnetic storage devices and the structure of Ni_2O_3 is orthorhombic are shown in Figure (1.5) [48].

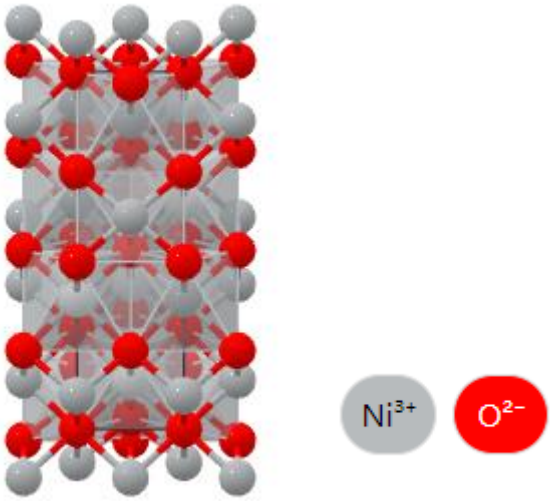

Fig. (1.5) The structure of Ni_2O_3 [48]

1.6 Literature Review

In (2017) K. S. Khashan, *et al*. [49] prepared NiO NPs via pulsed laser ablation in deionized water and their antibacterial activity. The X-ray diffraction (XRD), transmission electron microscopy (TEM), Fourier transform infrared spectroscopy (FTIR) and UV-Vis optical absorption spectra was tested. The results show that crystalline NiO NPs were produced. The antibacterial activity against *Escherichia coli, Pseudomonas aeruginosa, Proteus vulgaris,* and *Staphylococcus aureus* bacteria was then examined. It was found that the NiO

NPs have a synergistic effect on inhibiting *E. coli* and *S. aureus* growth; this effect was also tested using the well-diffusion method. In this method, NiO nanoparticles at a concentration of (0.001) g along with amoxicillin yielded an inhibition zone against E. coli of 14.3 ± 1.15 mm; this zone was 12.6 ± 0.57 mm against S. aureus.

In (2018) M. Irfan, *et al.* [50] prepared NiO NPs by chemical precipitation technique. Films of NiO doped PVA NCs are synthesized by solution casting process. NiO doped PVA films were characterized by XRD and FTIR techniques. XRD analysis revealed the NCs nature of amorphous. FTIR analysis revealed the existence of C-O and Ni-O in films. Dielectric properties were studied. The dielectric constant (ε′) of the sample is found to decreased with rise in frequency. The AC conductivity was found to rise with rise in frequency. The electrical conduction mechanism in present sample agrees with an electron-hopping model. Present NiO doped PVA NCs may find applications in the electronic energy storage devices.

In (2018) S. Ningaraju, *et al.* [51] prepared poly(vinyl alcohol)/nickel oxide (PVA/NiO) and poly(vinyl alcohol)/titanium dioxide (PVA/TiO_2) polymer nanocomposites by Positron Lifetime Technique (PLT). The FTIR and SEM demonstrated the formation of nanoclusters by the agglomeration of nanoparticles at higher wt.% of nanofiller loading. The increased AC/DC conductivity of PVA/NiO and at lower concentration of TiO_2 in PVA/TiO_2 polymer nanocomposites suggests the increased mobility of ions and electric charge carriers. The decreased conductivity at higher concentration of TiO_2 indicated the reduced conducting pathways for the mobility of ions and electric charge carriers due to the increased ion aggregation. The increased dielectric constant and dielectric loss up to 1.0 wt.% of NiO and 0.4 wt.% of TiO_2 suggests the increased dipole polarization.

In (2018) K. O. Ukoba, *et al*. [52] prepared NiO thin film by the spray deposition method. The physical, chemical, optical, structural characterization and properties of nanostructured NiO thin film have been investigated. NiO films are p-type semiconductors and as such possesses direct band gap suitable for various applications. The film has been categorized as an excellent material for optoelectronic applications because of its tune-ability for optimization. The wide band gap was in the range of 3.25–4.0 eV.

In (2019) P. Liu, *et al*. [53] studied a novel poly (vinyl alcohol) (PVA)/poly (ethylene glycol) (PEG) scaffold was carefully designed via thermal processing and subsequent supercritical fluid (SCF) foaming. The intermolecular interactions of the PVA/PEG blend were studied using X-ray diffraction and FTIR analysis. The results demonstrate that various types of hydrogen bonds among the hydroxyl groups on the PVA chains, PEG and water molecules are formed in the blend system. The realization of thermoplastic foaming of the PVA/PEG blend benefits from the interactions of complexation and plasticization between water and PEG molecules. The SEM images also revealed that L929 fibroblast cells were able to attach and spread on surfaces of the PVA/PEG samples. Thus, the PVA/PEG scaffold with unique bimodal cellular structure is nontoxic and favors the attachment and proliferation of cells.

In (2020) S. A. Bhat, *et al*. [54] prepared Ni_2O_3 thin films by spray pyrolysis technique. The XRD, UV visible spectroscopy, atomic force microscope (AFM). The XRD of the films was (002) oriented hexagonal. Average values of optical absorbance, extinction coefficient and optical conductivity in the visible region (λ = 380 – 740 nm) increased rapidly with molarity in the low molarity range 0.01 – 0.05M and rather slowly in the high molarity range (0.1 – 0.5 M). Both direct (3.99 – 4.045 eV) and indirect (3.37 – 3.52 eV) band gaps decreased whereas Urbach energy (0.33 – 0.42 eV) increased on increasing molarity. The average refractive index (1.33 –1.53) in the visible region decreased linearly with increase in molarity. Surface

morphology of the films consisted of random shape nanoparticles. Average surface roughness of the films (0.173 – 0.366 μm) increased rapidly with molarity in the range 0.01 – 0.03 M, and then decreased to an intermediate level (0.284 μm) around which it undulated in the range 0.05 – 0.5 M.

In (2021) N. M. Shaalan, *et al.* [55] prepared composites of functionalized polyvinyl alcohol with NiO nanoparticles with of 1.0–5.0 wt %. Crystal structure analysis were well studied by XRD and optical properties of the functionalized PVA have been deeply characterized. XRD analysis reveals the polycrystalline feature of pure and functionalized PVA, containing both amorphous and crystalline phases. The dual optical properties exhibit the features of both PVA and dopant materials. Clear change in the optical properties of PVA was observed with various NPs content that has been increased up to 5 %. The optical band gap of PVA was changed from 5.4 eV for 0.1% NiO up to higher value at 0.4% NiO. Interesting is the appearance of another indirect band at lower energy. This band gap energy was recorded at 3.8 and 3.36 eV at 0.1% NiO, and 2.85 and 2.3 eV at 0.5% NiO for various phonon energies.

In (2021) H. Ali, *et al* [56] prepared chitosan/PVA/NiO nanocomposite by casting method. Chitosan/PVA doped with different amounts of NiO NPs (0.5, 1.5, 3, 5 wt.%) were studied using XRD, HRTEM, FESEM, ATR-FTIR, UV–Vis spectrophotometer, and AC conductivity measurements. The antibacterial activity and dye removal of the prepared sample are investigated. The XRD and conductivity measurements proved that addition NiO NPs increases the crystallinity of nanocomposite system compared to pure chitosan/PVA. ATR-FTIR results affirmed the structural change in blend sample by the addition of NiO NPs. XRD and FTIR data confirmed the loading of NiO in chitosan/PVA membrane. Values of absorption coefficient and band gap indicated that addition of NiO NPs change the structure of chitosan/PVA, decreased the band gap, and creates localized states in the band gap. The AC

conductivity was decreased compared to polyblend sample because of the addition of NiO NPs. The results of antimicrobial test indicated that the NiO/chitosan/PVA nanocomposite films have better activity toward.

In (2022) T. Alrebdi, *et al* [57] prepared (NiO/PVA) doped by silver nanoparticles (Ag) to generate an Ag doped NiO/PVA nanocomposite structure prepared by multiple laser ablation process technique for removing phosphate. The characterization results of the prepared nanocomposites showed that NiO and Ag were successfully integrated into the PVA structure. After that, in the adsorption study, the most important aspect of the investigation was a series of phosphate adsorption tests from aqueous solutions, which showed that the efficiency of the adsorption process is dependent on the concentrations of the adsorbate and adsorbent, the pH, the reaction time, and the temperature.

1.7 The Aim of the Study

Studying and comparison effect of green and black nickel oxide nanoparticles on the structural, optical, and electrical properties of PVA-PEG polymer blend. Then this nanocomposite applied as the antibacterial.

CHAPTER Two

Theoretical Part

2.1 Introduction

The general overview of the theoretical part of this chapter focused on the description of classification of polymer and laws used to describe the optical and electrical properties results.

2.2 Classification Based on the Structure of Polymers.

The physical properties of any polymer are depending on two molecular characteristics [58] :

a) The length of the molecule

b) The functional group related with the repeating units.

By using different starting materials and processing techniques, it is possible to produce polymers having different molecular structures as the following [59].

1. Linear: The chains of polymer hold it together by many Vander Waals bonds. Examples of linear polymers are polyethylene, fluorocarbons, polystyrene, nylon, and polyvinyl chloride are shown in Figure (2.1 a).

2. Branched: Side-branch chains bond to the main ones during synthesis of the polymer. These reduce the packing efficiency, so lower density is shown in Figure (2.1 b).

3. Cross linked: Cross-linked polymers consist of smaller polymer chains which are bonded together. Each chain is bonded to many chains. Many of the rubber materials consist of polybutadiene cross linked with (S) atoms are shown in Figure (2.1 c).

4. Network: Mer units with three active covalent bonds are form 3D networks (e.g., epoxies) are shown in Figure (2.1 d).

.

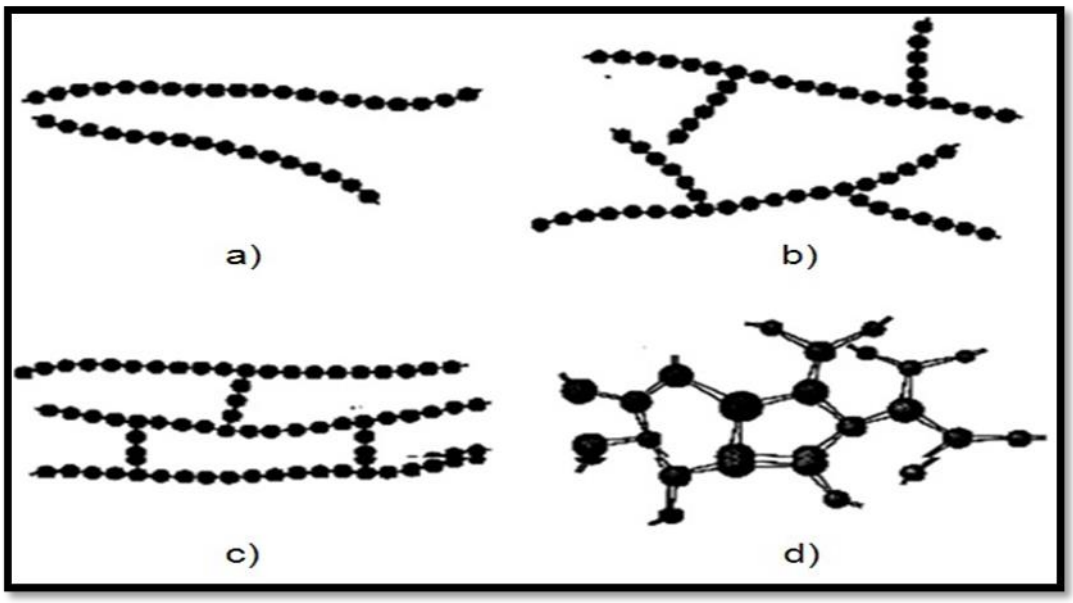

Fig. (2.1): The type of polymers (a) Linear polymer, (b) Branched Polymer, (c) Cross-linked polymer, (d) Network polymer [59].

2.3 Comparison Between Thermoplastic and Thermosetting Polymers

Thermoplastics are lengthy polymer chains that have a high molecular weight. These chains can be crystalline or amorphous, depending on the thermoplastic. The high molecular weights of polymers are what give them their useful features, including as superior mechanical capabilities and the capacity to be molded into a wide variety of different kinds of parts (injection molded, extruded, etc.).

Thermoplastics can have no crystallinity, making them amorphous. This causes the lengthy chains to become entangled with one another, giving the impression that the material is "like a bowl full of spaghetti." Since the polymer chains are going through random Brownian motion and slithering past one another, the late Professor Garth Wilkes from Virginia Polytechnic Institute used to compare molten polymers (like linear amorphous) to a bowl full of snakes [60]. He was referring to the fact that molten polymers are like linear amorphous.

Thermosets are a type of polymer that start out as small molecules (monomers and oligomers), but through the process of a chemical reaction, they are able to polymerize into a network structure. In the fully cured and final condition, the crosslinks bind the chains together, which provides both strong mechanical qualities and dimensional stability, but thermosets will not flow (and are not dimensionally stable) above their T_g [61]. Figure (2.2) explain the thermoplastic and thermosetting.

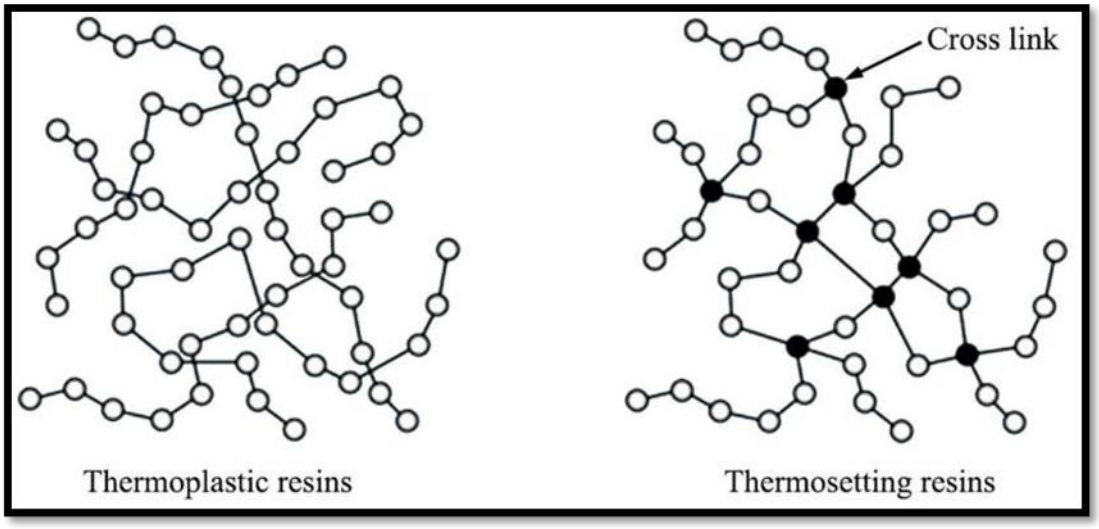

Fig. (2.2): Difference between thermoplastic and thermoset polymers [61].

2.4 Measurements of Structural Properties

2.4.1 Optical microscope (OM)

One of the first techniques used to study the topography of a surface is optical microscopy as shown in figure (2.3), also called light microscopy, is a type of microscope that uses visible light and a system of lenses to magnify images of small samples.

Optical microscopes are the oldest design of microscope and were possibly designed in their present compound form in the 17th century. An optical microscope usually has a single eyepiece which can often be fitted with a camera for photography [62].

Traditional optical microscopes have a resolution restricted by the size of submicron particles approaching the wavelength of visible light (400–700 nm) include:

1. Transmission: beam of light passes through the sample; and
2. Reflection: beam of light reflected off the sample surface.

An example is the polarizing or petrographic microscope for which the samples are usually fine powder or thin slices (transparent). Another example is the metallurgical or reflected light microscope which is used for the surfaces of materials, especially opaque ones [63].

The image from an optical microscope can be captured by normal light sensitive cameras to produce a micrograph. Typically, images were captured by photographic film but modern developments in supplementary metal oxide semiconductor and charge-coupled device (CCD) cameras permit the capture of digital images. Simply, digital microscopes are now available that use a CCD camera to examine a sample, showing the resulting image directly on a computer screen without the need for eyepieces [64].

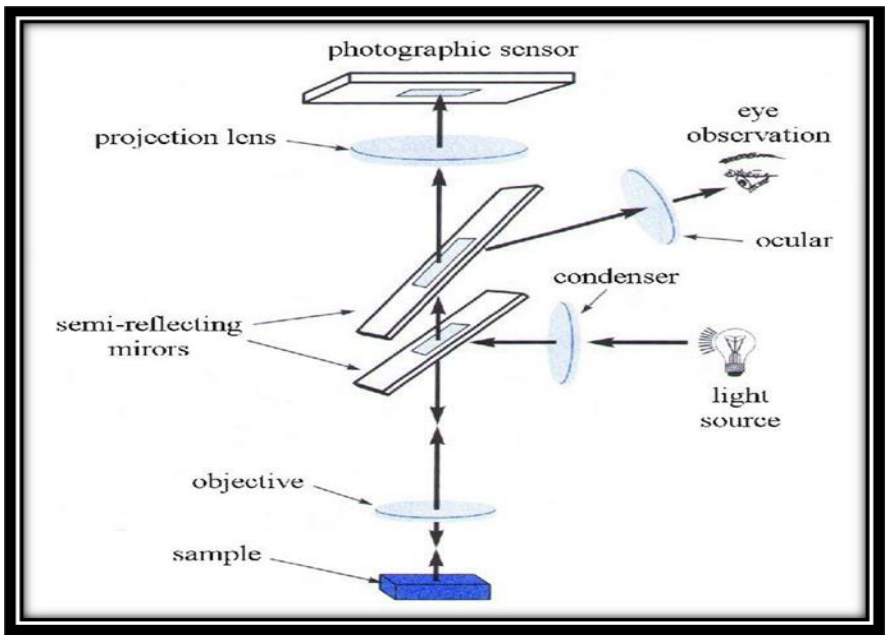

Fig. (2.3) The optical Microscope [63]

2.4.2 Fourier Transform Infrared (FTIR) Spectroscopy

FTIR is a tool that has been used over the years in chemical analysis for substance identification and is one that can be applied to describe microorganisms. FTIR spectroscopy is determined by the magnitude of the molecular bond vibration compounds, excited at an appropriate wavelength by radiation, given the conditions for the molecular absorption of energy. Figure (2.4) get the configuration of the FTIR system [65].

FTIR spectroscopy is a form of vibrational spectroscopy, which reflects both the molecular structure and the molecular environment. The approach is to irradiate the sample from an infrared source with infrared radiation, and the absorption of this radiation causes vibrational motions by vibration. In vibrational modes, quantum energy deposition [66]. Thus, a molecule is only absorbed at frequencies corresponding to its molecular vibration modes in the region of the electromagnetic spectrum between the visible (red) and the short (microwave) waves when exposed to radiation emitted by the thermal emission of a hot source (the source of IR energy) [67]. These variations in vibrational motion give rise to bands in the vibrational spectrum; each spectral band is characterized by its frequency and amplitude [68].

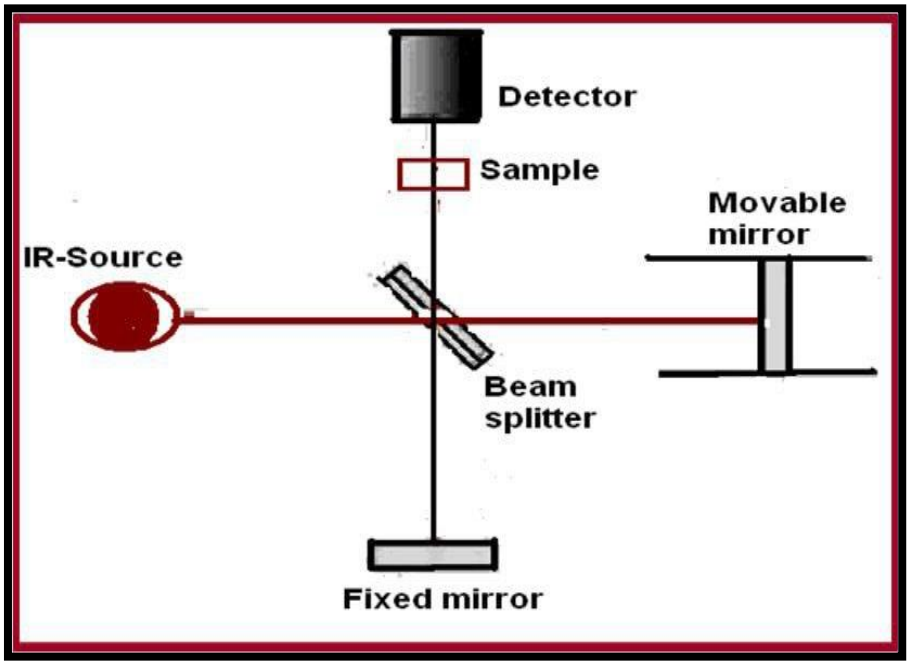

Fig.(2.4): Scheme of the FTIR system[65].

2.4.3 X-ray Diffraction (XRD)

The composition of atomic materials which used X-Ray-fluorescence (XRF) and its characterization used X-Ray diffraction (XRD). The technique is based on the fact that in condensed matter, the wavelength of X-rays is similar in size to the distances between atoms. So, when a substance exhibits a long-range (at least μm) periodic atomic order, such as a single crystal or polycrystalline powder, it is irradiated by X-rays and functions as an extended periodic grating creating a pattern of diffraction displaying various sharp points, called Bragg diffraction peaks. It is possible to define the spatial characteristics of the grating by measuring and analyzing the locations and intensities of the Bragg peaks. In the crystalline mat, to establish the three-dimensional (3D) atomic arrangement [69]. The XRD mechanism is simple when there are constructive diffractions (or interference) from parallel planes of atoms with inter-planar spacing (d) when a monochromatic X-ray beam occurs on a crystal sample, as shown in Figure (2.5) if Bragg 's law is satisfied [70].

$$2d\sin\theta = n\lambda \qquad (2.1)$$

Where n is an integer that indicates the order of the reflection, (d) the inter-planar distant, θ is the angle of Bragg, and λ is the x-ray beam's wavelength.

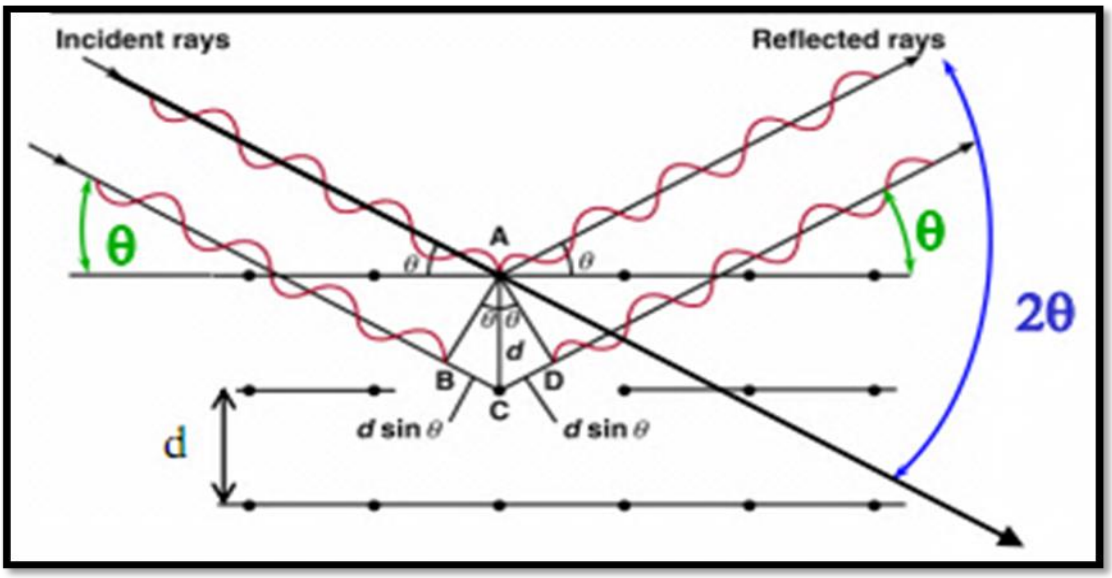

Fig.(2.5) Bragg diffraction[70]

The structural factors of any material are determined by X-ray diffraction, which is crucial in explaining many of the material's physical properties. In the case of the cubic structure, which represents the dominant pattern of the structure, (a, b, c) represent the lattice constants [71].

2.4.4 Field emission scanning electron microscope (FESEM)

FESEM is a type of electron microscope that produces images of a sample by scanning the surface with a focused beam of electrons. The electrons interact with atoms in the sample that contain information about the sample's surface topography [72]. The most common FESEM mode is detection of secondary electrons emitted by atoms excited by the electron beam. The number of secondary electrons can be detected depending on specimen topography. Electron microscopes use a particle beam of electrons to illuminate a specimen and create a highly magnified image [73]. The electrons from electron gun pass through anode, electromagnetic lenses, coils, detectors and strike the gold coated specimen placed on the stage. The electromagnetic lenses focus electron beam to a specific plane relative to the specimen and thereby forming the image. The secondary electrons generated because of electrons striking specimen surface are detected by secondary electron detector and converted into signal that is sent to a TV scanner [74]. Figure (2.6) shows schematic flow diagram of a FESEM [75] .

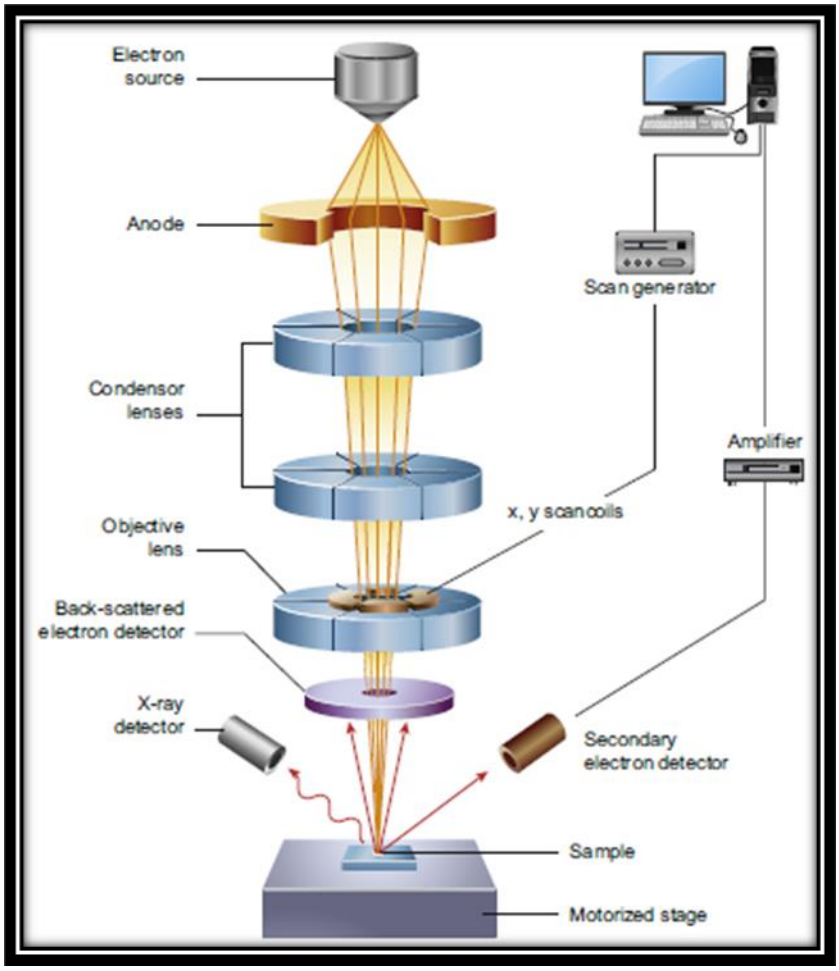

Fig.(2.6): Schematic diagram of the FESEM [75].

2.5 Optical properties of semiconductors

2.5.1 Absorbance (A)

The absorbance occurs when light passes through a material and the intensity is reduced based on the colors that are absorbed.

It can be defined as the ratio between absorbed light intensity (I_A) by material and the incident intensity of light (I_o) [76]:

$$A = \frac{I_A}{I_o} \qquad (2.2)$$

2.5.2 Transmittance (T)

The intensity of transmitted rays from the film (I_T) over the intensity of incident rays on the film (I_o) is called the transmittance (T), and can be obtained as follows [77]:

$$T=I_t / I_o \qquad (2.3)$$

2.5.3 Optical constants

There are many ways to find the optical constants of refractive index, extinction coefficient, optical conductivity, dielectric constant, and absorption coefficient.

2.5.3.1 Refractive index (n)

The refractive index can be defined as the ratio of the speed of light in vacuum (c) to the velocity of light in the medium (υ) according to [78]:

$$n = \frac{c}{\upsilon} \qquad (2.4)$$

The relation can be used to calculate reflectance ® from absorption A and transmission T spectra in accordance with the conservation of energy law [79]:

$$R + A + T = 1 \qquad (2.5)$$

The following equation can be used to calculate the refractive index [80]:

$$n = \frac{1+R}{1-R} + \left[\frac{4R}{1-R^2} - k_o^2\right]^{1/2} \qquad (2.6)$$

where: (k_0) is the extinction coefficient.

R: is the reflectance.

Depending on the refractive index, it can be determined the polarizability (P) by the relation [81]:

$$P = \frac{3}{4\pi}\left(\frac{n^2-1}{n^2+1}\right) \quad (2.7)$$

2.5.3.2 Extinction coefficient (k_o)

The electrical coefficient the amount of photons absorbed by the membrane, that is, the energy absorbed by the electrons of the material, and expresses the following relationship [82]:

$$k_o = \alpha\lambda/4\pi \quad (2.8)$$

Where (λ) is the wavelength of the incident light and (α) absorption coefficient.

2.5.3.3 Optical conductivity

The optical conductivity (σ_{op}) has been determined from the following equation [83]:

$$\sigma_{op} = \frac{nc\alpha}{4\pi} \quad (2.9)$$

Where n is the refractive index, α is the absorption coefficient and c are the speed of light.

2.5.3.4 Dielectric constant

The dielectric constant expresses a material's polarization ability, whose expression is computed using the following equation [84]:

$$\varepsilon = \varepsilon_1 - i\varepsilon_2 \quad (2.10)$$

$$\varepsilon = N^2 \quad B \quad (2.11)$$

$$(n - ik_o)^2 = \varepsilon_1 - i\varepsilon_2 \quad (2.12)$$

$$\varepsilon = (n^2 - k_o^2) - i(2nk_o) \quad (2.13)$$

The dielectric coefficient (ε) can be determined using the refractive index (n), join complex dielectric coefficient (ε) with complex refractive index (N). From equations (2.11) and (2.12) real and imaginary complex dielectric coefficient can be written as in following equation [84]:

$$\varepsilon_1 = (n^2 - k_o^2) \quad (2.14)$$

$$\varepsilon_2 = (2nk_o) \quad (2.15)$$

2.5.3.5 The absorption coefficient

It is defined as a ratio decrement in incident ray energy flux relative to distance unit in the direction of incident wave diffusion. The absorption coefficient (α) depends by the incident photon energy (hυ) as well as the properties of the sample, where electronic transitions type (n) or (p), and forbidden energy gap, photon energy give the following equation [85]:

$$E=h\upsilon \quad (2.16)$$

When the incident photon energy is lower than the forbidden energy gap, the photon is transmitted, and the transmittance equation is as follows [86]:

$$T = (1 - R)^2 . e^{-\alpha t} \quad (2.17)$$

If the incident ray intensity (I_o) that incident on blend film material of thickness (t), the intensity of transmittance ray (I) is determined by the beer Lambert law [87].

$$I = I_o e^{(-\alpha t)} \quad (2.18)$$

a means the absorption coefficient (cm^{-1}).

$$\alpha t = 2.303 \log \frac{I}{I_o} \quad (2.19)$$

Where the quantity of log (I/I_o) indicates the absorbance (A). The following equation can be used to compute the absorption coefficient[88]:

$$\alpha = 2.303 \left(\frac{A}{t}\right) \quad (2.20)$$

Where (t) represent a thickness of sample.

2.5.4 Fundamental absorption edge

The fundamental absorption edge can be characterized as the quick increase in absorbance when the amount of energy absorbed is nearly equal to the band energy gap; Thus, the fundamental absorption edge denotes the less difference in the energy between up point in valance band to bottom point in conduction band [89].

2.5.4.1 Absorption regions

There are three different types of absorption regions [90]:

A) High absorption region

This region is shown in Figure (2.7). In part (A), the absorption coefficient's magnitude (α) is greater than or equal to (10^4 cm^{-1}). The magnitude of the forbidden optical energy gap ($E_g{}^{opt}$) can be introduced from this region.

B) Exponential region

This region is shown as in Figure (2.7). In part (B) The absorption coefficient (α) equals ($1\ cm^{-1} < \alpha < 10^4\ cm^{-1}$). It describes the transition from extensive levels in the Valens band (V.B.) to local levels in the conductive band (C.B.) and vice versa, transitioned from local levels in (V.B.) to extended levels at the conductive band's bottom (C.B.).

C) Low absorption region

The absorption coefficient (α) is extremely small in this region. it is about ($\alpha < 1\ cm^{-1}$). The transition occurs in this region as a result of state density inside space motion caused by structural faults [91] as in Figure (2.7), the part (C).

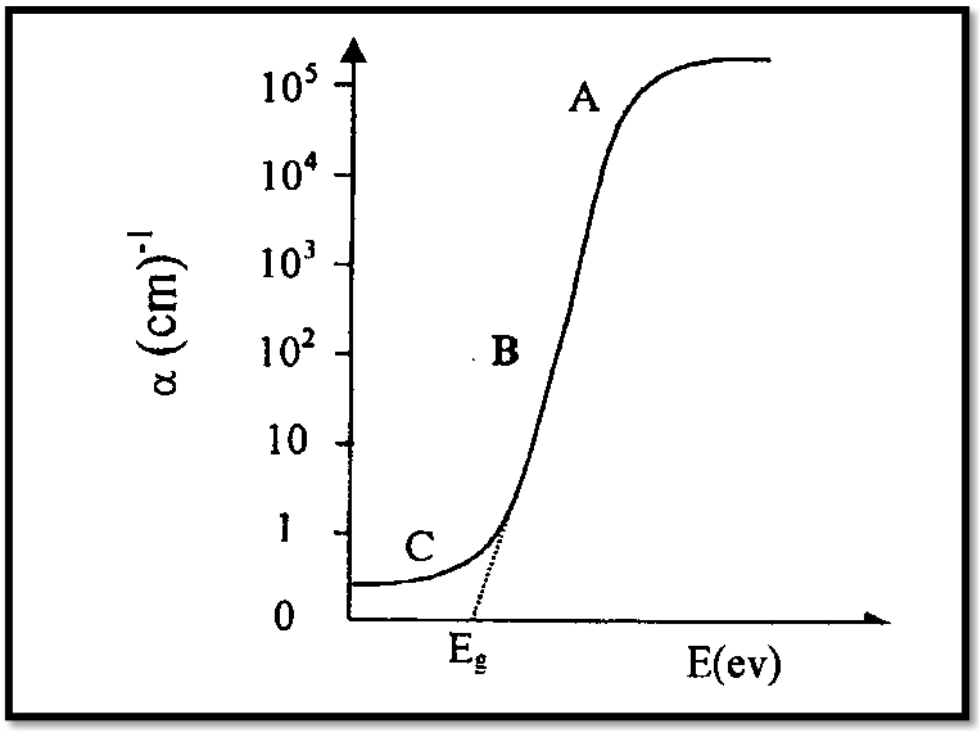

Figure.(2.7): The variation of absorption edge with absorption regions [91]**.**

2.5.4.2 The electronic transitions

There are two basic forms of electronic transition: direct and indirect transition.

1. Direct transitions

This kind of transitions occurs in semi-conductors, where the bottom of the conduction is precisely above the top of the valance band, thus implying that they share similar wave vector values i.e. ($\Delta K= 0$). In such a case, the absorption would occur at ($h\upsilon = E_g^{opt}$.). Therefore, the phonons do not take part in direct transition since the phonon's wave vector (K) is much greater than that of the photons. This transition type requires the laws of conservation in momentum and energy. The direct photon transition to the energy of the minimum gap reaches no satisfaction of the demand for conserving the wave vector, as the photon wave vectors could be neglected in the given energy range [92]. There are two kinds of direct transitions[93].

a. Direct allowed transition

This transition occurs from the top points in the (V.B.) and the bottom point in the (C.B.), as shown in Figure (2.8).

b. Direct forbidden transitions

This transition occurs from near top points of (V.B.) and the bottom points of (C.B.).

The absorption coefficient for this type of transition is equal to [94]:

$$\alpha h\nu = B\,(h\nu - E_g^{opt.})^n \qquad (2.21)$$

Where E_g is the energy gap of direct transition.

B: the constant depended on the type of material

n: the exponential constant, its value depended on type of transition.

n =1/2 for the allowed direct transition.

n =3/2 for the forbidden direct transition.

2. Indirect transitions

In these transitions type, the bottom of (C.B.) is not over the top of (V.B.), in curve (E-K). The electron transits from (V.B.) to (C.B.) is not perpendicularly when the value of the electron's wave vector before and after the transition is not equal ($\Delta K \neq 0$), this transition type occurs with the help of a particle named Phonon. For conservation of the energy and momentum law. Indirect transitions are classified into two types [93], they are:

a. Allowed indirect transitions:

This type of transition occurs in a different region of K-space that is the electrons transmitted between the V.B. top and the C.B. bottom, as exposed in Figure (2.8).

b. Forbidden indirect transitions:

Forbidden indirect transitions are displayed between the nearest points in the top and the bottom of the valance and conductive bands respectively.

The equation (2.22) giving the transition absorption coefficient and the phonon absorption [95]:

$$\alpha h\upsilon = B(h\upsilon - E_g{}^{opt} \pm E_{ph})^n \qquad (2.22)$$

E_{ph} is the phonon energy, where the sing (-) applied when phonon absorption, whereas the sing (+), used when phonon emission. The exponential constant is represented as r in the equation, in which its value is determined by the transition n=2 and n=3 for the allowed indirect, and forbidden indirect transitions, respectively.

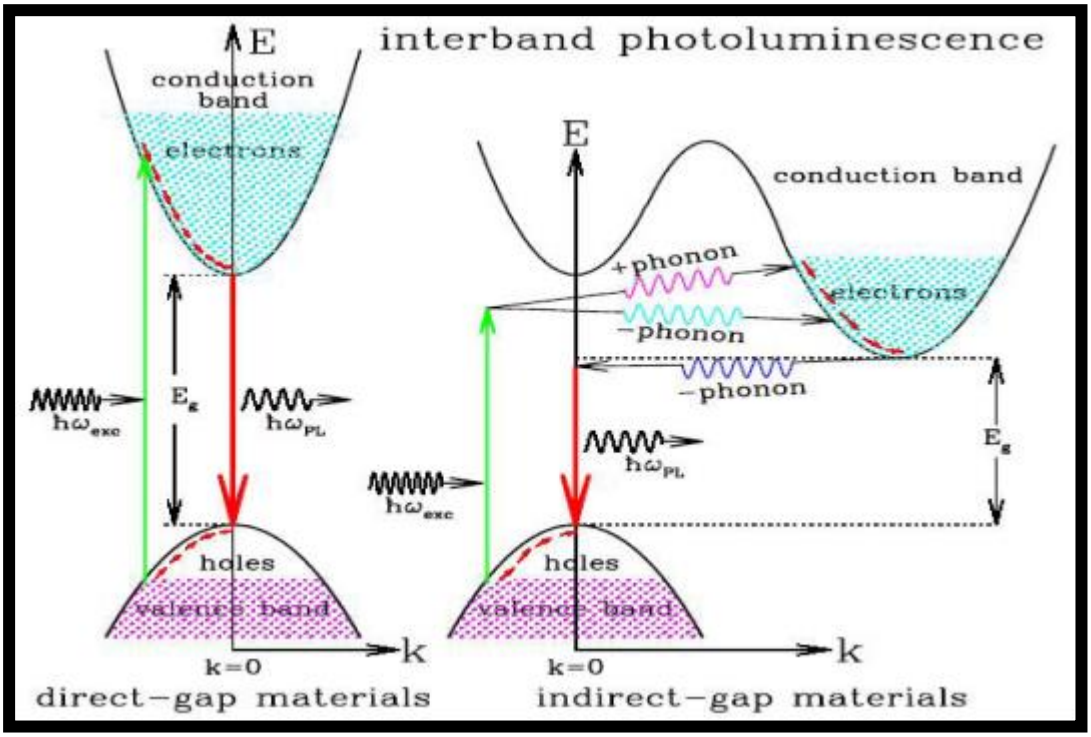

Fig. (2.8): The electronic transition types (a) Allowed direct transition (b) Forbidden direct transition,(c)Allowed indirect transition and (d) Forbidden indirect transition[95].

2.6 The A.C Electrical Conductivity

A.C conductivity affects the frequency of the electrical field [96]. Dielectric spectroscopy is based on the calculation of current and voltage phases and the amplitude A.C system. It is commonly used for the study of dielectric properties of polymers e.g. (ε', tanδ) [97]. The electrical conductivity of isolation

polymer materials can be improved through adding certain conductive fillers [98]. The dielectric constant represents the ratio of the capacitance of the condenser that contains an insulator material between its conductive plates, to the capacity of the same size but with vacuum between its plates. Its value varies from material to material based on the amount of polarization that occurs in the material [99].

When an alternating potential $V = V_m e^{i\omega t}$ is applied through a capacitor (C) loaded with an insulator, the current going through the capacitor will precede the potential by π/2[100].

$$I = j\omega c v_m \qquad (2.23)$$

Where (ω) is the applied angular frequency of the filed (ω=2πf), (j) refers to the number of imaginary and is equal to $\sqrt{-1}$, (C) is the capacitance of a capacitor, and (V_m) is the highest voltage. The angle between electric current and voltage is less than π/2, as seen in figure (2.9). The sum of the conduction current (I_p) is assumed to be electric current. This is in the same phase with voltage, whereas the capacitates current (I_q) is with the phase variation (π/2). The current can be obtained through the equation below [100]:

$$I = I_P + jI_q \qquad (2.24)$$

The capacitance of a condenser consisting of two parallel plates can be defined through the following equation [101]:

$$C = \frac{A_r}{d}\varepsilon \qquad (2.25)$$

where A_r is the area, and (d) is the thickness.

The dielectric constant is then viewed as a complex quantity (ε). The difference of the real and imaginary components of the complex dielectric constant is defined as follows [102]:

$$\varepsilon = \varepsilon' - i\,\varepsilon'' \qquad (2.26)$$

where (ε") is the dielectric loss which given by the equation [102]:

$$\varepsilon'' = 1 / \omega R_P C_o \qquad (2.27)$$

where R_P is the resistance parallel. The dielectric constant is obtained from the relation [102]:

$$\varepsilon' = C_P / C_o \qquad (2.28)$$

where C_P is the capacitance in the presence of an insulator and C_o is the capacitance in the presence of a vacuum. The dissipated power in the insulator is represented by the existence of alternating potential as a function of the alternating conductivity, as explained in the following equation [99]:

$$\sigma_{A.C}=2\pi f \acute{\varepsilon}\, d\, \varepsilon_o \qquad (2.29)$$

where $\sigma_{A.C}$ represents the measurement of the temperature produced by the insulation material arising from the vibration of the charges or rotation of the dipoles in their positions, f is the frequency, έ is the dielectric constant, ε_o is the permittivity of the free space and d is the sample thickness. This is the result of the alternation of the field [103].

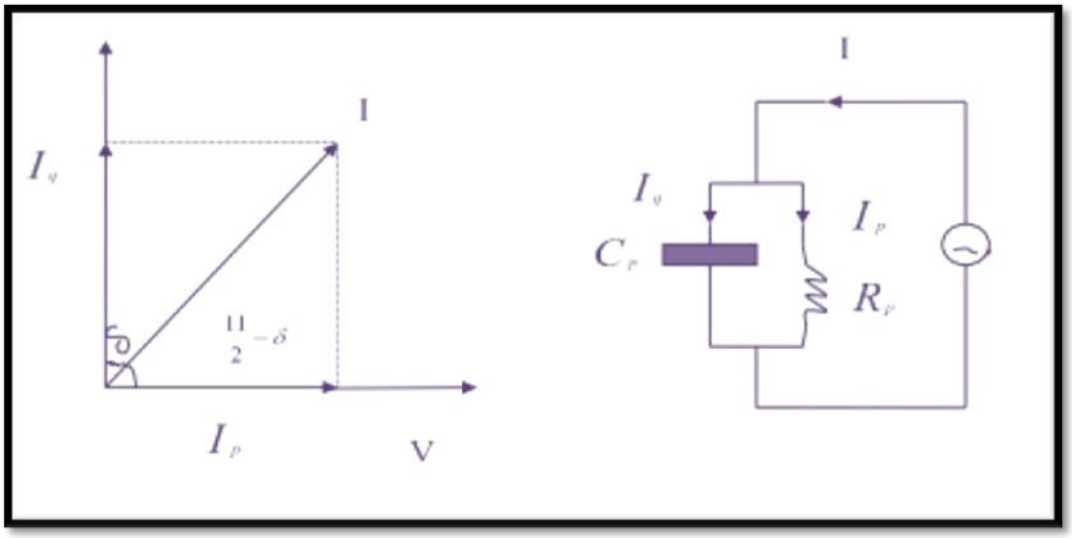

Fig.(2.9): The circuit equivalent to non-ideal capacitor [103].

2.7 Antibacterial Activity

Infectious disease development in general poses a severe threat to public health worldwide, particularly with the emergence of antibiotic-resistant bacterial species. As a result, there is an incentive to develop new bactericidal [104]. In general, both gram-negative and gram-positive bacterial strains are considered to be a significant public health threat. Antibiotics are used to control infections caused by both community and hospital environments pathogens for many years [104,105] .

Recent advancements in the domain of nano biotechnology, especially the ability to prepare metal oxide nanoparticles with precise size and shape specifications, are anticipated to result in the development of new antibacterial agents. The size of nanoparticles has a major effect on their functional properties. As a result of their unique chemical, physical, and biological characteristics, nanoparticles have garnered considerable attention in various fields, including medicine [106 -108] .

Due to the widespread use of the antibiotics in prevention and treatment of bacterial infections, resistant microorganisms have developed, necessitating

the creation of new active molecules against bacteria. The size of nanoparticles is approximately the same as that of biological molecules and less than that of human cells. Nano treatment strategies could be used to improve medical treatments [109-111].

2.7.1 Bacterial Strain

1. *Staphylococcus aureus (S. aureus)*

Staphylococci are gram-positive bacteria that have individual cocci that separate in several planes to form grape-like clusters. They are often non-motile and do not produce spores [112]. S. aureus are facultative anaerobes that can grow by aerobic respiration or fermentation and can grow at temperatures ranging from 15 to 45 °C and at NaCl concentrations as high as 15%. The hard protective layer, (microbial surface components recognizing adhesive matrix molecules) produced on the surface of S. aureus boosted antibiotic resistance and boosted the bacteria's adherence to host proteins such as fibronectin and fibrinogen. *S. aureus* is considered to be a major pathogen that colonizes and infects both hospitalized patients with decreased immunity, and healthy immuno-competent people in the community [113].

2. *Escherichia coli (E. coli)*

It’s one of the most popular gram-negative bacteria. E. coli is considered as a facultative anaerobic bacterium that can live in the presence or absence of oxygen. It characterized by a non-spore forming, motile, rode- shaped bacteria that ferments lactose [114]. *E. coli* is one of the most common inhabitants of the human intestinal tract, its optimal growth occurs at 37°C and the optimum pH growing in a culture at 37°C is 6.0-7.0 also it has a minimum pH level of 4.4 and a maximum level of 9.0 required for growth [115].

CHAPTER Three

Experimental Part

3.1 Introduction

This chapter covers the preparation steps of the sample, as well as a description of the equipment and method used and measuring process such as FTIR, XRD, FESEM, OM, optical spectrometer and AC electrical properties and then measuring the application for antibacterial activity.

3.2 The Utilized Materials

The utilized materials in this study:

3.2.1 Matrix Material

Polymers: there are two types of polymers were used in this work:

- **Polyvinyl alcohol (PVA):** The polymer is used as granular form and could be obtained from (Alpha Chemika, India) with high average molecular weight 160,000 g/mol and high purity (99.98 %).
- **Polyethylene glycol (PEG):** The polymer is used as granular form and could be obtained from (Central Drug House, Ltd, Company, India) with average molecular weight 20,000 g/mol and high purity 99%.

3.2.2 Additive Nanomaterial

1. **Green nickel oxide powder (NiO):** NiO nanoparticles (Sigma Aldrich) with purity 99.8%, (Mol. wt. = 74.69 g/mol) is a white powder that is insoluble in water with a particle size of ≤ 40 nm.
2. **Black nickel oxide powder (Ni_2O_3):** Ni_2O_3 nanoparticles (Sigma Aldrich) with purity 99.8%, (Mol. wt. = 74.69 g/mol) is a white powder that is insoluble in water with a particle size of ≤ 40 nm.

3.3 Purification of (PVA-PEG/NiO) and (PVA-PEG/Ni_2O_3) NCs

Firstly, 0.9 g of commercially available PVA in 50 mL distilled water dissolve with continuous stirring for 2 h. In the first hour, the mixing is without heat, and in the second hour, at a temperature of 70^{o}C, then 0.1g of PEG (after leaving the aqueous solution cooled to 40^{o}C) was added to synthesis the polymer blend. The resulting solution was cast IN clean glasses Petri dish and kept it under air at RT for 240 h for drying process till the solvent gets completely evaporated as shown in Figure (3.1).

PVA-PEG with green NiO and black Ni_2O_3 NPs were fellow individually the same procedure to prepare nanocomposite films as shown in Figure (3.2). The method summarized in Table (3.1) and Table (3.2) respectively. The thickness of the produced films was about (120 ± 4 μm).

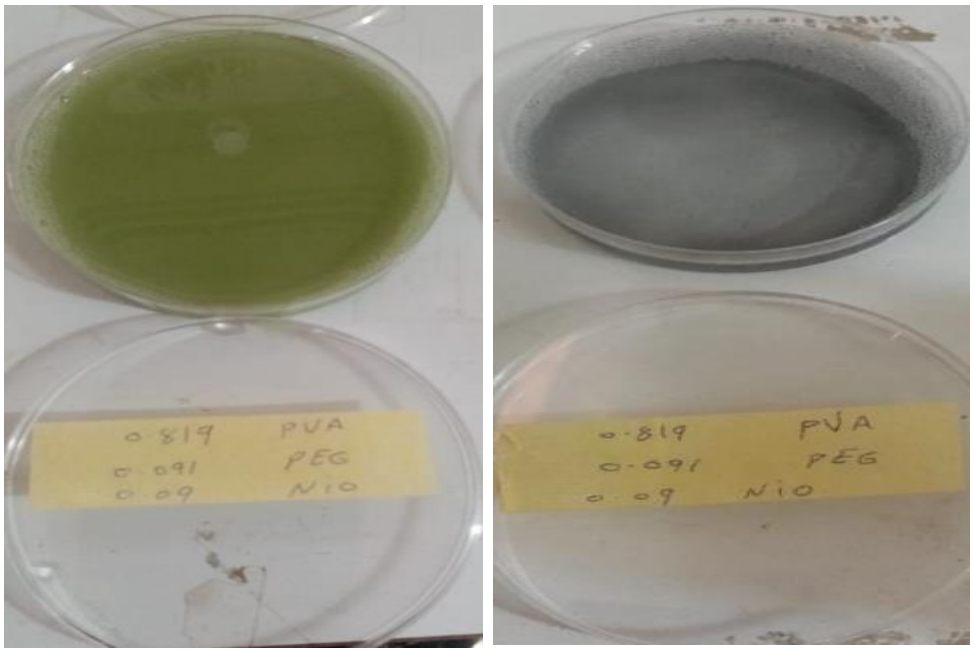

Fig. (3.1): Preparation of (PVA-PEG/NiO) and (PVA-PEG/Ni_2O_3) NCs

Table (3.1): Summarized the purification of PVAs, PEGs with NiO NPs.

Sample	PVA (g)	PEG (g)	Green NiO (g)
PVA-PEG	0.9	0.1	0
3 wt.% NiO	0.873	0.097	0.03
4.5wt.% NiO	0.8595	0.0955	0.045
6 wt.% NiO	0.846	0.094	0.06
7.5 wt.% NiO	0.8325	0.0925	0.075
9 wt.% NiO	0.819	0.091	0.09

Table (3.2): Summarized the purification of PVAs, PEGs with Ni_2O_3 NPs.

Sample	PVA (g)	PEG (g)	Black Ni_2O_3 (g)
PVA-PEG	0.9	0.1	0
3 wt.% Ni_2O_3	0.873	0.097	0.03
4.5wt% Ni_2O_3	0.8595	0.0955	0.045
6 wt.% Ni_2O_3	0.846	0.094	0.06
7.5 wt.% Ni_2O_3	0.8325	0.0925	0.075
9 wt.% Ni_2O_3	0.819	0.091	0.09

3.4 Measurements of Structural Properties for (PVA-PEG/NiO) and (PVA-PEG/Ni_2O_3) Nanocomposites

3.4.1 X-ray diffraction (XRD)

The crystal structure of the prepared nanocomposites has been determined by using (Rigaku-binary (RAW), Ultima Iv, Japan). The following are the specifications for an X-ray diffractometer (XRD):

(Target Cu Kα1 radiation of 1.54060 Å, Current = 30 mA, Voltage = 40 kV, Step = 0.08 deg, scanning speed= 0.25 deg/min., and measurement temperature 25 °C). X-ray diffraction was examined at university of Tehran.

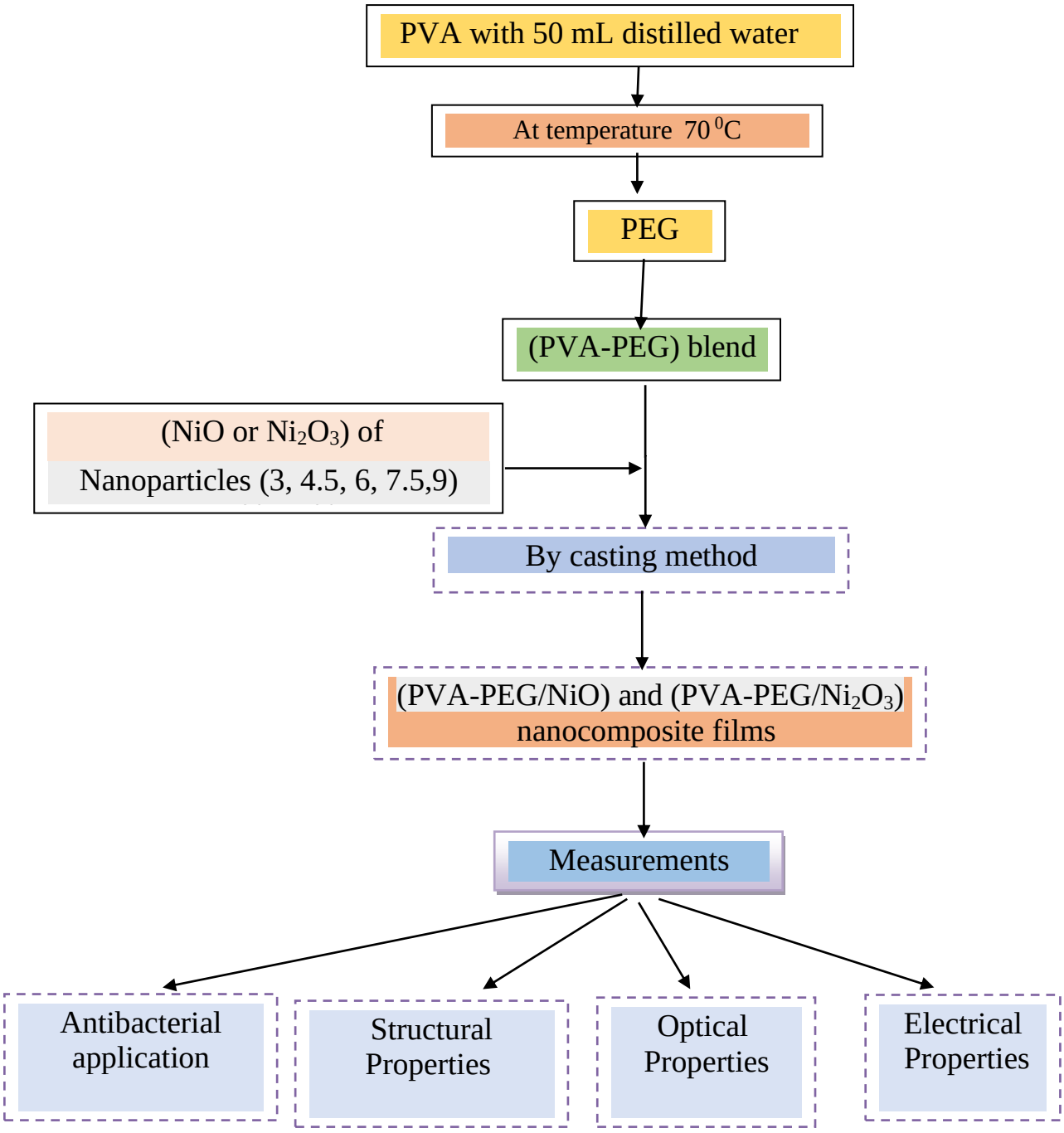

Fig. (3.2): Scheme of experimental part.

3.4.2 Optical microscope (OM)

The change of surface morphology samples of (PVA-PEG/NiO) and (PVA-PEG/Ni_2O_3) nanocomposites is observed applying the optical microscope. This used OM was provided by Olympus (Top View, type Nikon-73346). It is used in the university of Babylon/ Physics department/ college of education for pure sciences.

3.4.3 Field emission scanning electron microscope (FESEM)

The structural properties and nanoparticles size, shape, and morphology of NCs films were analyzed by field emission scanning electron microscope (FESEM) (TESCAN Mira3, Company TESCAN, Czech Republic). The examination was carried out in the laboratory of the university of Tehran, Iran

3.4.4 Spectral characterization for FTIR

FTIR Spectra were captured using an FTIR (Bruker company type vertex -70, German origin). The spectrum of wave numbers considered is (500–4000) cm^{-1}. FTIR was introduced in the physics department/ Education college for pure science/ University of Babylon, Iraq.

3.5 Optical Properties Measurements.

The absorption spectrum of polymer blend (PVA-PEG) and (PVA-PEG/NiO) and (PVA-PEG/Ni_2O_3) nanocomposites have been recorded in the wavelength range (200-1100) nm by using the double beam spectrophotometer (Shimadzu, UV-1800 Å). The absorption spectrum has been recorded at room temperature. A computer program (UV Probe software) was employed to obtain the absorbance, optical constants, transmittance, absorption coefficient, extinction coefficient, dielectric

constant (real and imaginary parts), refractive index and energy gaps. It is implemented at the university of Babylon /college of education for pure sciences/ department of physics.

3.6 Measurement of A.C. Electrical Conductivity

The A.C. electrical conductivity was measured by LCR meter type (HIOKI 3532-50 LCR Hi TESTER (Japan)) in university of Babylon/ college of education for pure sciences/ department of physics. Figure (3.3) demonstrates a diagram for the system of A.C electrical measurement. Only 1cm from each one of the samples were taken and put between two electrodes and by different frequencies from 100Hz-6MHz at room temperature. The capacity (C_P) and dissipated factor (D) have been recorded for all samples. Dielectric constant, dielectric loss and conductivity were calculated from this data.

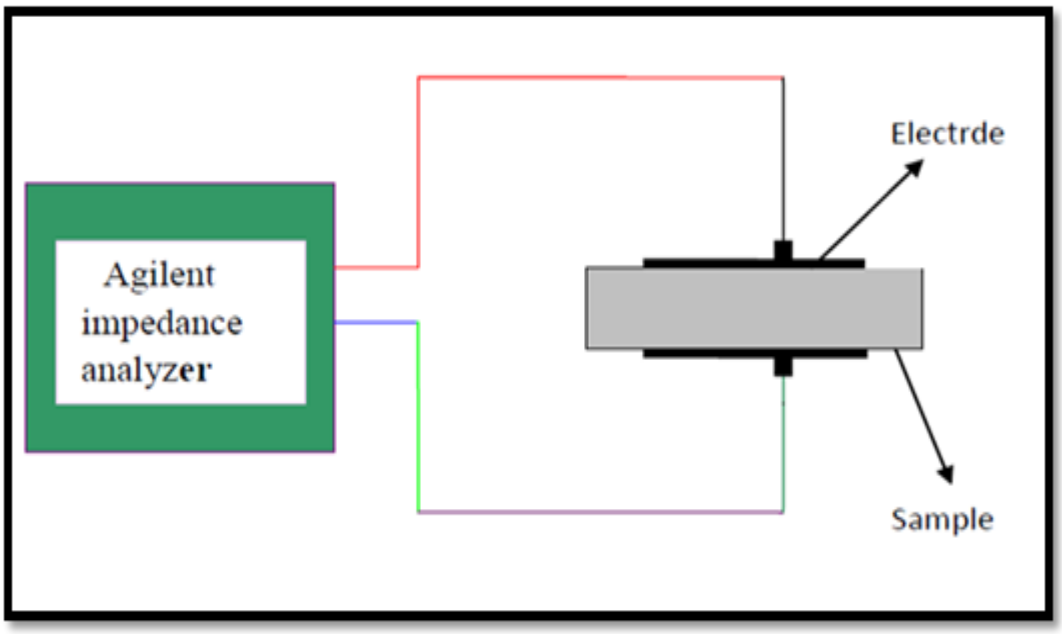

Fig. (3.3): Schematic diagram for A.C Cell.

3.7 Application of (PVA-PEG/NiO) and (PVA-PEG/Ni_2O_3) NCs for antibacterial activity

3.7.1 The preparation of the Bacterium Inoculum

Four- five isolated colonies were selected from an 24h culture and diluted in Mueller Hinton broth to a turbidity like to 0.5 McFarland turbidity standard.

3.7.2 Antibacterial Susceptibility Test for Nanocomposites

The antibacterial susceptibility test of synthesized NCs was made by agar disk diffusion method.

3.7.3 Agar Disk Diffusion Method:

Antibacterial activity of synthesized NCs was performed by Agar disk diffusion method. 20 mL of sterilized Mueller Hinton agar was placed in Petri dishes. After media solidification, 0.1 mL of each bacterial isolates were spread on the surface of media, the petri dishes were left for 5 minutes, then 6 mm diameter disk from each NCs were placed in each petri dish. The polymer blend pure was considered as negative control, the Petri dishes then incubated at 37^{o}C for 24 h. The zones of inhibition were measured and expressed as millimeter in diameter, the experiment was performed in triplicate.

CHAPTER Four

Results and Discussion

4.1 Introduction

This chapter includes the results and discussion of structural, morphological, optical measurements, (A.C) electrical properties and antibacterial application for PVA-PEG polymer blend (PVA-PEG/NiO) and (PVA-PEG/Ni_2O_3) NCs.

4.2 The Structural Properties of (PVA-PEG/NiO) and (PVA-PEG/Ni_2O_3) Nanocomposites

4.2.1 X-ray diffraction

The crystallographic structure of PVA-PEG polymer blend and the NC films based on different ratios (3, 4.5, 6, 7.5 and 9) wt.% of green NiO and black Ni_2O_3NPs were determined by XRD patterns recorded between 10^o to 80^o, as shown in Figures (4.1) and (4.2). This result is agree with researchers [116] . In this work, the film polymeric blend is displayed to have a semicrystalline nature whose peak observed at $2\theta=19.42°$ accordance with the plane (101) reflection and it deviates to 19.91° with the addition of NiO and Ni_2O_3 NPs respectively. The broad of peaks a sign the interaction happening between PVA and PEG. The XRD pattern of the synthesized films based on NiO NPs displayed sharp and intense diffraction peaks that perfectly matched well with the standard JCPDS file No: 4-0835. It shows the presence of readily indexed (111), (200), (220), (311), and (222) crystal planes. It can be noticed that no impurity peak was observed in XRD spectra and the characteristics predominant peak at 43.5◦ is attributed to (200) reflection, which are indexed to plane of face centered cubic (FCC) NiO phase. Its structure has space group Fm3m [225] and parameter a= 4.176 Å [117]. The XRD pattern of the synthesized films based on Ni_2O_3 NPs shows the presence of readily indexed (111), (200), (220), and (311) crystal planes affiliated to NiO phase on the top surface of the films, which may be attributed to the effect of PEG polymer as a reducing agent, as well as this transformation may be attributed to the heat

of reaction, and also the appearance of $(002)^*$, $(200)^*$, $(004)^*$ with less intensity affiliated to Ni_2O_3 (an unstable oxide type [118], which are indexed to plane of hexagonal phase , and its structure has space group P63mc and parameters a= 4.61 Å and c=5.61 Å`. This matches well with the standard JCPDS file No: 14-0481, and lookup values [119]. The position of the diffraction patterns was slightly changing in all prepared samples, while the intensity gradual increase by increasing the concentration of NiO and Ni_2O_3 NPs inside the polymer matrix when compared to blend (PVA-PEG) film. The incorporated of both nano additives into blended polymer act a change in the crystallinity from what it is in the initial state.

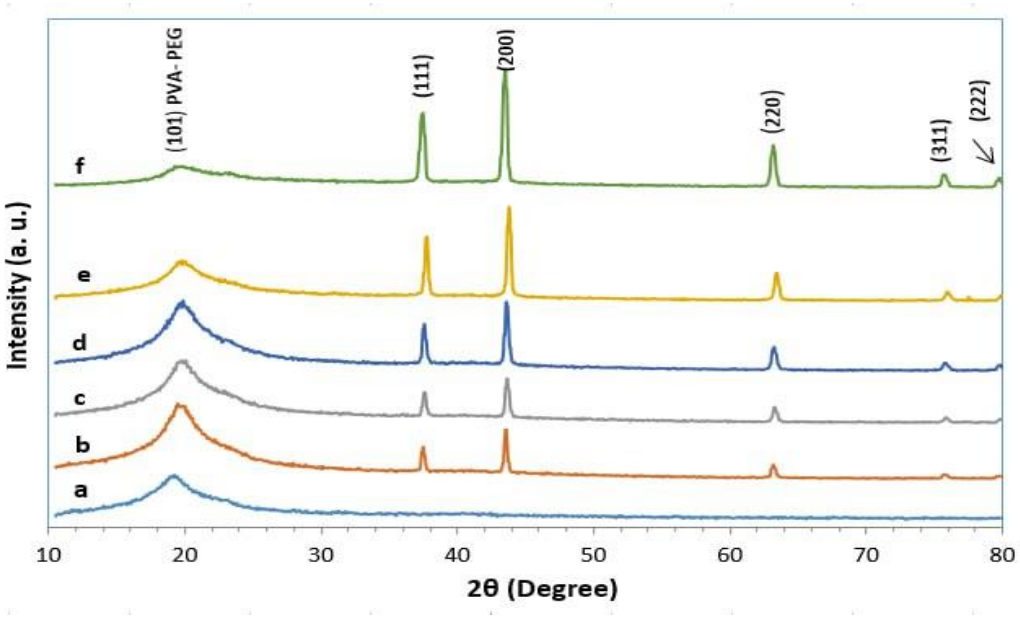

Fig. (4.1): XRD patterns of blended polymer PVA-PEG (a) with 3wt.% (b), 4.5wt.% (c), 6wt.% (d), 7.5wt.% (e), and 9wt.% (f) of NiO NPs.

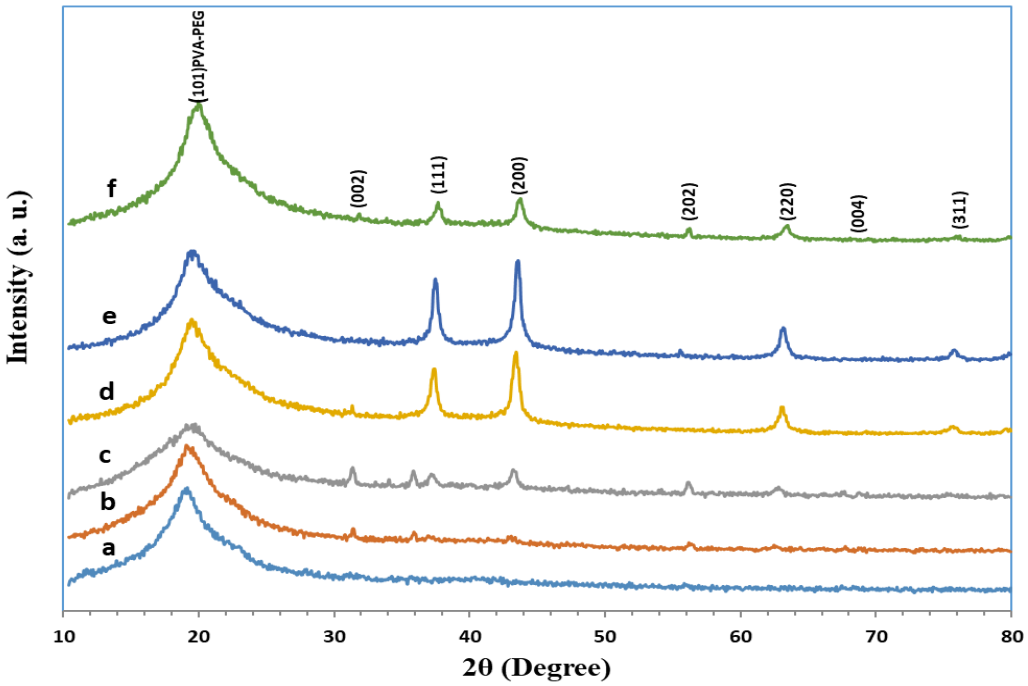

Fig. (4.2): XRD patterns of blended polymer PVA-PEG (a) with 3wt.% (b) , 4.5wt.% (c) , 6wt.% (d) , 7.5wt.% (e) , and 9wt.% (f) of Ni_2O_3 NPs.

4.2.2 Optical and field emission scanning electron microscopy

The surface of blended polymer PVA-PEG and the NC films based on different ratios (3, 4.5, 6, 7.5 and 9) wt.% of green NiO and black Ni_2O_3NPs at Zoom in (10x) were seen in Figures (4.3) and (4.4), respectively. It is clear from the surface images of both cases the NiO nanoparticles exhibited uniform density of grain distribution at surface morphology more homogeneity than the cases of Ni_2O_3 nanoparticles, and the NPs are appearing many aggregates randomly distributed on the films surface at the lower concentration, and when increasing the concentration of additives NPs its form a network of paths within the polymeric blend.

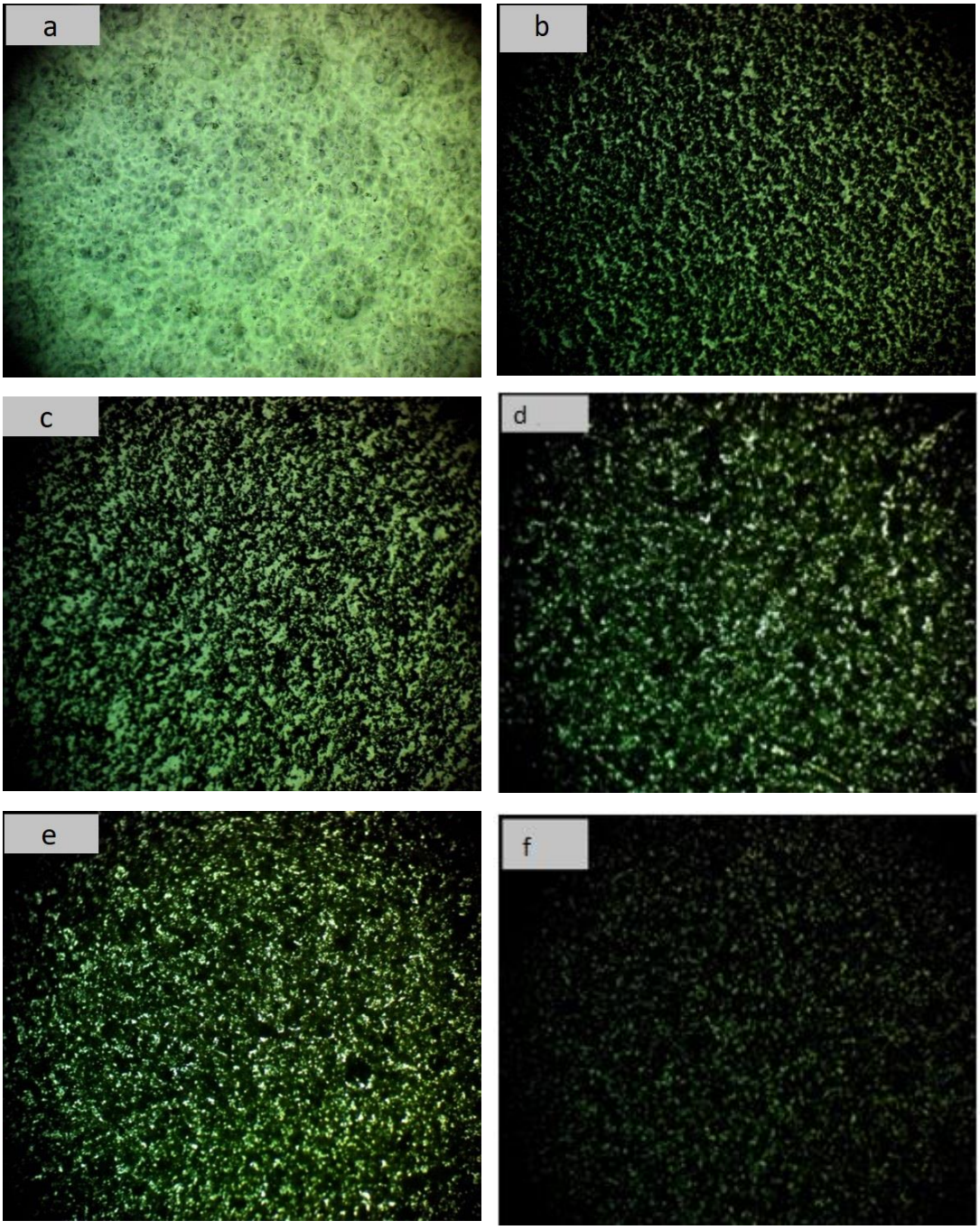

Fig. (4.3): Photomicrographs (10X) of blended polymer PVA-PEG (a) with 3wt.% (b), 4.5wt.% (c), 6wt.% (d), 7.5wt.% (e), and 9wt.% (f) of NiO NPs.

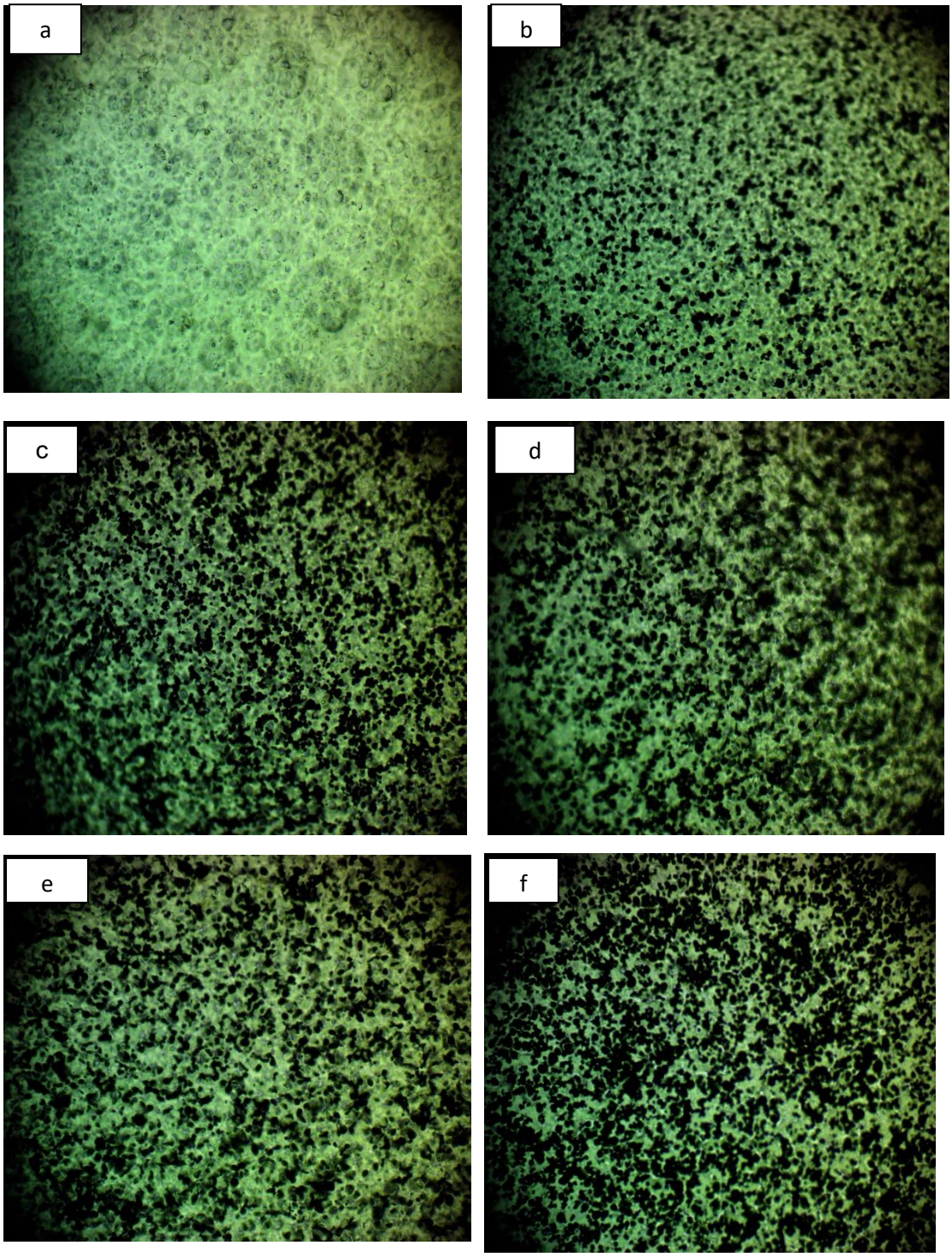

Fig. (4.4): Photomicrographs (10X) of blended polymer PVA-PEG (a) with 3wt.% (b) , 4.5wt.% (c) , 6wt.% (d) , 7.5wt.% (e) , and 9wt.% (f) of Ni_2O_3 NPs.

FESEM analysis was carried out on blended polymer and its NC films based on (3, 4.5, 6, 7.5 and 9) wt.% of NiO and Ni_2O_3 NPs to show the surface morphologies of prepared films, as seen in Figures (4.5) and (4.6) respectively. The images were taken at a magnification of 20.00 kx. The films showed many aggregates or chunks randomly distributed of NPs on the films surface. The results show an increase in the number of aggregations on the surface in accordance with increasing the amount of Ni_2O_3.

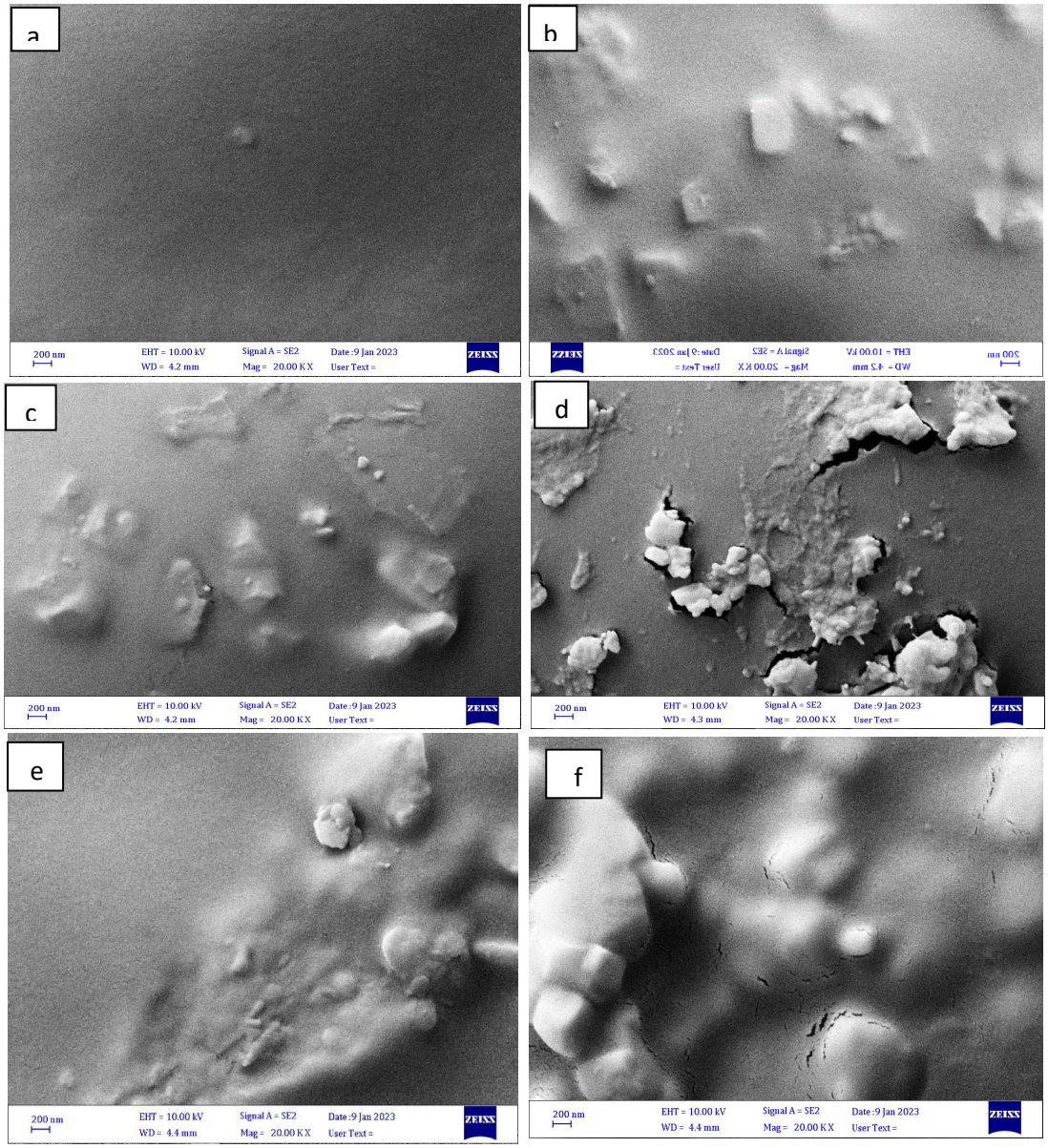

Fig. (4.5): FESEM of blended polymer (a) pure PVA-PEG, (b) 3wt.% , (c) 4.5wt.%, (d) 6wt.% (e) 7.5wt.% , and (f) 9wt.% of NiO NPs.

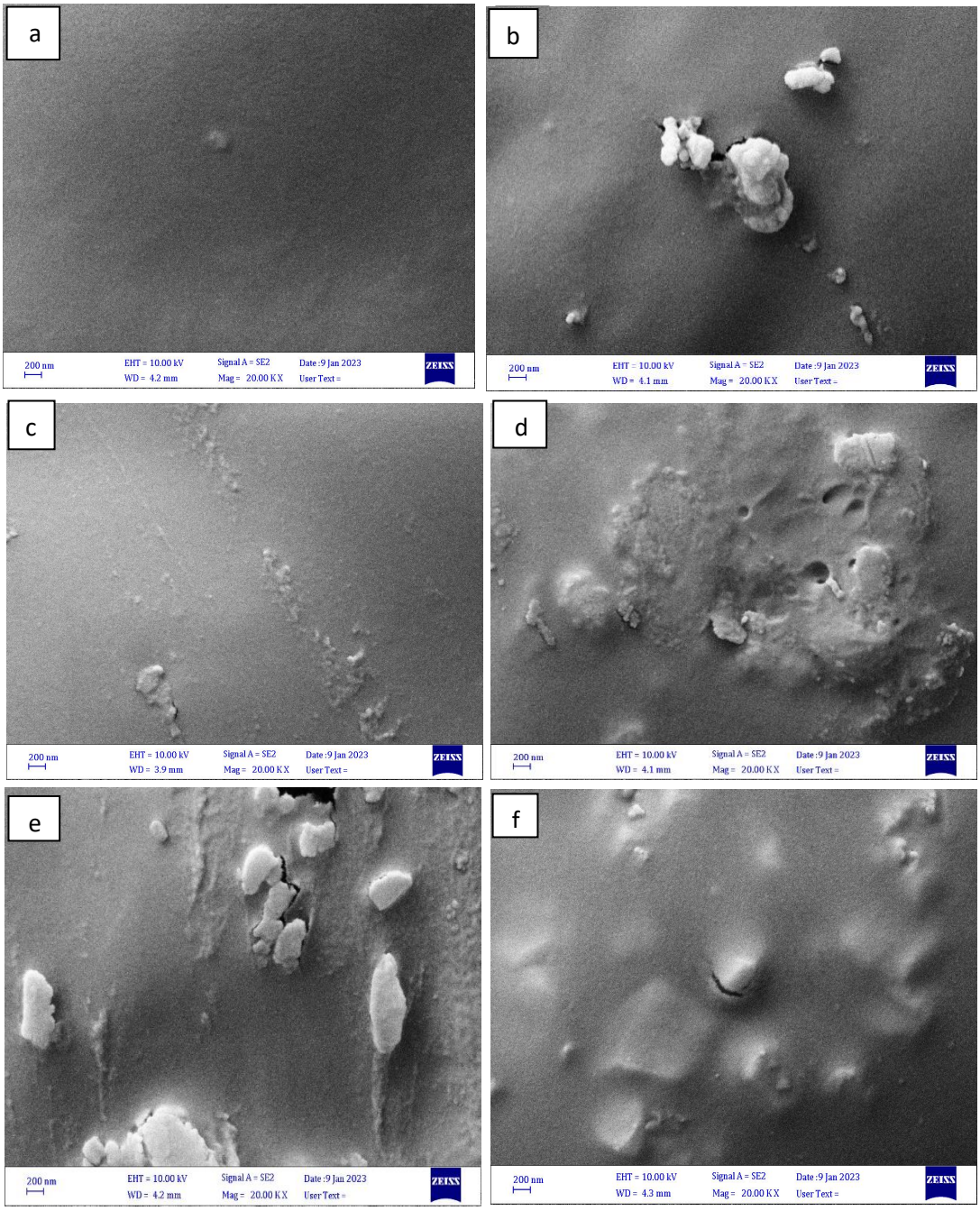

Fig. (4.6): FESEM of blended polymer (a) pure PVA-PEG, (b) 3wt.% , (c) 4.5wt.%, (d) 6wt.% (e) 7.5wt.% , and (f) 9wt.% of Ni_2O_3 NPs.

4.2.3 Fourier transform infrared radiation (FTIR) of (PVA-PEG/NiO) and (PVA-PEG/Ni_2O_3) NCs

FTIR spectroscopy examination to identify intermolecular connections between the polymer blend and the nanoparticles. The FTIR spectra of PVA-PEG blend and its NC films based on green NiO and black Ni_2O_3NPs as shown in the Figures (4.7) and (4.8). Its exhibit eight major absorption peaks. The broad peak at 3278.90 cm^{-1} assigned to the stretching vibration of the alcohol group (OH) in the polymer matrix chain [120]. The two intense peaks at 2908.33, and 2360.00 cm^{-1} corresponds to the Methyl C-H_3 asymmetric and strong O=C=O stretching vibration [121]. Additionally, the peak at 1716.51 cm^{-1} corresponds to the C=O stretching band, which is actually attributed to carboxylic acid, aliphatic ketone, aldehyde, or quinine groups [122]. The peak at 1340.55 cm^{-1} is attributed to the deformation stretching vibration of the strong N-O . The peak at 1239.16 cm^{-1} is attributed to the deformation stretching vibration of the C-N link [121]. Moreover, the peaks observed at 1085.02, and 830.52 cm^{-1} could be attributed to the twisting vibration of strong C-O-C and medium C=C bending vibrations [123]. As was mentioned, the intensity of these bands decreased and slightly shifted toward higher wavenumbers, which is a sign that hydrogen bonds were formed by the physical contact between the functional groups in the polymer blend and both NiO and Ni_2O_3 NPs. Strong incorporations with Ni^{+2} ions are another potential cause of intensity alterations and broadening of the functional groups in the polymeric matrix's backbone [123] . The peaks for the (PVA-PEG)/NiO and (PVA-PEG)/NiO (Fig.1and2,b-f) are alike to the spectrum of (PVA-PEG), showing this blend polymer make up a big part of the NCs. This can approve the successful synthesis of the (PVA-PEG)/NiO NCs. The figures indicate the bonding nature between (PVA-PEG/NiO) and (PVA-PEG/Ni_2O_3) NPs and polymers .

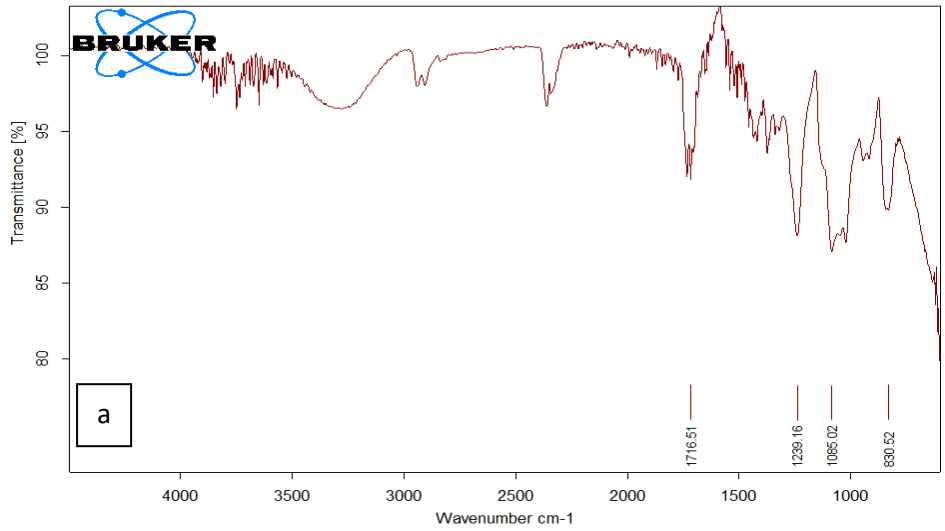

C:\OPUS_7.2.139.1294\MEAS\Sample description.1816	Sample description	Instrument type and / or accessory	01/01/2004

Page 1/1

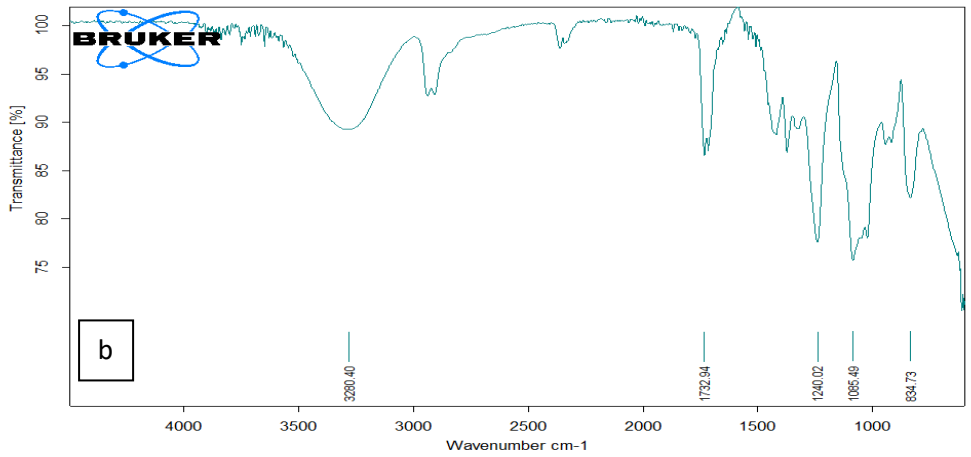

C:\OPUS_7.2.139.1294\MEAS\Sample description.1804	Sample description	Instrument type and / or accessory	01/01/2004

Page 1/1

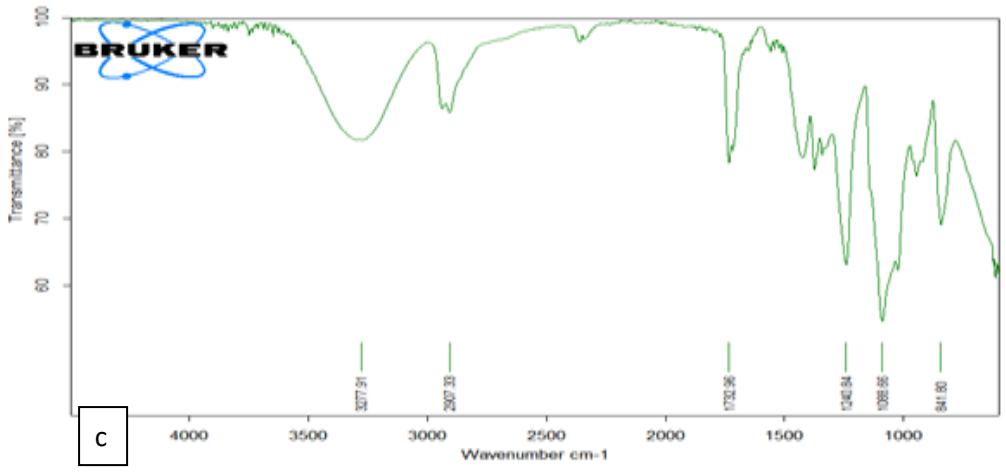

C:\OPUS_7.2.139.1294\MEAS\Sample description.1803	Sample description	Instrument type and / or accessory	01/01/2004

Page 1/1

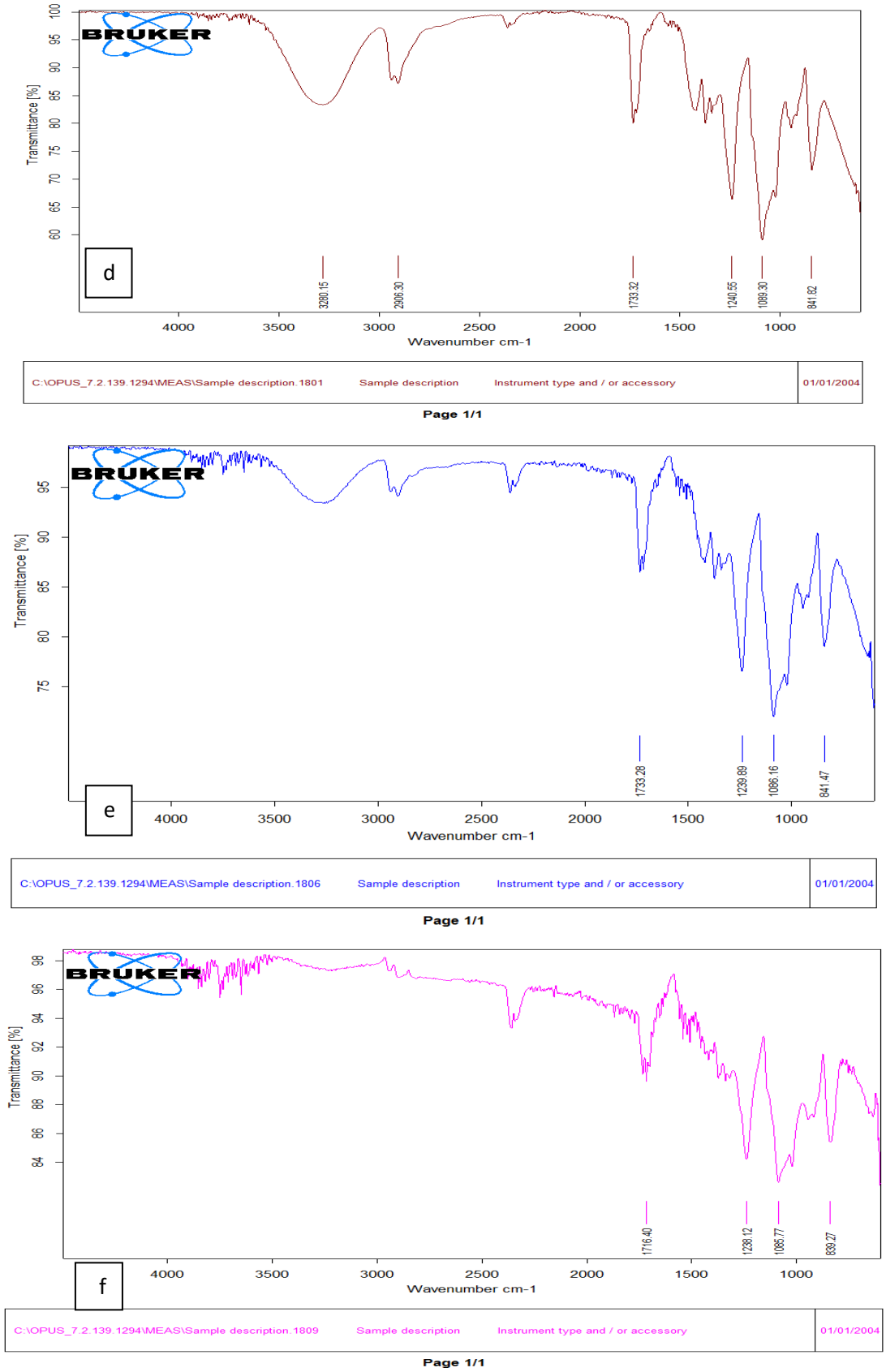

Fig. (4.7): FTIR of blended polymer PVA-PEG (a) with 3wt.% (b), 4.5wt.% (c) , 6wt.% (d) , 7.5wt.% (e) , and 9wt.% (f) of NiO NPs.

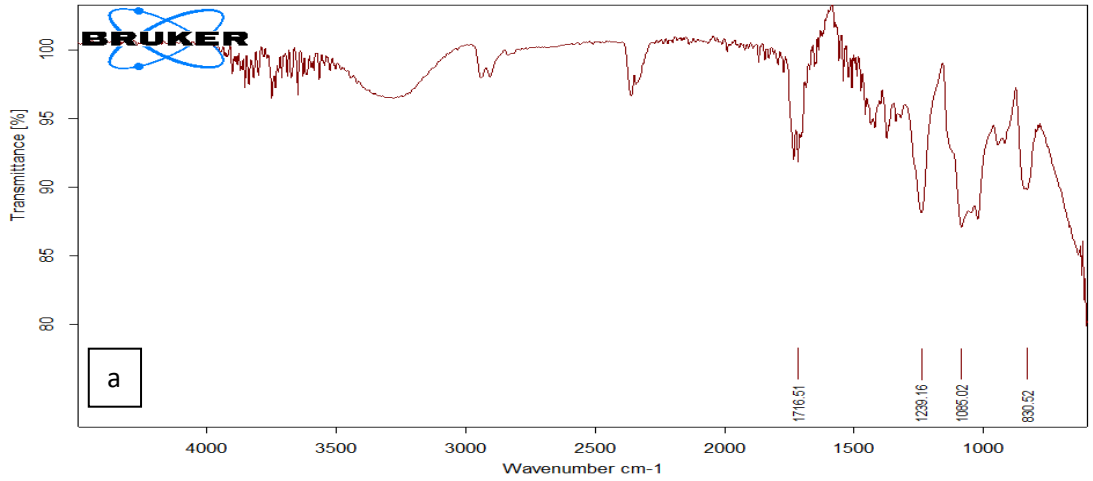

C:\OPUS_7.2.139.1294\MEAS\Sample description.1816	Sample description	Instrument type and / or accessory	01/01/2004

Page 1/1

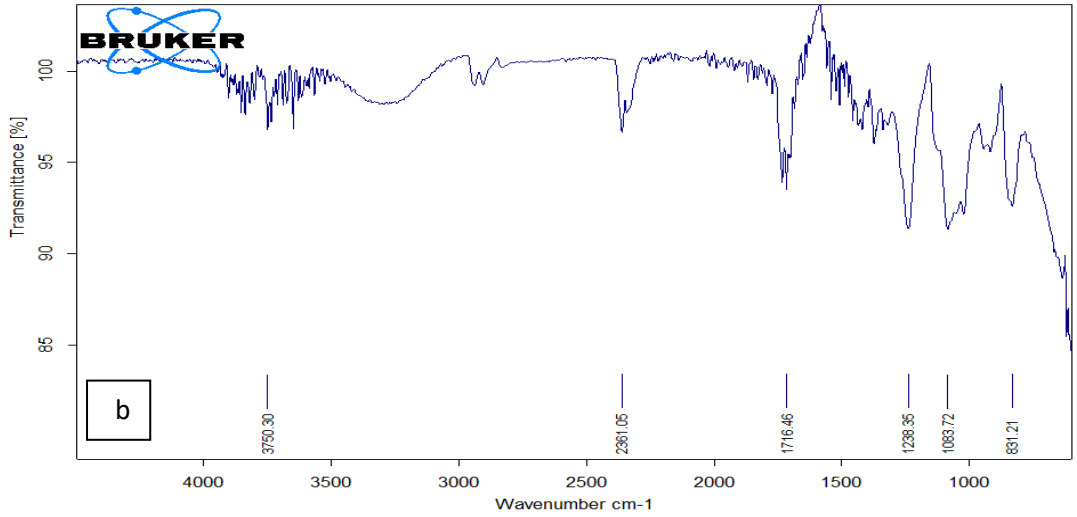

C:\OPUS_7.2.139.1294\MEAS\Sample description.1815	Sample description	Instrument type and / or accessory	01/01/2004

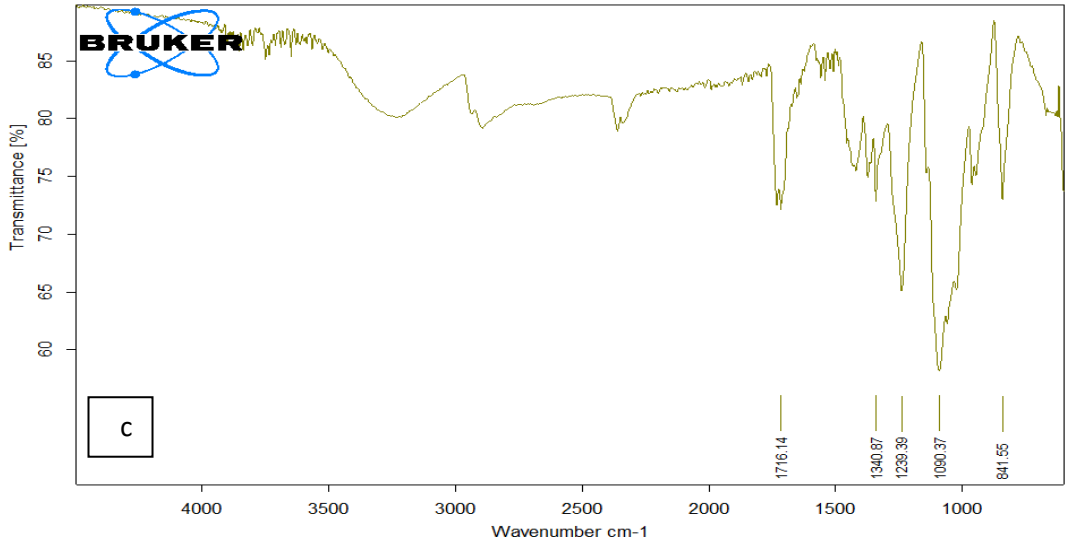

C:\OPUS_7.2.139.1294\MEAS\Sample description.1813	Sample description	Instrument type and / or accessory	01/01/2004

Page 1/1

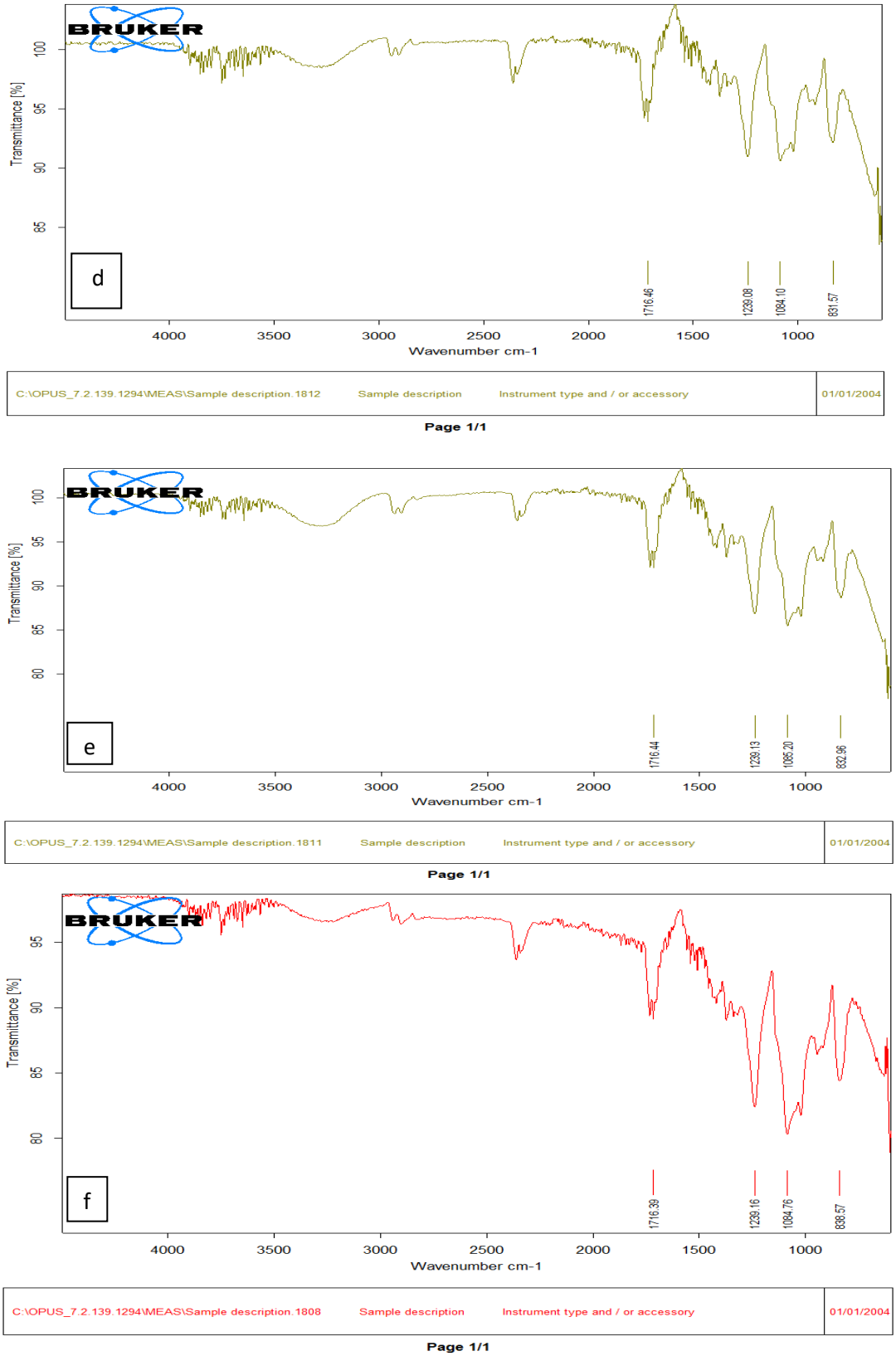

Fig. (4.8): FTIR of blended polymer PVA-PEG (a) with 3wt.% (b) , 4.5wt.% (c) , 6wt.% (d) , 7.5wt.% (e) , and 9wt.% (f) of Ni_2O_3 NPs.

4.3 The Optical Properties of (PVA-PEG/NiO) and (PVA-PEG/ Ni_2O_3) NCs

The effect of adding the NiO and Ni_2O_3 NPs on the optical properties of PVA - PEG considered as a main purpose of this study. The research covers the recording of the spectrum of absorbance for the PVA-PEG blend and (PVA-PEG/NiO), (PVA-PEG/Ni_2O_3) films at RT and calculating the transmittance, absorption coefficient, extinction coefficient, real and imaginary dielectric constant and optical conductivity as well as identifying the types of electronic transitions and calculating energy gaps.

4.3.1 The absorbance and transmittance

At room temperature, the absorbance spectra of blended polymer (PVA-PEG) and its nanocomposites (NCs) with (3, 4.5, 6, 7.5, and 9) wt.% of NiO and Ni_2O_3 films for the wavelength (200-1100) nm are shown in Figures (4.9) and (4.10), respectively. Regarding all tasters, in the poorer wavelength range (UV region), where NC films absorbs a lot of light, and then drops as the wavelength increases in the Vis and NIR regions. The absorption spectra for all samples show a minor drop in the visible and NIR regions and tend to steady at high wavelengths (400-1100) nm. This can be attributable to the incident photons' low energy, which prevents any interaction with the polymer structure. This implies that photons will transmit and scatter with high probability via polymer sheets.

The results show that the absorbance was increasing with the rising loading ratio of NiO $_{and}$ Ni_2O_3 NPs in the PVA-PEG matrix. In all NC films, the shift of absorption maxima towards greater wavelengths in the absorption edge near the lower band gap indicates that the NiO and Ni_2O_3 grains have irregular shapes and different sizes distributed on the films surface. The strong absorption peak at 280 nm for the (PVA-PEG/Ni_2O_3) films was due to the band gap-excitation of electrons in Ni_2O_3 NPs [124]. The results refer to can be candidate the prepared 9wt.% NC films.

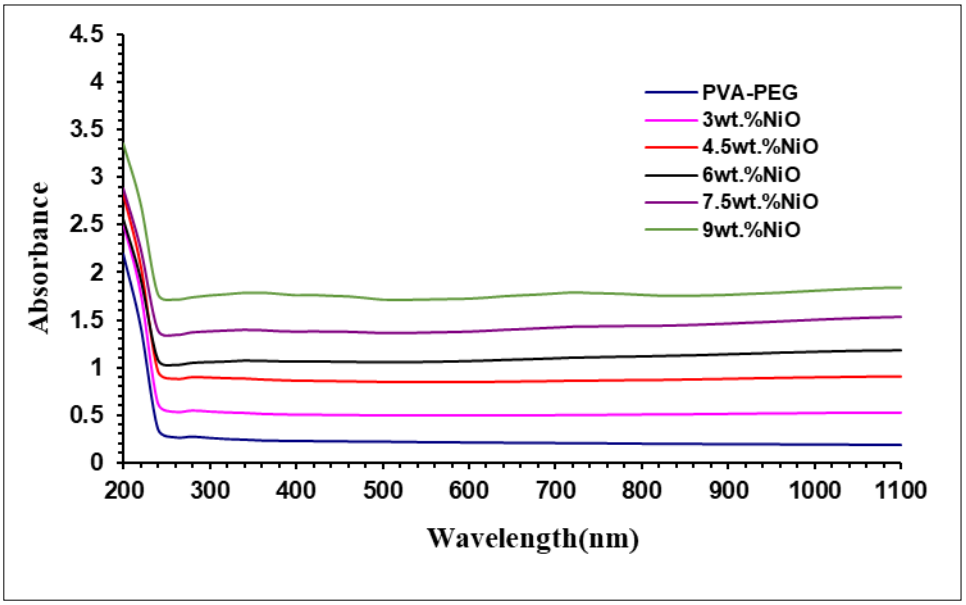

Fig. (4.9): Variation of absorbance for (PVA-PEG/NiO) NCs with wavelength.

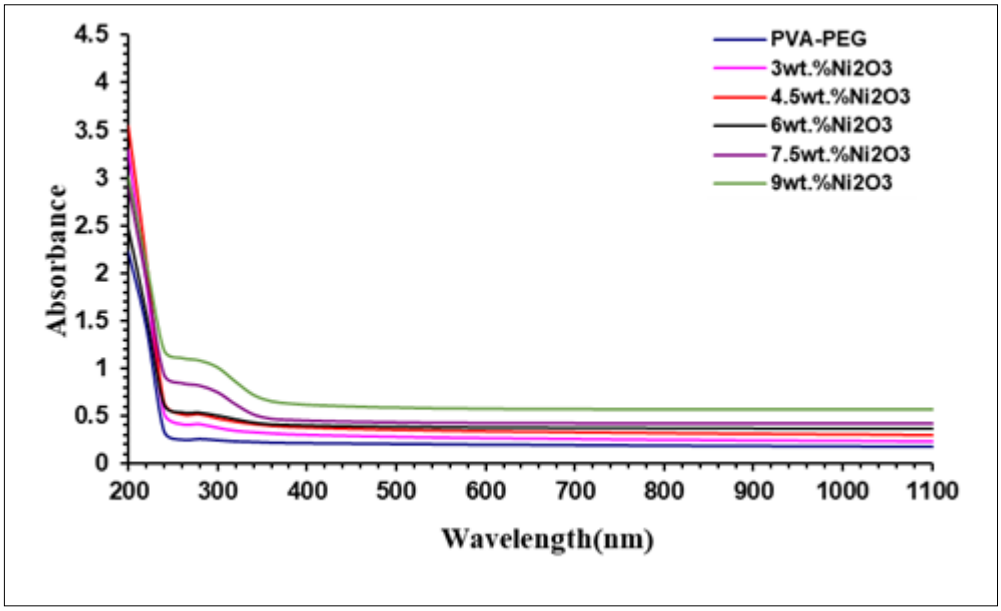

Fig. (4.10): Variation of absorbance for (PVA-PEG/Ni_2O_3) NCs with wavelength.

The transmittance spectra of blended polymer and its NCs with (3, 4.5, 6, 7.5, and 9) wt.% of NiO and Ni_2O_3 films are shown in Figures (4.11) and (4.12), respectively. Above 300 nm, the transmittance curves of all samples show a tendency towards saturation, and the highest rated average transmittance of the blended polymer is ~ 88% in the Vis and NIR areas of spectrum, but it decreases almost gradually with increasing the weight

reaching to 66% at 9 wt.% Ni_2O_3. This feature was ascribed to the film surface morphology and the absorption. Ni_2O_3 contribution exhibited absorbance peaks at ~ 280 nm, which could appear through the charge transfer from the ligand to the metal. Also, the decrease in the transmittance of the prepared films in UV region comes from increasing the nanoparticle concentrations that makes it suitable for different applications, as packaging for storage drugs regardless of cost or for solar cell applications[125].

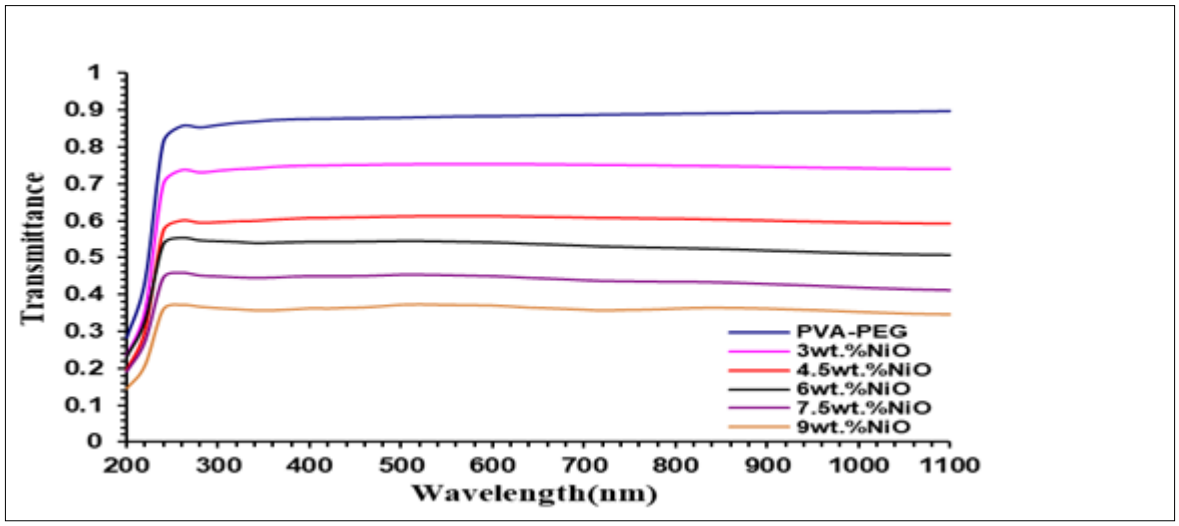

Fig. (4.11): Variation of transmittance for (PVA-PEG/NiO) NCs with wavelength.

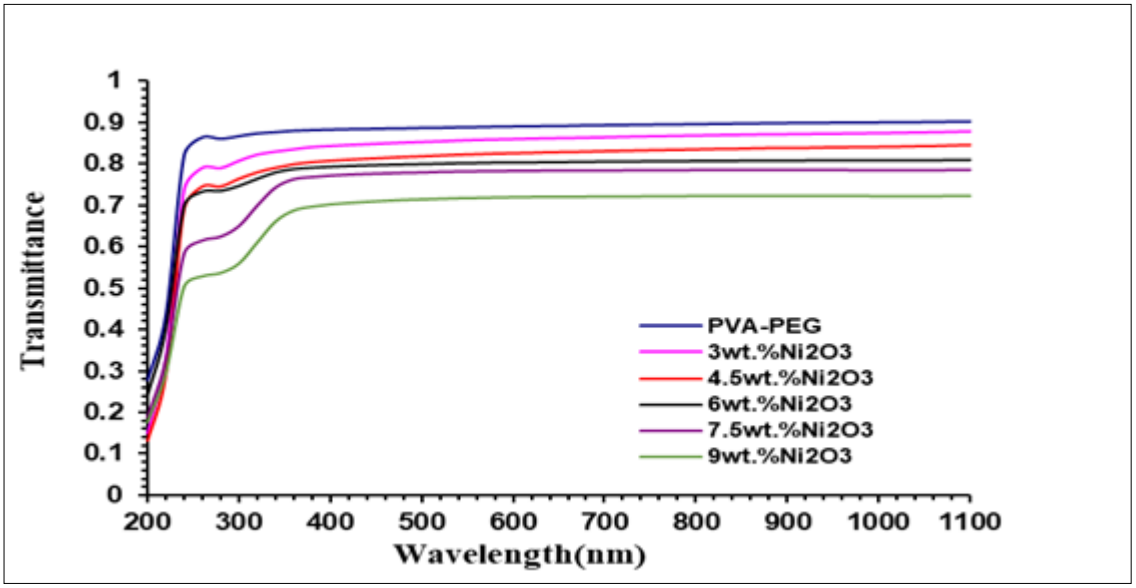

Fig. (4.12): Variation of transmittance for (PVA-PEG/Ni_2O_3) NCs with wavelength.

4.3.2 The absorption coefficient and energy band gap

The absorption coefficient of blended polymer (PVA-PEG) and the NC films with (3, 4.5, 6, 7.5, and 9) wt.% of NiO and Ni_2O_3 was calculated from relation (220), which are taken into consideration as an inspection tool to ascertain the film's light-intensity attenuation, are shown in Figures (4.13) and (4.14), respectively . On the other hand, depending on the energy of the incident light, this is a sensitive physical way to give us vital information about the sorts of charges transported in a band and around the value of the band gap energy. From such figures it is noted the shift in the absorption edge towards the lower energy with the rising loading ratio of the additives. This result reveals the decline of the optical energy gap as the percentage of the additive increases.

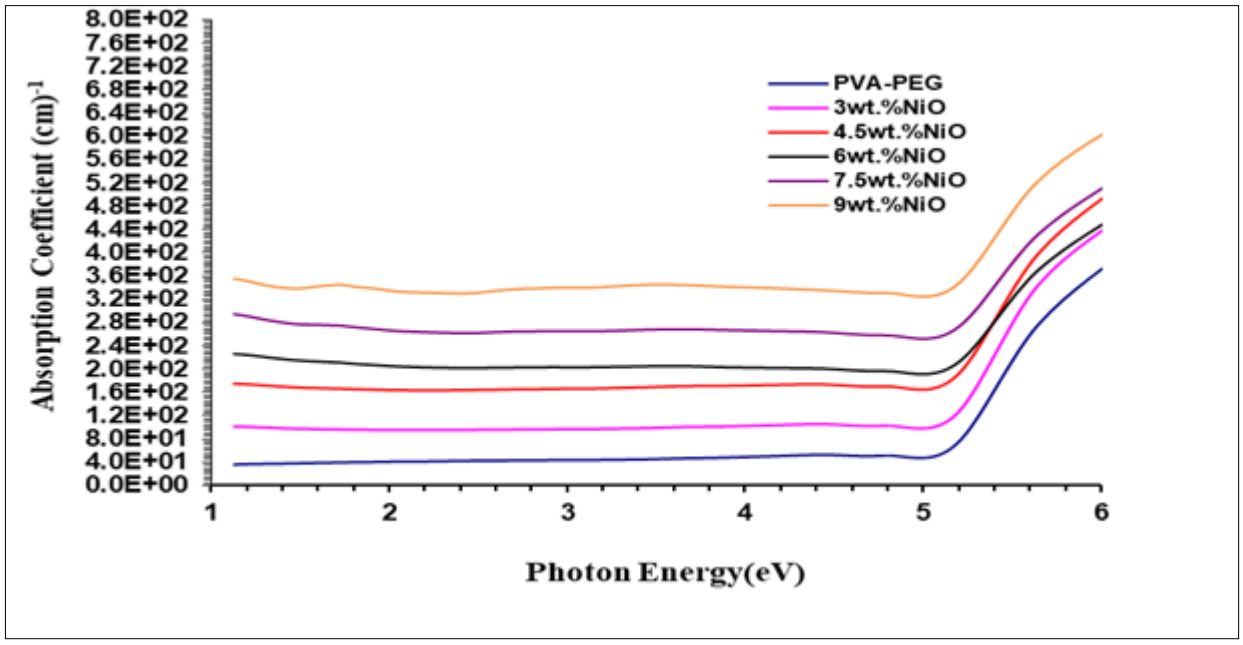

Fig. (4.13): Variation of absorption coefficient (α) for (PVA-PEG/NiO) NCs with photon energy.

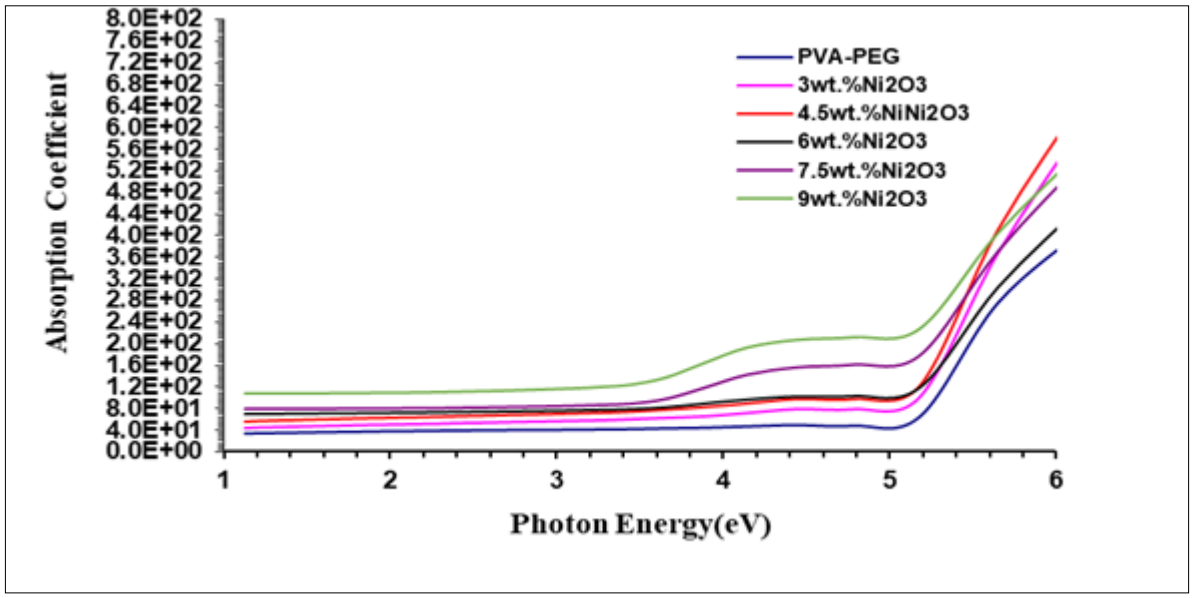

Fig. (4.14): Variation of absorption coefficient (α) for (PVA-PEG/Ni_2O_3) NCs with photon energy.

The energy band gap is calculated using the classical relation (2-22) for near edge optical absorption. The energies gap for allowed indirect transitions of (PVA-PEG/NiO) and (PVA-PEG/ Ni_2O_3) NCs are shown in Figures (4.15) and (4.16), respectively. The energies gap for forbidden indirect transitions of (PVA-PEG/NiO) and (PVA-PEG/ Ni_2O_3) NCs are shown in Figs. (4.17) and (4.18), respectively. The indirect band gap (IBG) obtained with procedure PVA-PEG/ 3-9wt.%NiO and Ni_2O_3 NC films, calculated by projecting the linear portion of the curve to the hν axis. In the Tables (4.1) and (4.2), the energies gap for allowed and forbidden indirect transitions of NCs are decreased with the increasing of the NiO and Ni_2O_3 NPs concentration. Change in the crystallinity of the films [126] and oxygen ion vacancies[127] may cause reduction in optical energy gap; these positively charged vacancies may capture some free electrons and act as donor centers leading to the reduction in optical energy gap. From another point of view the formation of imperfections and disarrays into the materials, which is close to the conduction band, may explain why the

optical energy gap has reduction. As a result, it can soak up low-energy photons. These matches the lookup values [128, 129],

It can be concluded from the cases of NiO and Ni_2O_3 additions, and according to the results presented in Tables (4.1) and (4.2), that the values of the energy gaps for (PVA-PEG/NiO) are differ than their values for (PVA-PEG/ Ni_2O_3), and this is probably due to the difference in the density values of nano-additives NiO (6.67 g/cm^3) and Ni_2O_3 (4.84 g/cm^3), in addition to the nature of their diffusion on the surface of the films prepared according to the results of the optical microscope test.

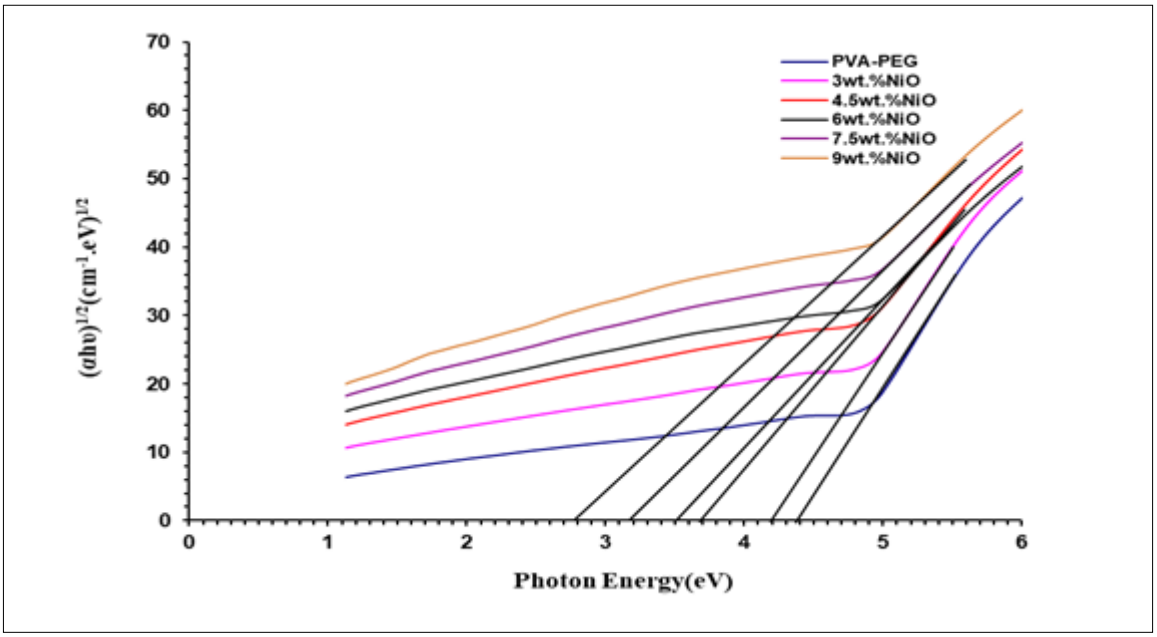

Fig. (4.15): Variation of $(\alpha h\upsilon)^{1/2}$ for (PVA-PEG/NiO) NCs with photon energy.

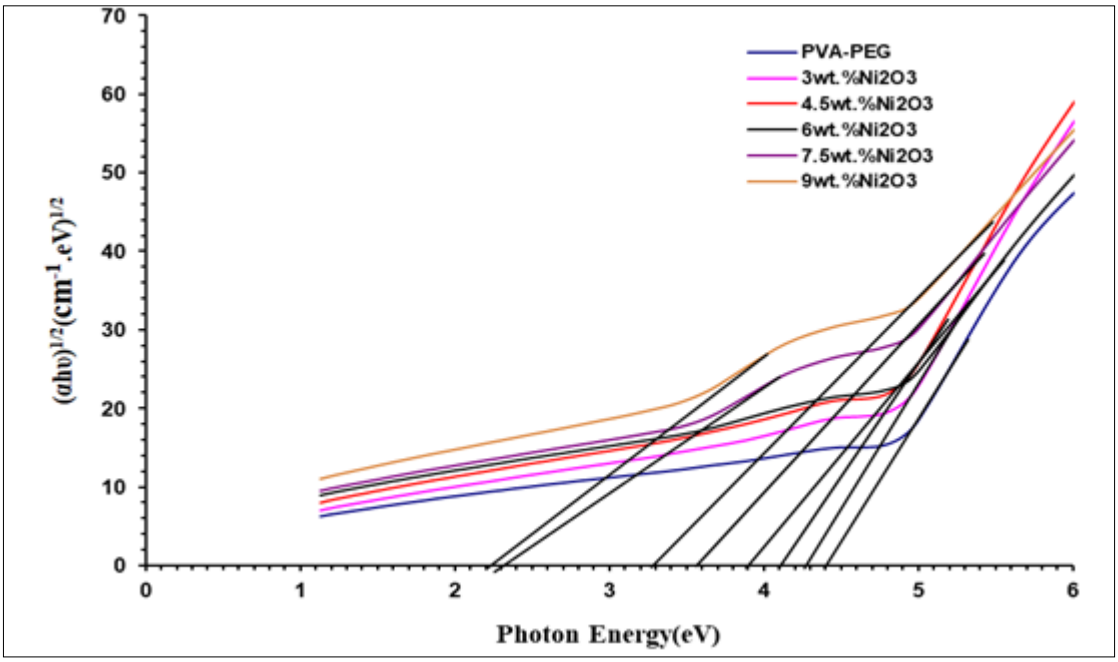

Fig. (4.16): Variation of $(\alpha h\upsilon)^{1/2}$ for (PVA-PEG/Ni_2O_3) NCs with photon energy.

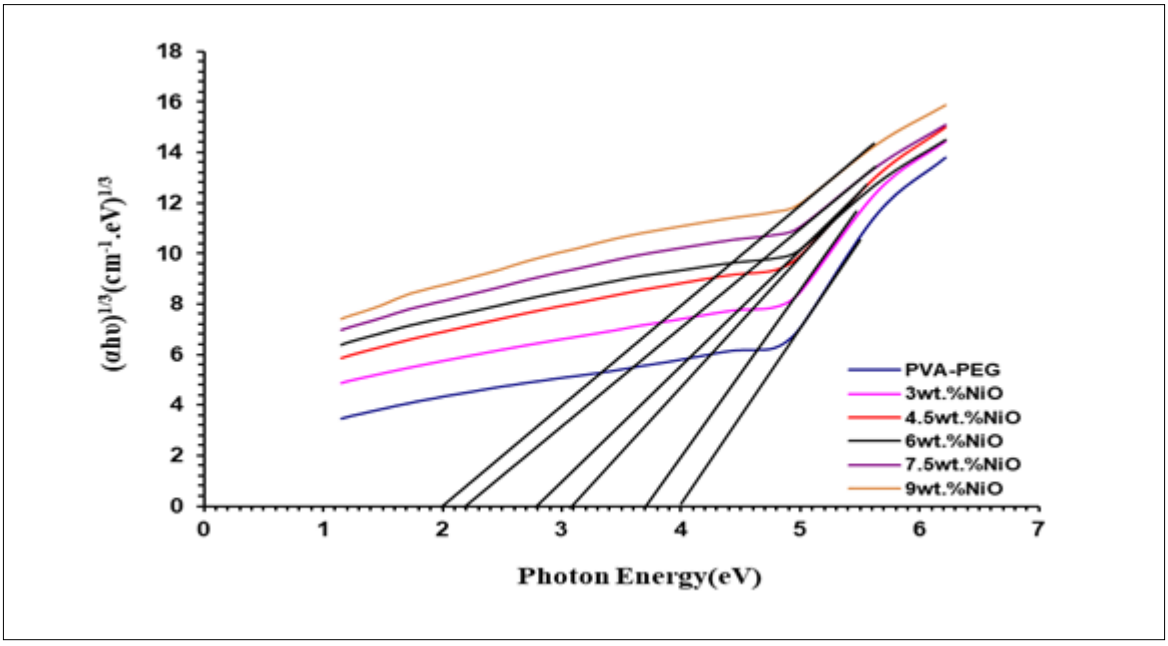

Fig. (4.17): Variation of $(\alpha h\upsilon)^{1/3}$ for (PVA-PEG/NiO) NCs with photon energy.

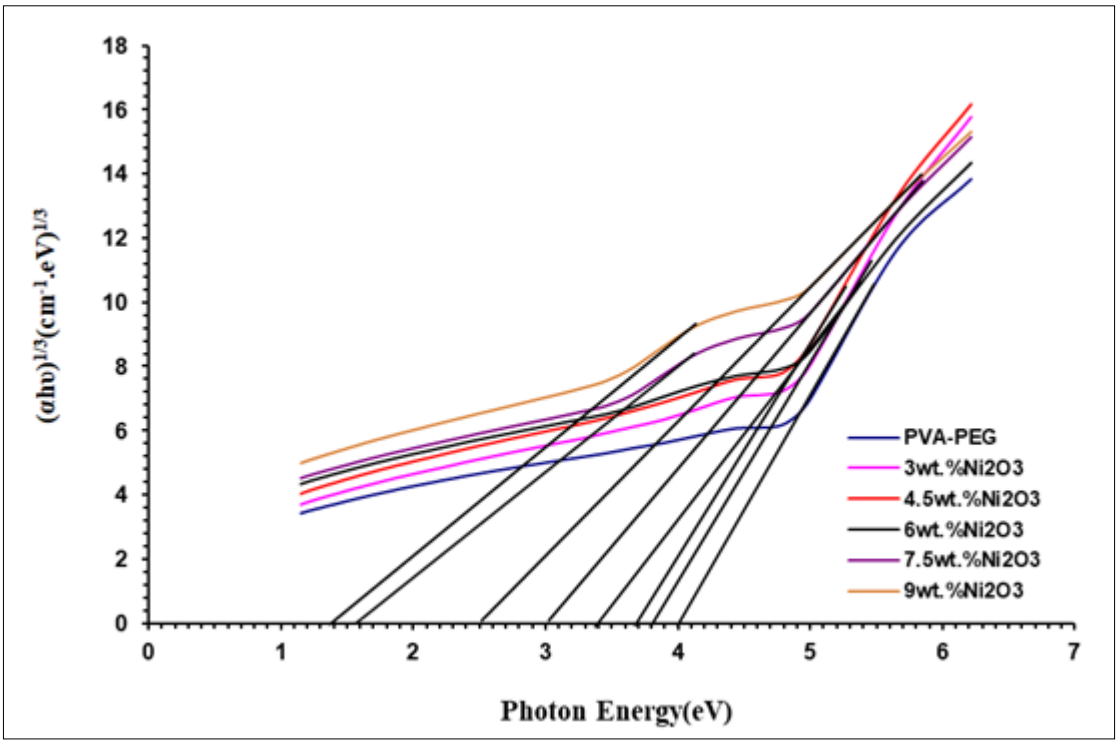

Fig. (4.18): Variation of $(\alpha h\upsilon)^{1/3}$ for (PVA-PEG/Ni_2O_3) NCs with photon energy.

Table (4.1): E_g^{opt} values for the allowed and forbidden indirect transition of blended polymer (PVA-PEG) and its NCs.

Sample	Allowed (eV)	Forbidden (eV)
PVA-PEG	4.385	4.000
3 wt.% NiO	4.200	3.680
4.5wt.% NiO	3.695	3.080
6 wt.% NiO	3.520	2.800
7.5 wt.% NiO	3.180	2.200
9 wt.% NiO	3.000	2.000

Table (4.2). E_g^{opt} values for the allowed and forbidden indirect transition for (PVA-PEG/Ni_2O_3) NCs.

Sample	Allowed (eV)	Forbidden (eV)
PVA-PEG	4.385	4.000
3wt.% Ni_2O_3	4.280	3.810
4.5wt.% Ni_2O_3	4.100	3.685
6 wt.% Ni_2O_3	3.920	3.390
7.5 wt.% Ni_2O_3	3.57, (2.31)	3.072 and (1.580)
9 wt.% Ni_2O_3	3.39, (2.22)	2.580 and (1.390)

4.3.3 Index of refractive (n), polarizability (P) and extinction coefficient (k_o) of (PVA-PEG/NiO) and (PVA-PEG/Ni_2O_3) NCs.

The index of refractive (n), polarizability (P) and extinction coefficient (k_o) of PVA-PEG/3-9wt.%NiO and PVA-PEG/3-9wt.%Ni_2O_3 NC films were considered from the equations 2.6, 2.7 and 2.8 respectively. When developing a variety of electronic devices, such as those for optoelectronic, photonic, and cable applications, the evaluation of refractive index (n) is thought to be a crucial factor [130]. Figures (4.19) and (4.20) elucidate the dependence of refractive index on different ratios of NiO and Ni_2O_3 NPs in blended polymer (PVA-PEG) , respectively. From the photodarkening phenomenon, the (n) was found to be increased with the additives of NiO and Ni_2O_3 NPs increases, and the structural change criteria is what causes the fluctuation in the value of (n). Also, the decrease in the refractive index values towards longer wavelength may be attributed to the effect of lattice absorption [131].

The refractive index values obtained in the case of PVA-PEG/3-9wt.%NiO are higher than it is in the case of PVA-PEG/3-9wt.%Ni_2O_3 NC films. This is due to a difference in the density values of nano-additives NiO (6.67 g/cm^3) and Ni_2O_3 (4.84 g/cm^3), where the refractive index is

directly proportional to the density, as well as the nature of their diffusion on the surface of the films prepared according to the results of the optical microscope test. The results refer to can be candidate the prepared 9wt.% NC films.

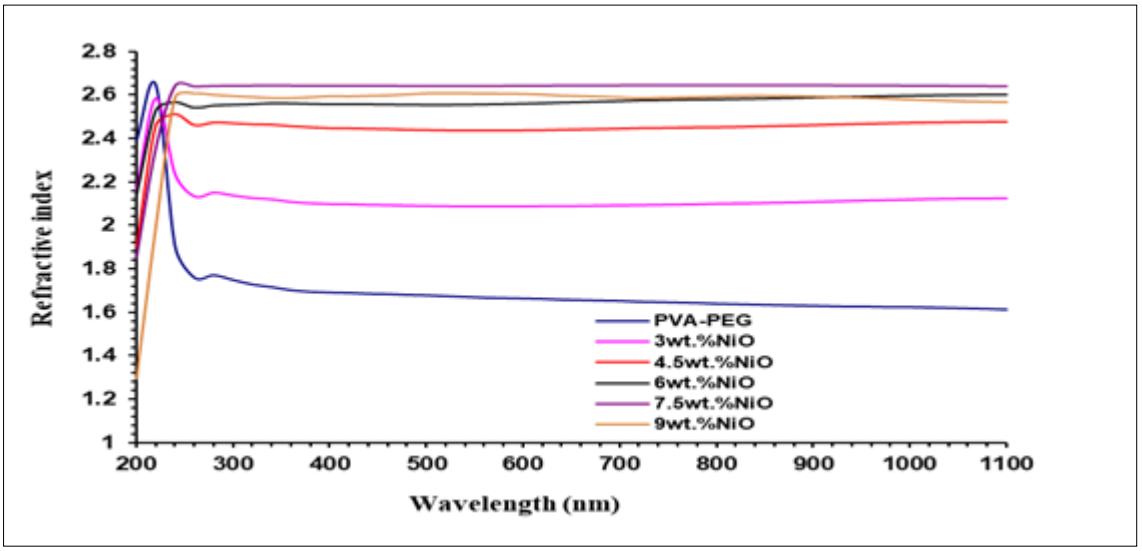

Fig. (4.19): Variation of refractive index for (PVA-PEG/NiO) NCs with wavelength.

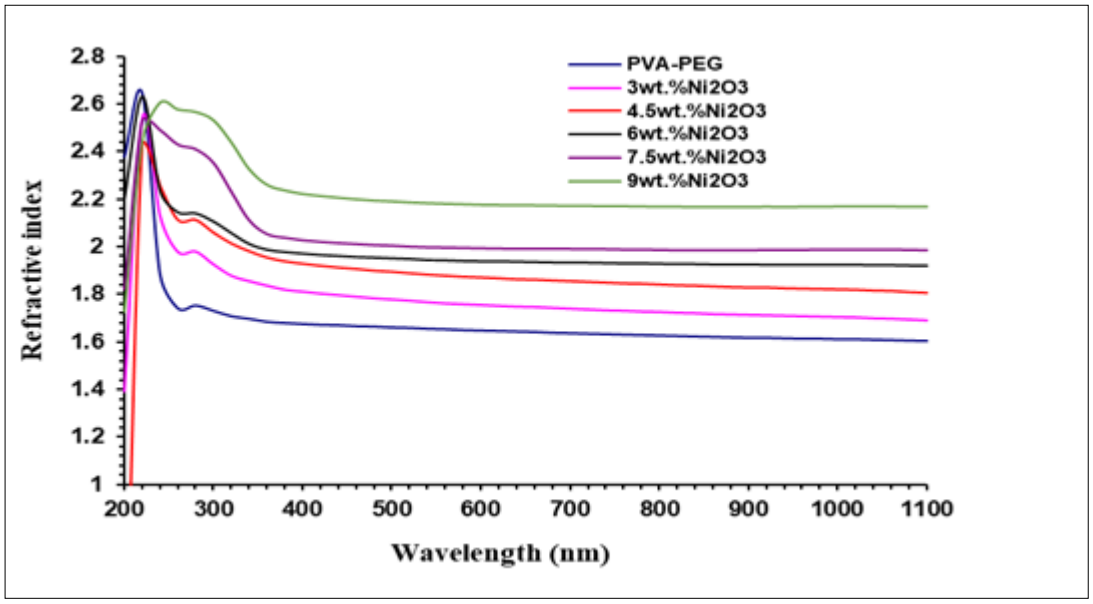

Fig. (4.20): Variation of refractive index for (PVA-PEG/Ni_2O_3) NCs with wavelength.

According to the literature [132] the larger the polarizability, the greater the refractive index, and non-polarizing materials don't change the speed of light, and therefore n=1. Decreasing in the E_g^{opt} with the increase the ratio of the additive NiO and Ni_2O_3 NPs means that the electrons can

move to other levels and thus an increase in the polarizability of the material, as shown in Figures (4.21) and (4.22). Due to the dipoles created being unable to maintain the high frequency, polarization can be seen to diminish at lower wavelengths as the incident photon's energy increases (high energies).

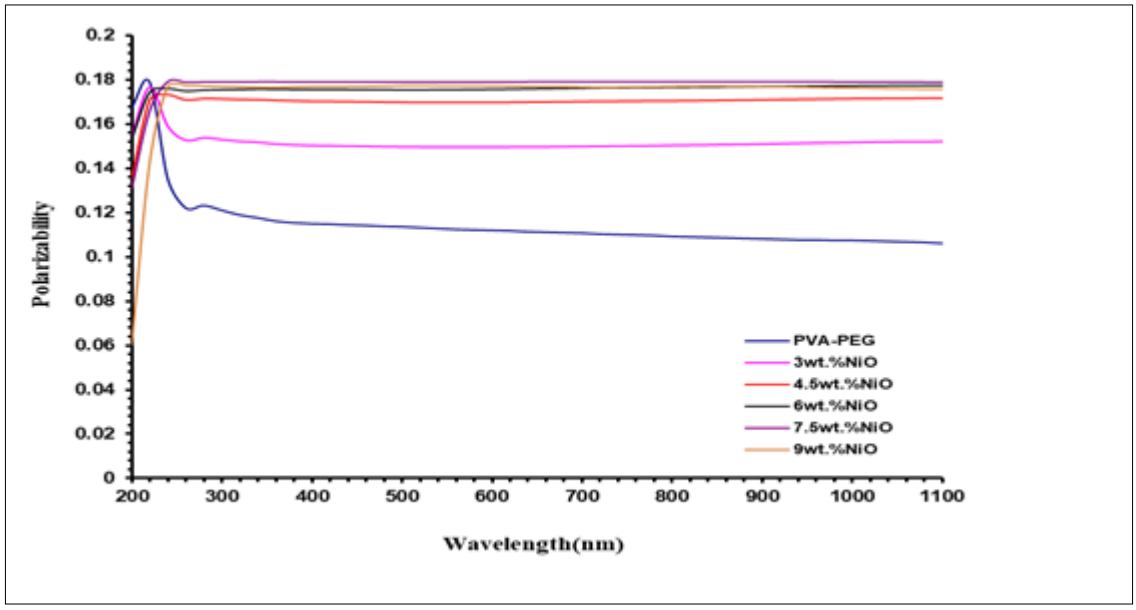

Fig. (4.21): Variation of polarizability for (PVA-PEG/NiO) NCs with wavelength.

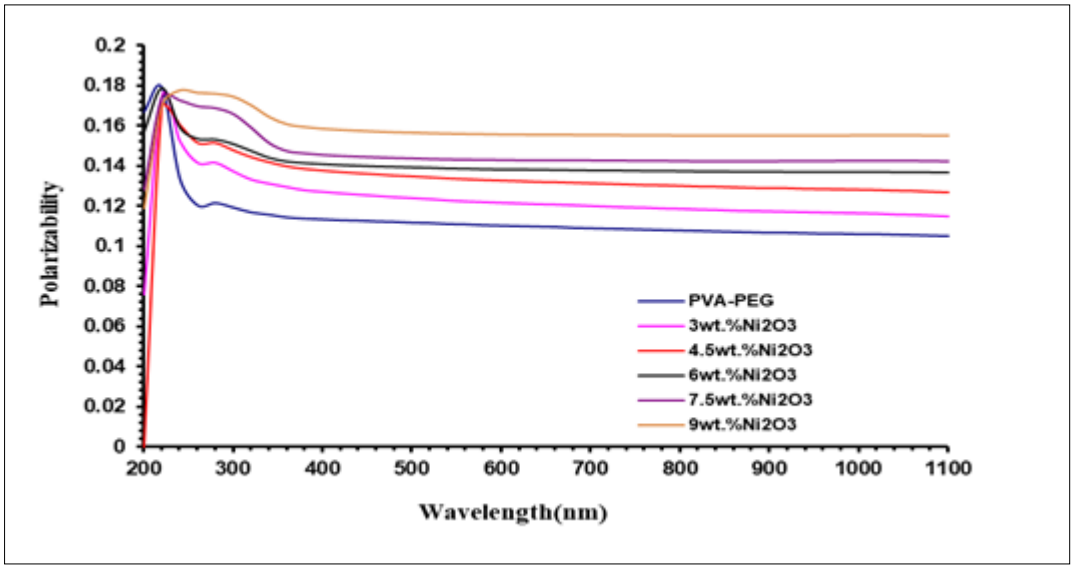

Fig. (4.22): Variation of polarizability for (PVA-PEG/Ni_2O_3) NCs with wavelength.

According to our analysis of Figures (4.23) and (4.24), the extinction coefficient results of the NC films are much higher than those of the blended polymer (PVA-PEG) in all regions. This behavior attributed to increase of the absorption of the incident light [132].

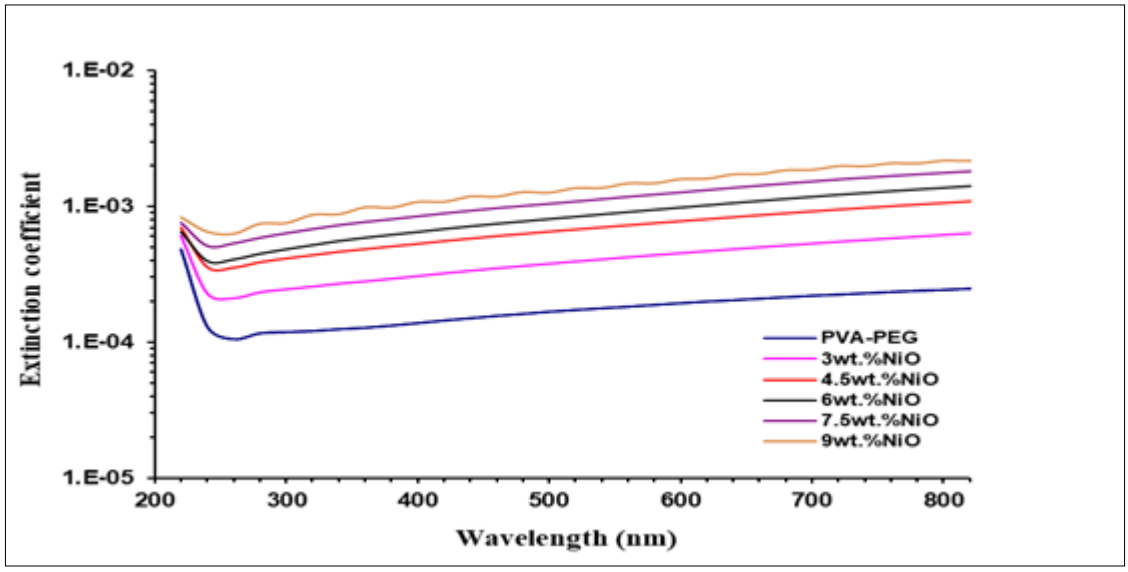

Fig. (4.23): Variation of extinction coefficient for (PVA-PEG/NiO) NCs with wavelength.

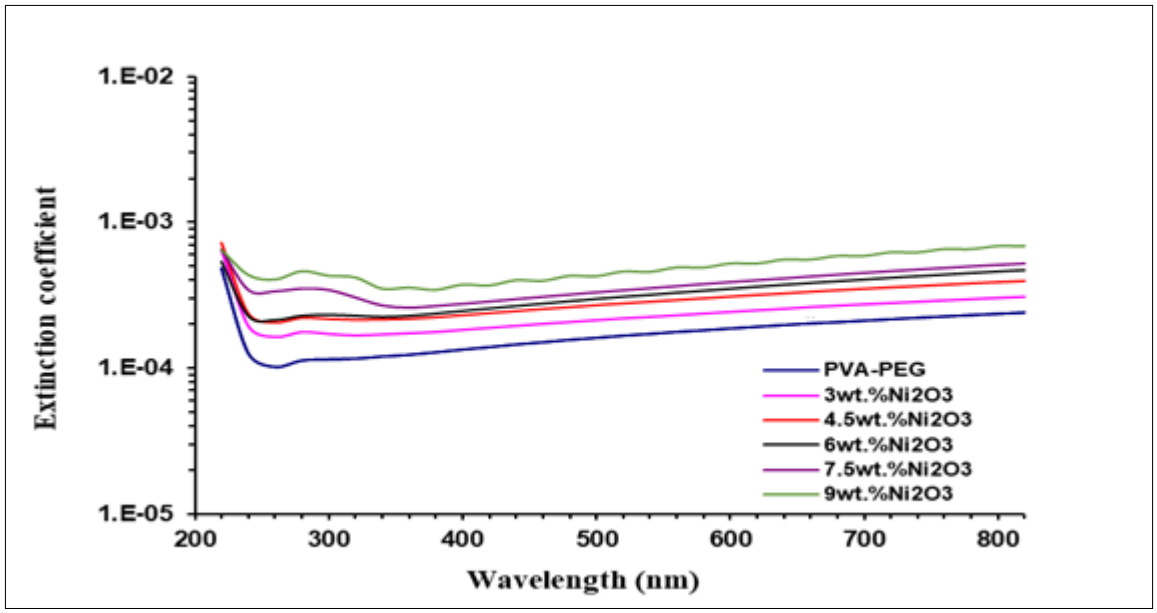

Fig. (4.24): Variation of extinction coefficient for (PVA-PEG/Ni_2O_3) NCs with wavelength.

4.3.4 The real and imaginary parts of dielectric constant.

Dielectric constant of any solid is a measure of its polarizability [133]. The real and imaginary parts of dielectric constant are calculated using equations (2.14) and (2.15), respectively. The real part (ε_1) is attributed to the slowing down phenomenon of the speed of light in solid and the imaginary part (ε_2) pertains to dipole motion due to absorption of energy from electric field [134]. Figures (4.25) and (4.26) show the effect of NiO and Ni_2O_3 NPs on the real dielectric constant for (PVA-PEG/NiO) and (PVA-PEG/Ni_2O_3) NCs, respectively. The effect of NiO and Ni_2O_3 NPs on the imaginary part of dielectric constant for (PVA-PEG/NiO) and (PVA-PEG/Ni_2O_3) NCs is shown in Figures (4.27) and (4.28), respectively. For a given wavelength, ε_1 and is ε_2 increasing with the increase in NiO and Ni_2O_3 NPs concentration and is minimum for polymeric blend film. As shown in the figures, the real and imaginary parts of dielectric constant of (PVA-PEG) blend are changed with the wavelength, this is due to the real part of dielectric constant depending on refractive index because the effect of extinction coefficient is very small and the imaginary part of dielectric constant depends on extinction coefficient especially in the visible and NIR regions of wavelength where the refractive index is approximately constant while extinction coefficient increases with the increase of the wavelength.

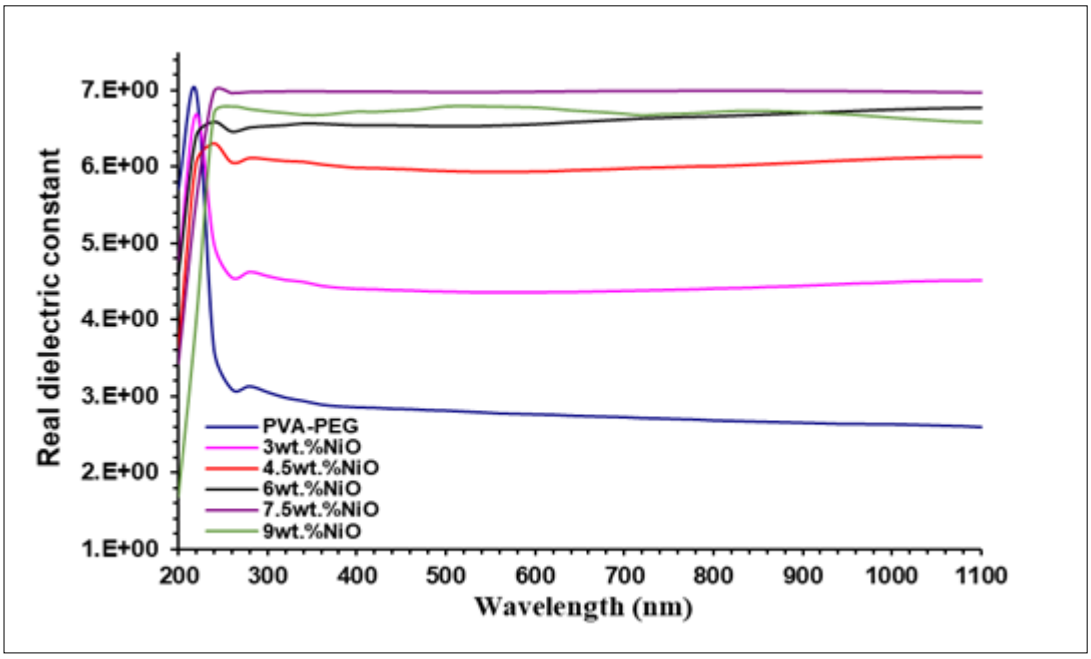

Fig. (4.25): Values of real part of dielectric constant for (PVA-PEG/NiO) NCs as a function of wavelength.

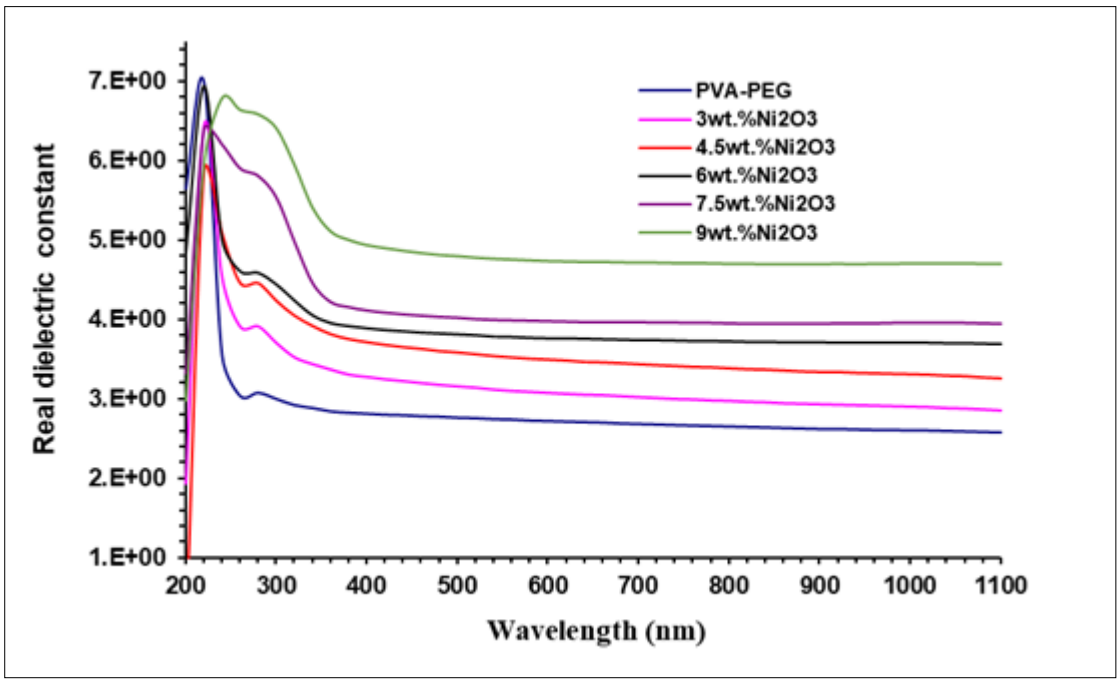

Fig. (4.26): Values of real part of dielectric constant for (PVA-PEG/Ni_2O_3) NCs with wavelength as a function of wavelength.

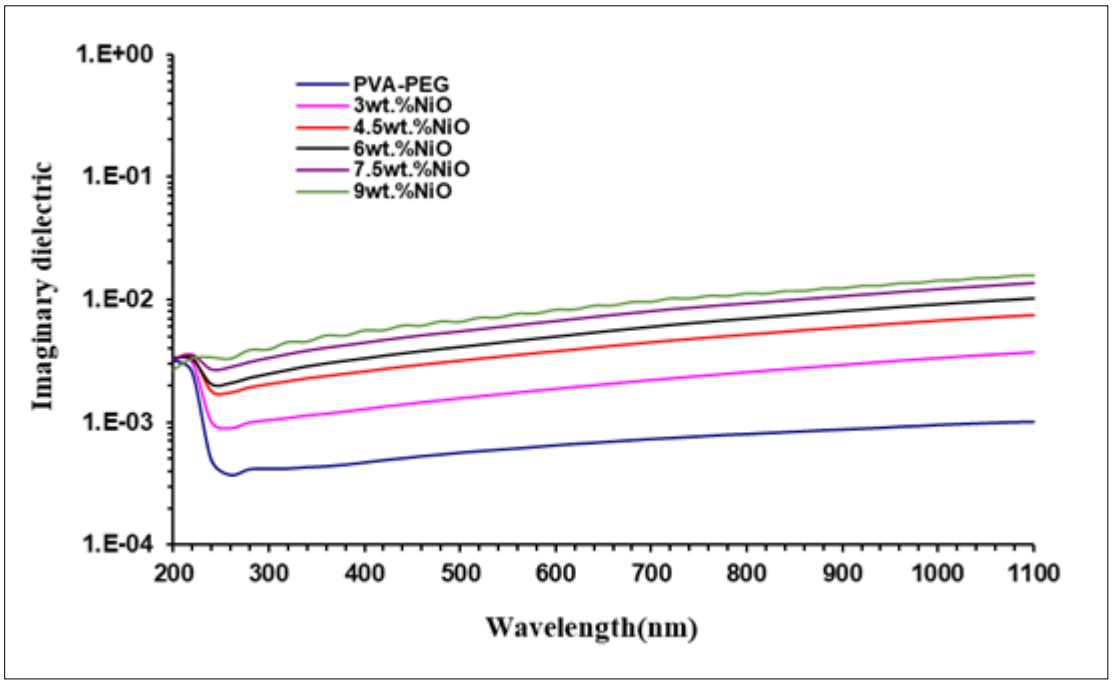

Fig. (4.27): Variation of imaginary part of dielectric constant for (PVA-PEG/NiO) NCs with wavelength.

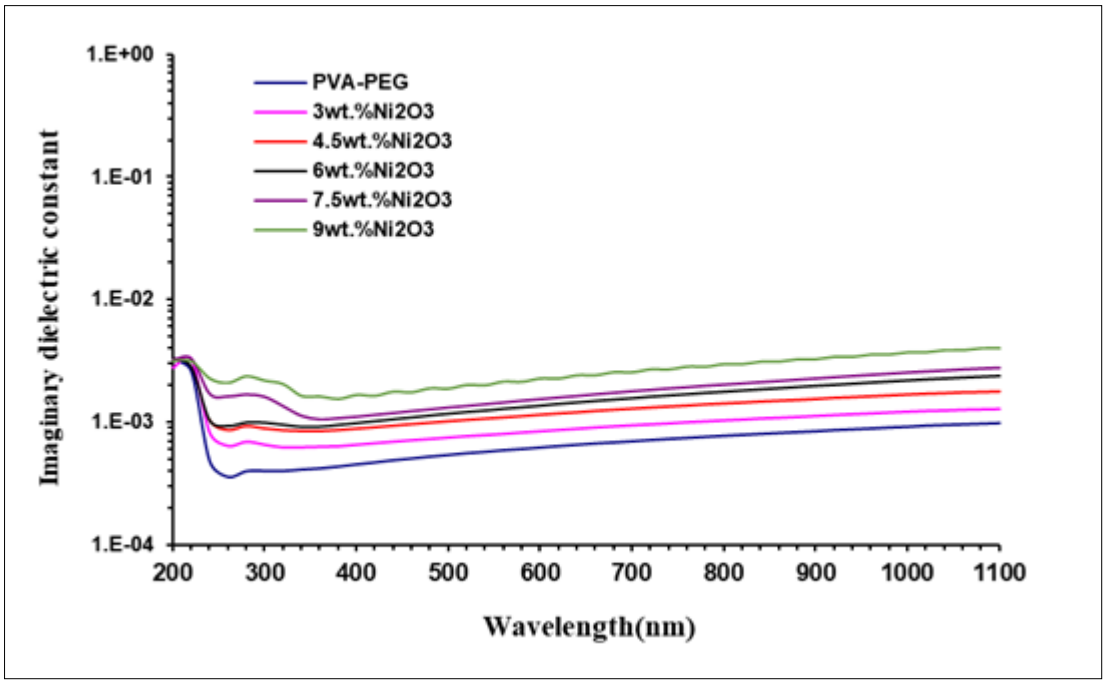

Fig. (4.28): Variation of imaginary part of dielectric constant for (PVA-PEG/Ni_2O_3) NCs with wavelength.

4.3.5 The optical conductivity

The optical conductivity (σ_{op}) is obtained by via the relation (2.9). Figures (4.29) and (4.30) elucidates the dependence of optical conductivity on different ratios of NiO and Ni_2O_3 NPs in blended polymer (PVA-PEG) , respectively . The optical conductivity of the prepared samples increases with the increase in the concentration of the nano-additive and reaches its highest value in the UV region. This tendency results from the band structure's localized stages becoming denser, which raises the absorption coefficient and, in turn, the optical conductivity. The optical conductivity spectra confirm the transmittance behavior within the Vis and NIR regions, noting that its values in the case of (PVA-PEG/NiO) NCs are higher than it is in the case of (PVA-PEG/Ni_2O_3) NCs**.**

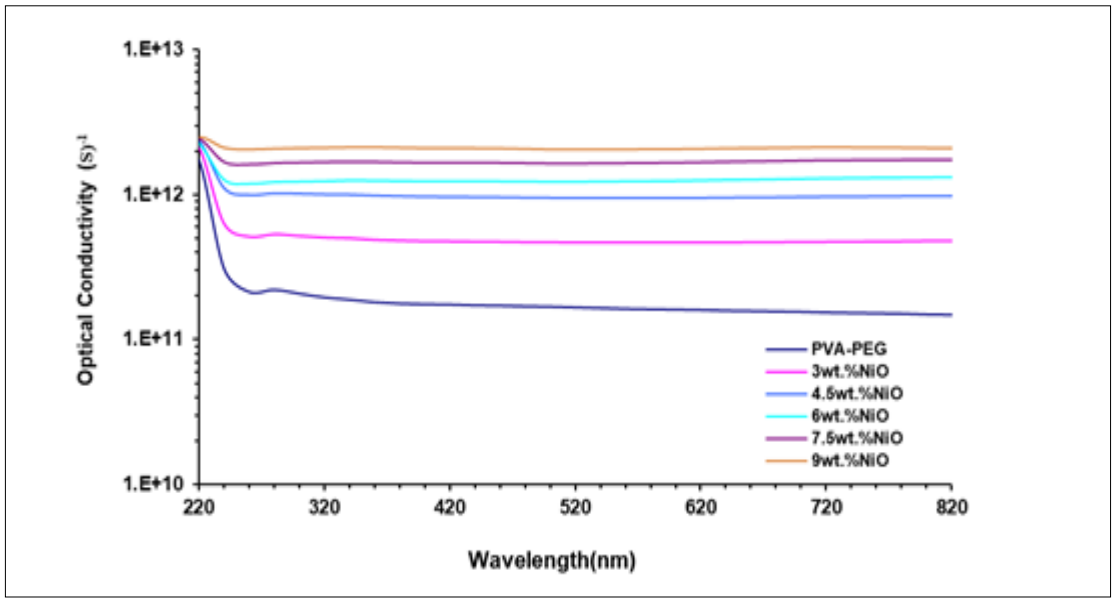

Fig. (4.29): Variation of optical conductivity for (PVA-PEG/NiO) NCs with wavelength.

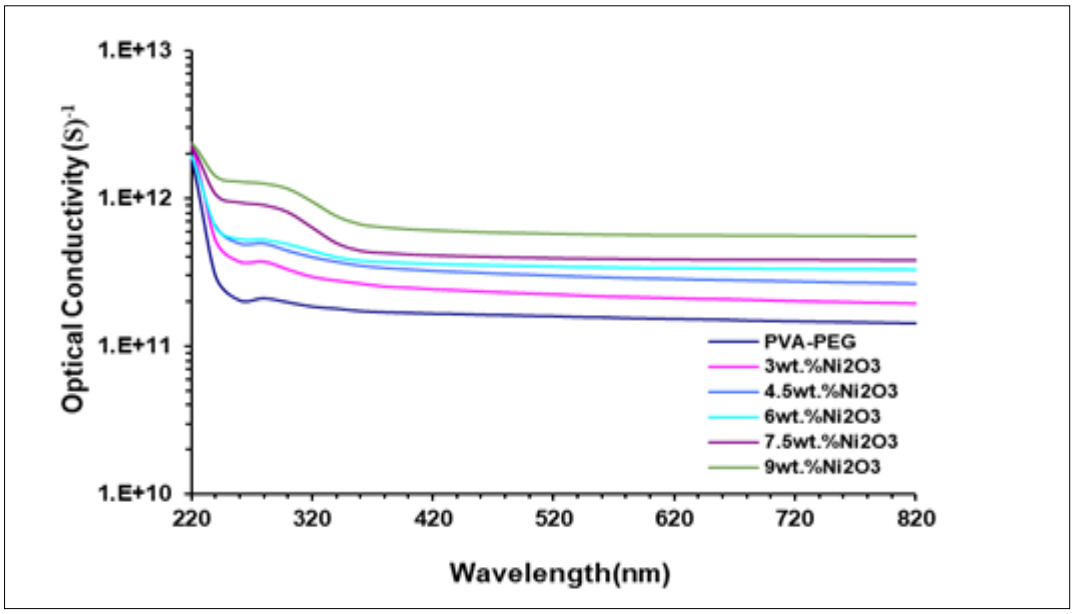

Fig. (4.30): Variation of optical conductivity for (PVA-PEG-Ni_2O_3) NCs with wavelength.

4.5 The A.C Electrical Properties of (PVA-PEG/NiO) and (PVA-PEG/Ni_2O_3) NCs

The A.C electrical properties of (PVA-PEG/NiO) and (PVA-PEG/Ni_2O_3) NCs include dielectric constant, dielectric loss, and A.C electrical conductivity which were studied in frequency ranging between 10^2 to 10^6 Hz at RT.

4.5.1 The Dielectric Constant of (PVA-PEG/NiO) and (PVA-PEG/Ni_2O_3) NCs

The dielectric constant of blended polymer's (PVA-PEG) and its NC films with (3, 4.5, 6, 7.5, and 9) wt.% of NiO and Ni_2O_3 NPs at 100Hz are shown in Figures (4.31) and (4.32), respectively. The dielectric constant is calculated using equation (2.28). As shown in the figures, the dielectric constant of NCs increases with the increasing of the NiO and Ni_2O_3 NPs concentration. This behavior can be explained by the interfacial polarization within the nanocomposites in the applied alternating electric field and the increase of charge carriers [135]. From Figures (4.33) and (4.34), it is noted

that increasing the frequencies causes a decrease in the space charge polarization relative to the total polarization and this causes a decrease in the dielectric constant values for all (PVA-PEG/NiO) and (PVA-PEG/Ni_2O_3) NC samples, and thus becomes space charge polarization contributes more to polarization at lower frequencies.

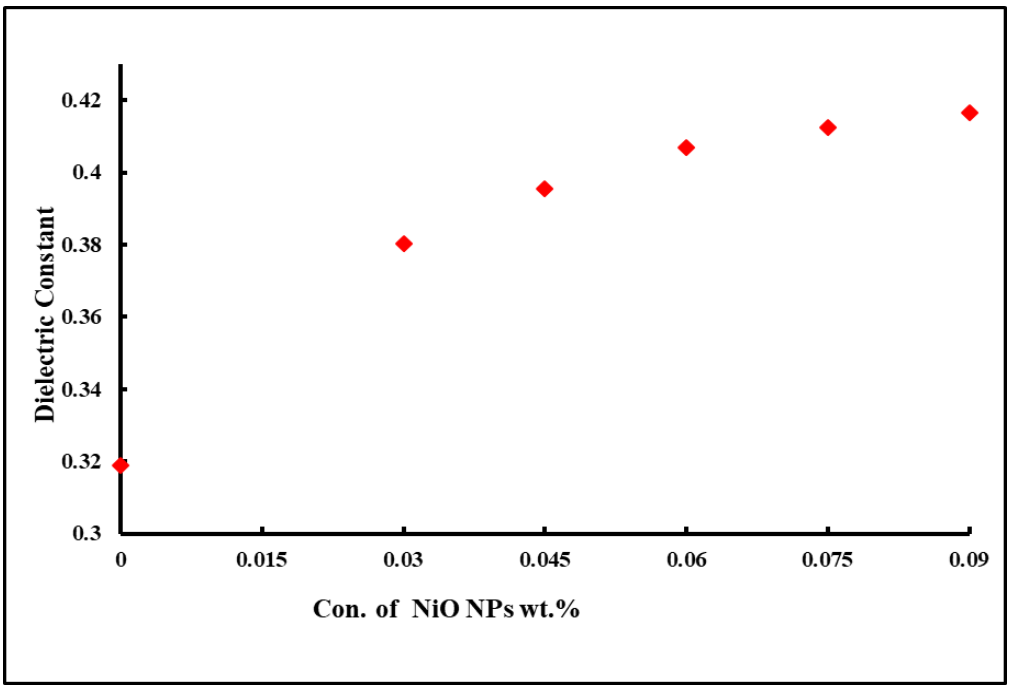

Fig. (4.31): Effect of NiO concentrations on dielectric constant for (PVA-PEG/NiO) NCs at 100Hz

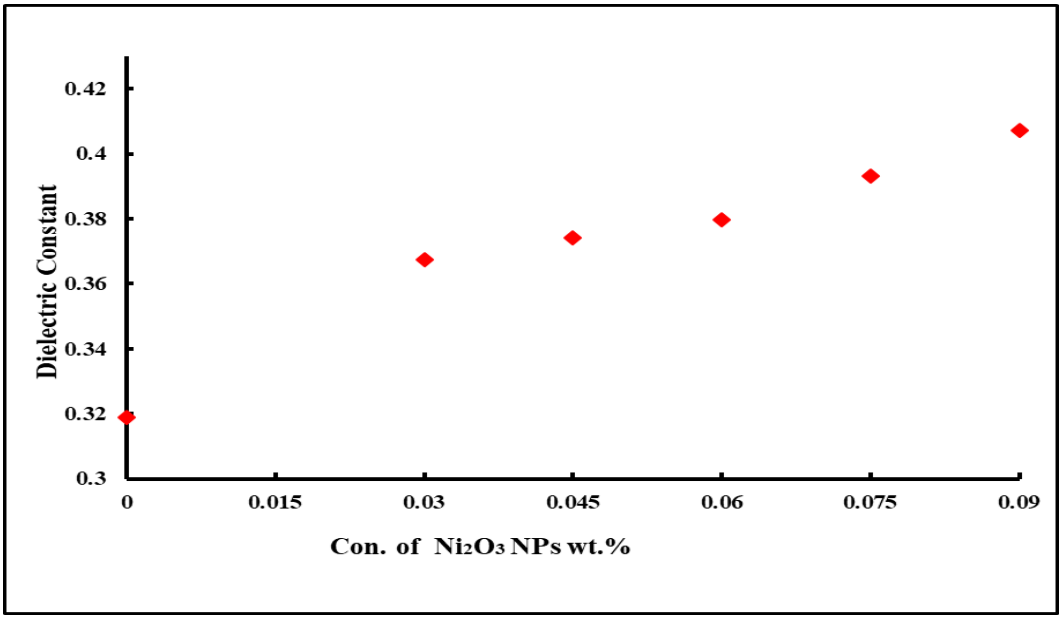

Fig. (4.32): Effect of Ni_2O_3 concentrations on dielectric constant for (PVA-PEG/NiO) NCs at 100Hz.

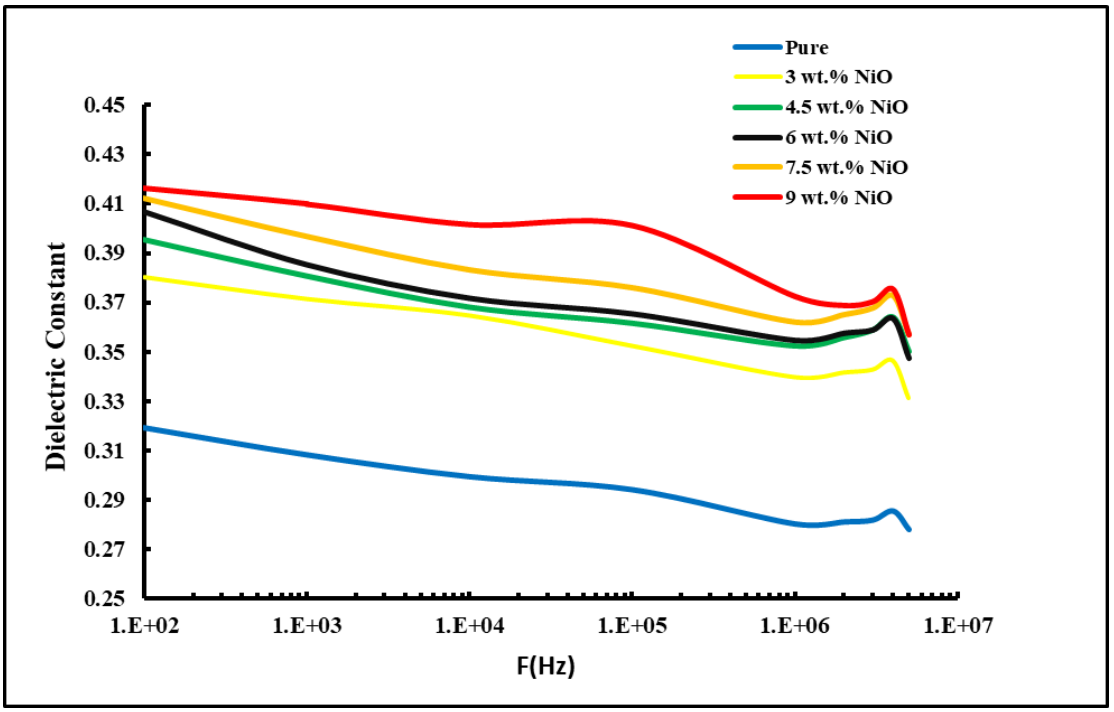

Fig. (4.33): Variation of dielectric constant for (PVA-PEG-NiO) nanocomposites with frequency at RT.

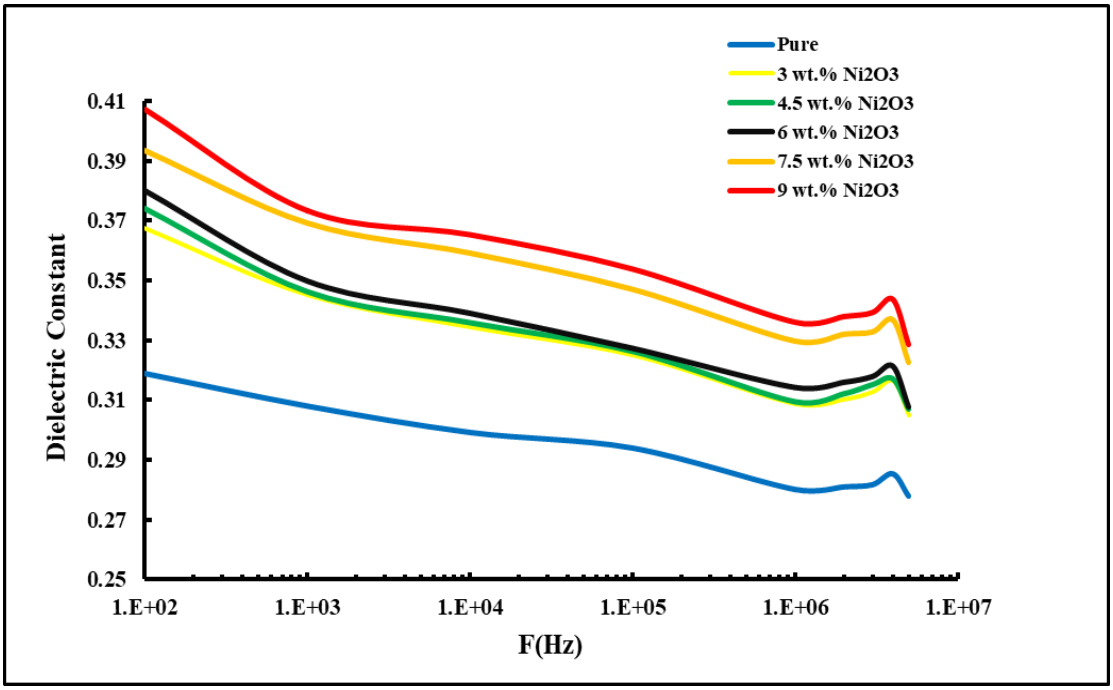

Fig.(4.34): Variation of dielectric constant for (PVA-PEG-Ni_2O_3) nanocomposites with frequency at RT.

4.5.2 Dielectric Loss of (PVA-PEG/NiO) and (PVA-PEG/Ni_2O_3) NCs

The dielectric loss measures the lost electrical energy in the sample from the applied field which is transformed to thermal energy in the sample. The dielectric loss of nanocomposites is calculated by using equation (2.27). The dependence of dielectric loss on electric field frequency of both NiO and Ni_2O_3 NPs in the PVA-PEG blends at RT shown in Figures (4.35) and (4.37), respectively. The figures show that the dielectric loss of nanocomposites decreases with increase of electric field frequency for all samples. This behavior is attributed to a decrease of the space charge polarization contribution. In addition, the maximum dielectric loss for NC films of 9 wt.% NiO and Ni_2O_3 NPs at low frequency (10^2Hz) are 0.0749 and 0.0692.

The dielectric loss of nanocomposites based on NiO and Ni_2O_3 increases with increasing of the nanoparticles concentration as shown in Figures (4.37), and (4.38), respectively. This related to the increases of the charge carrier's number. Similar behavior was reported in [136].

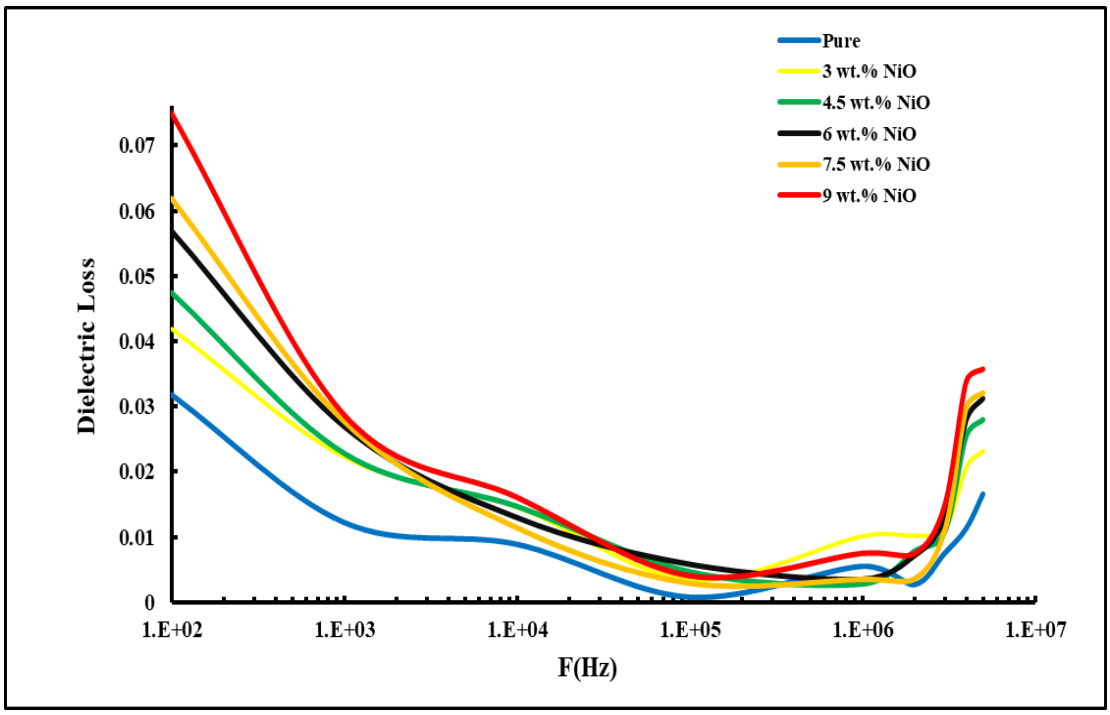

Fig. (4.35): Variation of dielectric loss for (PVA-PEG/NiO) NCs with frequency at RT.

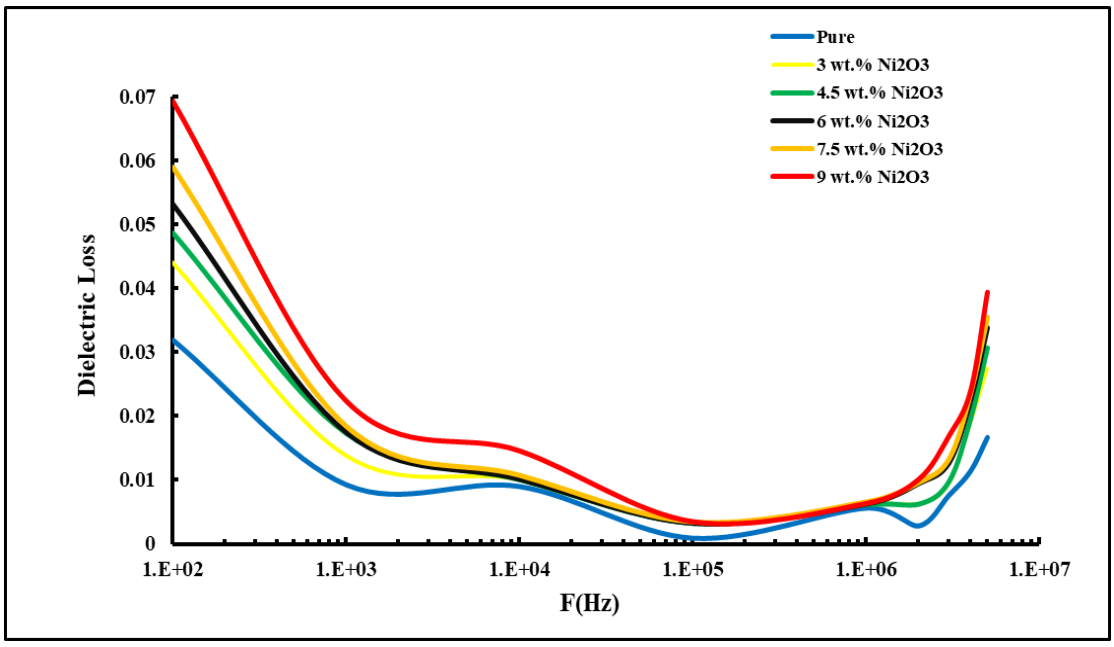

Fig (4.36): Variation of dielectric loss for (PVA-PEG/Ni_2O_3) NCs with frequency

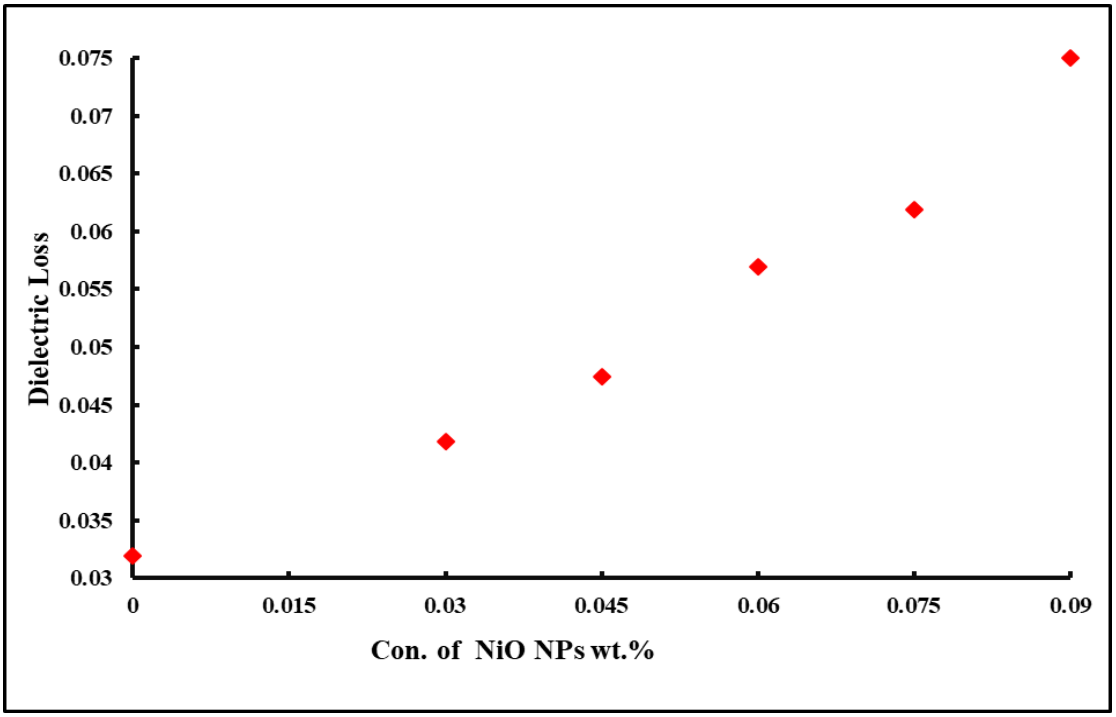

Fig. (4.37): Effect of NiO nanoparticles concentrations on dielectric loss for (PVA-PEG) blend at 100Hz.

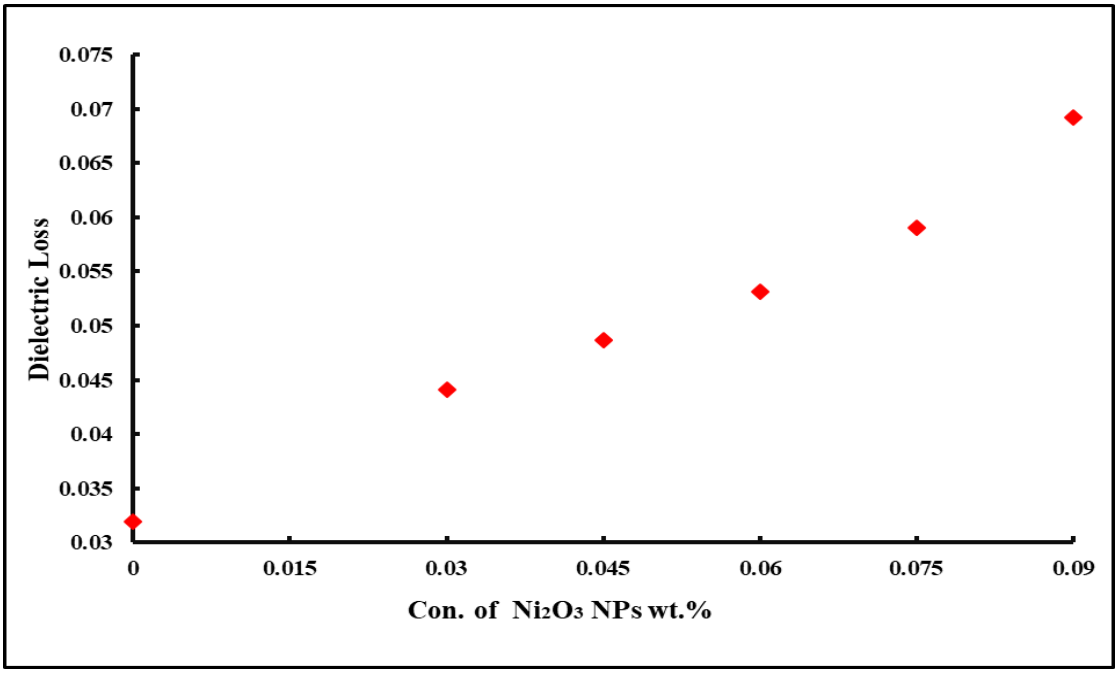

Fig. (4.38): Effect of Ni_2O_3 nanoparticles concentrations on dielectric loss for (PVA-PEG) blends at 100Hz.

4.5.3 The A.C Electrical Conductivity of (PVA-PEG/NiO) and (PVA-PEG/Ni_2O_3) NCs

The A.C electrical conductivity of nanocomposites is calculated by using equation (2-29). The dependence of A.C electrical conductivity on electric field frequency of both NiO and Ni_2O_3 NPs in the PVA-PEG blends at RT shown in Figures (4.39) and (4.40), respectively. The A.C conductivity increases considerably with the increase of electric field frequency for all samples, This behavior is attributed to the space charge polarization at low frequencies, and to the motion of charge carriers by hopping process [136]. Also, the conductivity increases with the increasing wt.% of the both NiO and Ni_2O_3 NPs in the PVA-PEG blends at 10^2Hz as shown in Figures (4.41) and (4.42), respectively. This increases the conductivity caused by the increase in the number of charge carriers due to additives nanoparticles composition which reduces the resistance of nanocomposite and increases the A.C electrical conductivity. Similar behavior was reported in [136].

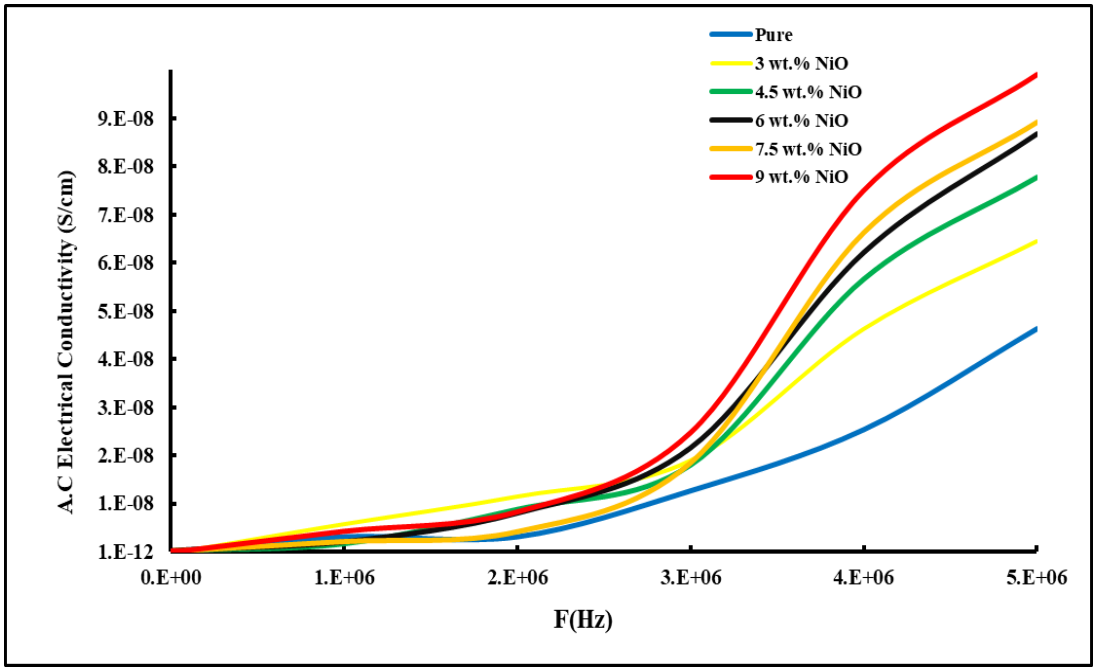

Fig. (4.39): Variation of A.C electrical conductivity for (PVA-PEG/NiO) NCs with frequency at RT.

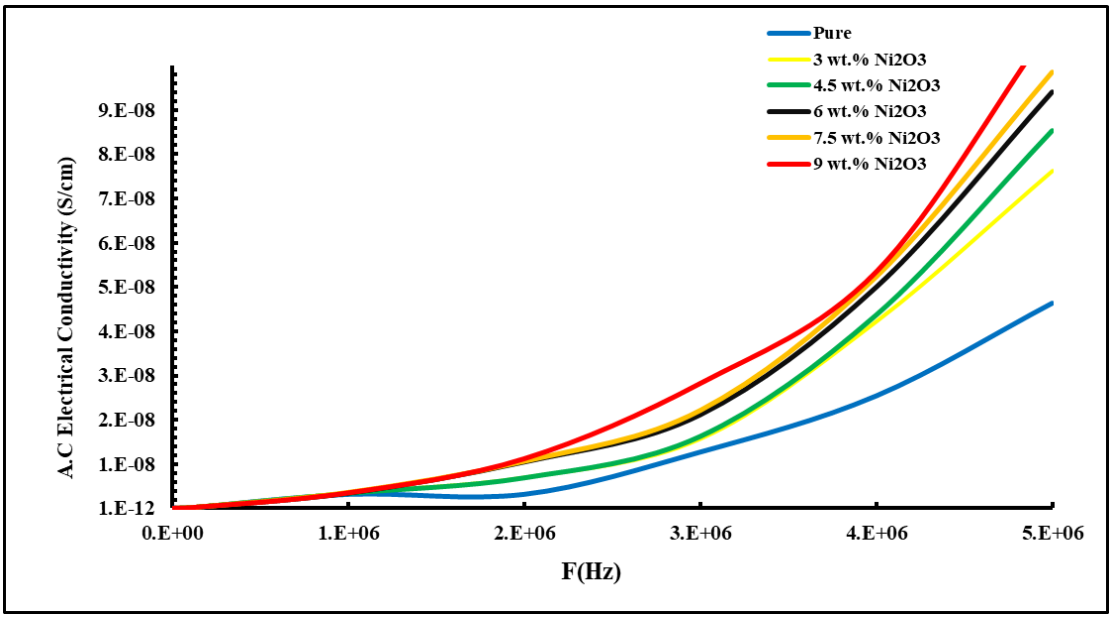

Fig. (4.40). Variation of A.C electrical conductivity for (PVA-PEG/Ni_2O_3) NCs with frequency at RT.

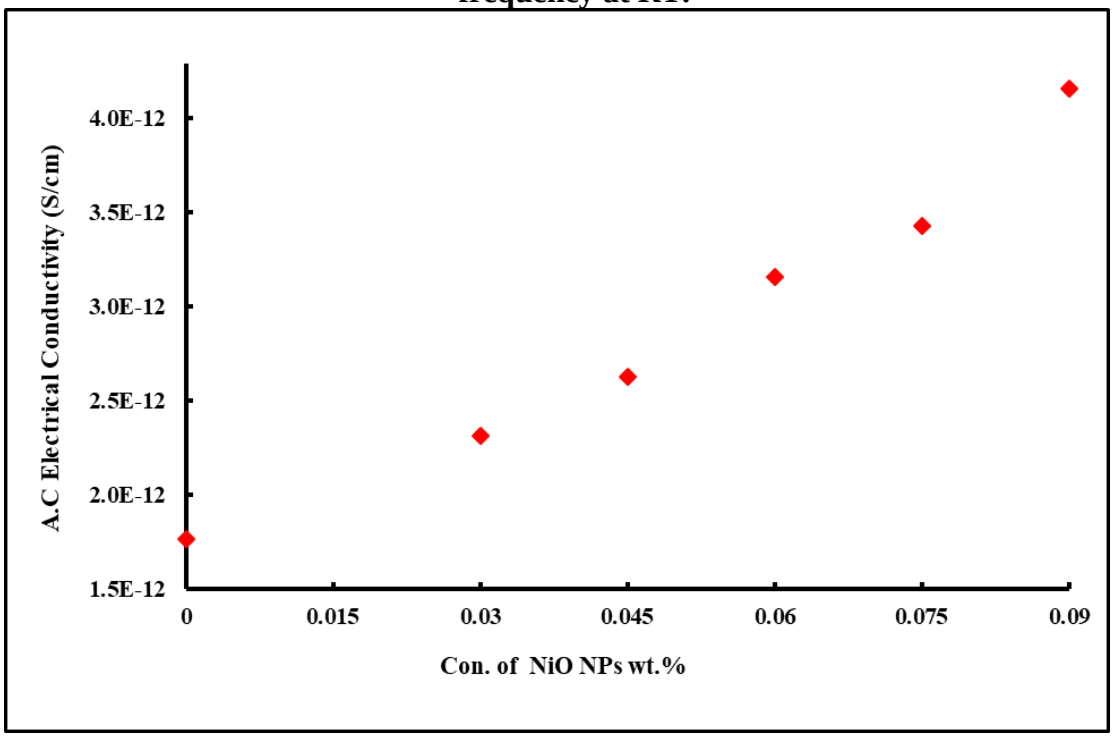

Fig. (4.41): Effect of NiO nanoparticles concentrations on A.C electrical conductivity for (PVA-PEG) blend at 100Hz.

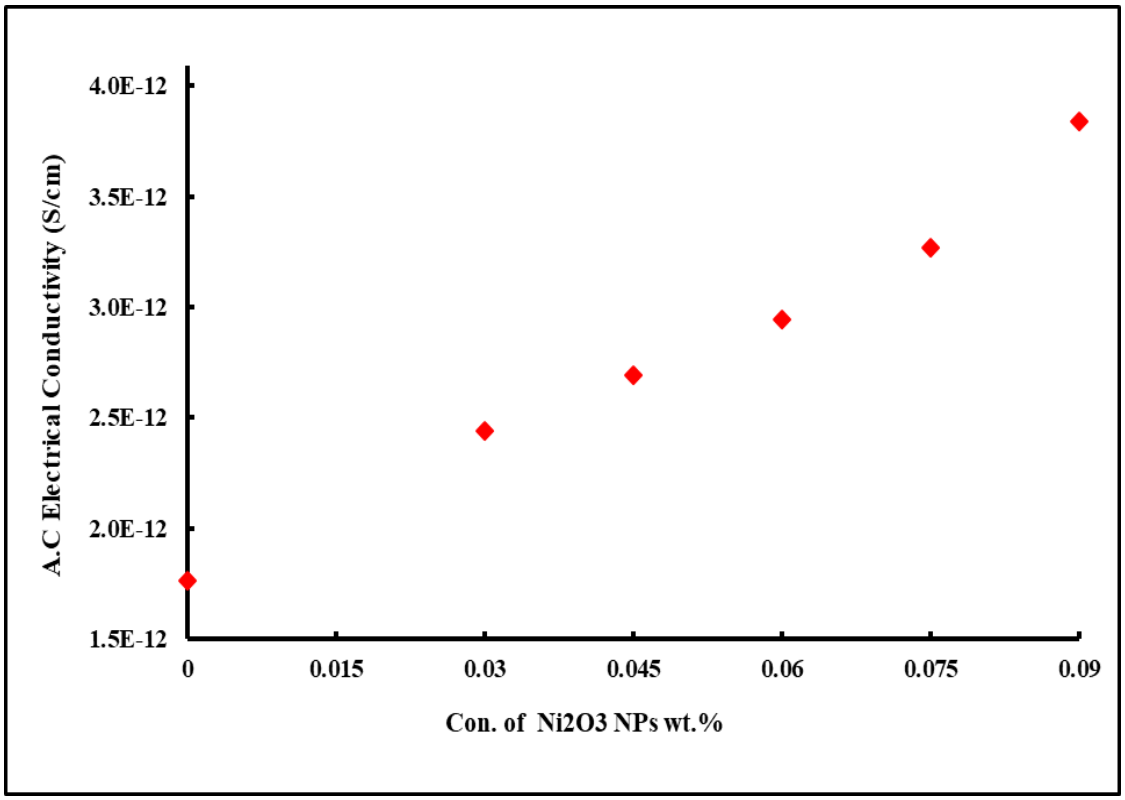

Fig. (4.42): Effect of Ni_2O_3 nanoparticles concentrations on A.C electrical conductivity for (PVA-PEG) blend at 100Hz.

4.5 Application of (PVA-PEG-NiO) and (PVA-PEG-Ni_2O_3) nanocomposites for antibacterial activity.

According to the conclusion that the best results can be candidate the prepared 9wt.% NC films, the antibacterial activity of (PVA-PEG/9wt.%NiO) and (PVA-PEG/9wt.%Ni_2O_3) NC films was tested against *Staphylococcus aureus* (*S. aureus*) and *Escherichia coli* (*E. coli*) using the disk diffusion method, and the results are shown in Figures (4.43) and (4.44). From these figures, the inhibition zone for NC films was greater in gram-positive (*Staphylococcus aureus*) compounds than in gram-negative (*Escherichia coli*). The width of the inhibition zone rises with additives metal oxides (NiO and Ni_2O_3), individually, and reaches its maximum value (24mm) in the case gram-positive (*Staphylococcus aureus*) for the additive Ni_2O_3 NPs. The reason for the bacterial activity of nanostructures is may be

due to the presence of reactive oxygen species ROS (which includes radicals like super oxide radicals O^{-2}, hydroxyl radicals OH, and hydrogen peroxide H_2O_2), generated by Ni_2O_3 NPs is more than that generated by NiO NPs. Also the nanoparticles of Ni_2O_3 can interact well with the membranes of bacteria because they have a lot of surface area and this makes them more effective at killing bacteria [137].

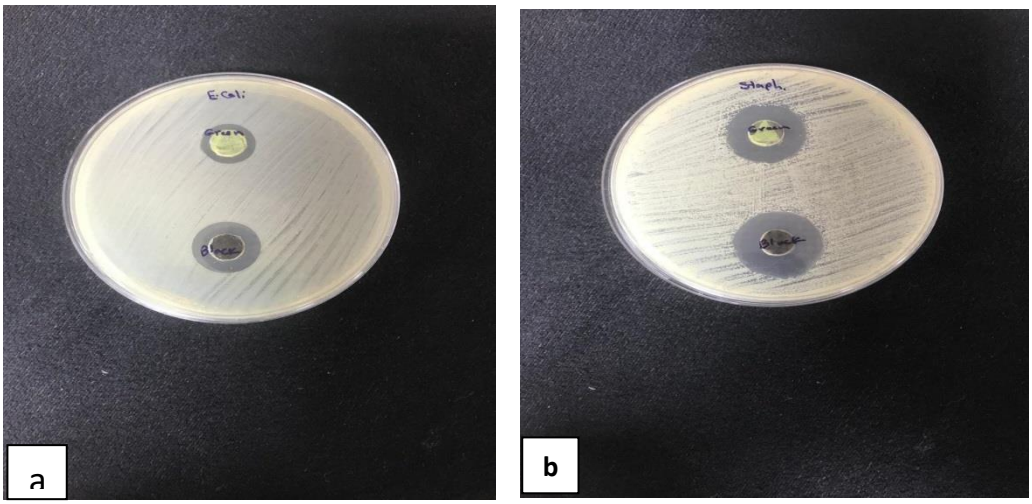

Fig. (4.43). Image for inhibition zones of (PVA-PEG/NiO) and (PVA-PEG/Ni_2O_3) nanocomposite films on a) *E. coli*. and b) *S. aureus*.

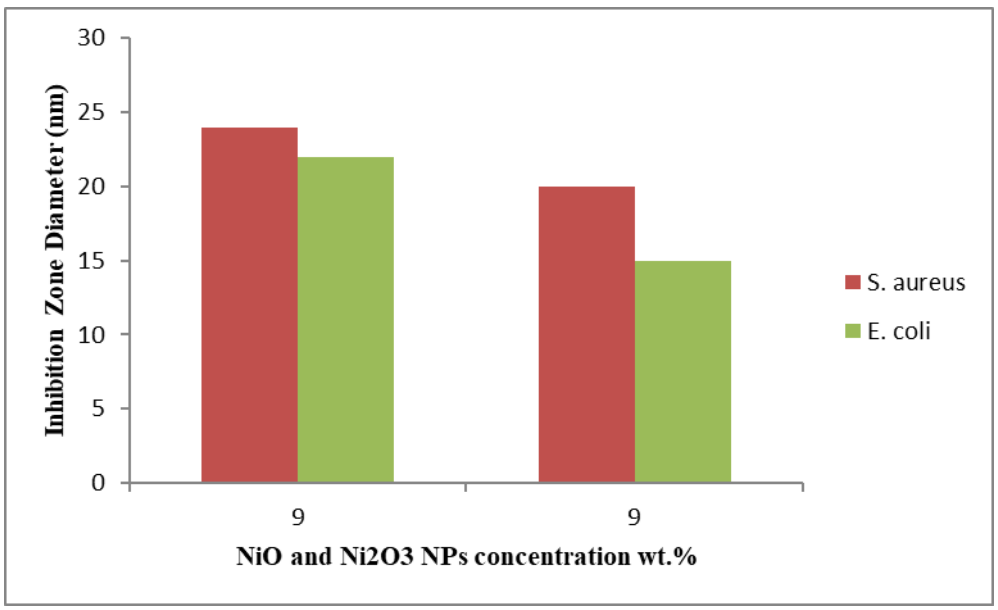

Fig. (4.44). Antibacterial effect of (PVA-PEG) as a function of NiO and Ni_2O_3 NPs concentrations on *S. aureus* and *E. coli*.

4.6 Conclusions

At the end of the current study and based upon the experiment conducted and the results reach at, the following conclusions are put forward:

1. According to XRD analysis, the polymeric blend is shown to have a semi-crystalline nature whose peak is in accordance with the plane (101) reflection, and the incorporated of NiO and Ni_2O_3 nanoparticles into blended polymers act noticeable change in the crystallinity of the films.
2. The optical microscope images denote a well distribution of NiO and form a network of paths charge transfer within the polymeric blend. FESEM images showed an increase in the number of aggregations on the surface of the polymeric matrix as a result of adding different amount of NiO and Ni_2O_3 nanoparticles.
3. The analysis of FTIR spectra confirms the presence of functional groups belonging to the polymer systems.
4. the absorbance, absorption coefficient, refractive index, polarizability, extinction coefficient, real and imaginary dielectric constant increase with increasing concentration of NiO and Ni_2O_3 NPs respectively, while the transmittance and indirect energy gap decrease with increasing concentration of NiO and Ni_2O_3 NPs respectively. these results can be used as solar collectors, UV shielding and wrapper for storing medicines.
5. The AC electrical properties exhibit that the dielectric constant and dielectric loss for (PVA-PEG/NiO) and (PVA-PEG/Ni_2O_3) films are increased with the increase in the amount of nano-additives and decreasing with the increase of frequency of the applied electric field, on the other hand, the A.C electrical conductivity increased with the increase in the amount of nano-additives and decreasing with the increase of frequency of the applied electric field.

6. The antibacterial examined of (PVA-PEG/9wt.%NiO) and (PVA-PEG/9wt.% Ni_2O_3) films exhibited that the best growth inhibition zone was observed with ratio 9wt.% of Ni_2O_3 (24 mm) against *Staphylococcus aureus*.

4.7 Future Works

Below are some ideas for future work to be conducted:

1. Study the mechanical properties of (PVA-PEG/NiO) and (PVA-PEG/Ni_2O_3) NC films.
2. Apply the (PVA-PEG/NiO) and (PVA-PEG/Ni_2O_3) NC films as the photodetector.
3. study of the pressure sensors application of the (PVA-PEG/NiO) and (PVA-PEG/Ni_2O_3) NC films**.**

[1] D. R. Paul and L. M. Robeson, “Polymer nanotechnology: nanocomposites,” *Polymer (Guildf).*, vol. 49, no. 15, pp. 3187–3204, 2008.

[2] R. V Kurahatti, A. O. Surendranathan, S. A. Kori, N. Singh, A. V. R. Kumar, and S. Srivastava, “Defence applications of polymer nanocomposites,” 2010.

[3] R. O. Ebewele, “Polymer and Technology,” *CRC Press. Raton-New York*, 2000.

[4] F. J. Davis, *Polymer chemistry: a practical approach*. Oxford University Press on Demand, 2004.

[5] R. K. Tubbs, “Sequence distribution of partially hydrolyzed poly (vinyl acetate),” *J. Polym. Sci. Part A-1 Polym. Chem.*, vol. 4, no. 3, pp. 623–629, 1966.

[6] Y. Khairy, M. I. Mohammed, H. I. Elsaeedy, and I. S. Yahia, “Optical and electrical properties of SnBr2-doped polyvinyl alcohol (PVA) polymeric solid electrolyte for electronic and optoelectronic applications,” *Optik (Stuttg).*, vol. 228, p. 166129, 2021.

[7] J. E. Mark, *Physical properties of polymers handbook*, vol. 1076. Springer, 2007.

[8] A. P. Mouritz and A. G. Gibson, *Fire properties of polymer composite materials*, vol. 143. Springer Science & Business Media, 2007.

[9] S. Kubo and J. F. Kadla, “The formation of strong intermolecular interactions in immiscible blends of poly (vinyl alcohol)(PVA) and lignin,” *Biomacromolecules*, vol. 4, no. 3, pp. 561–567, 2003.

[10] U. İbrahim, S. Keskin, G. Ü. L. Ali, T. C. Karabulut, and M. L. Aksu, “Preparation and properties of electrospun poly vinyl alcohol blended hybrid polymer with Aloe vera and HPMC as wound dressing,” *Hacettepe J. Biol. Chem.*, vol. 38, no. 1, pp. 19–25, 2010.

[11] E. Reis, E. F. D. Campos, F. S. Lage, A. P. Leite, R. C. Heneine, L. G.

Vasconcelos, and H. S. Mansur, “Synthesis and characterization of poly (vinyl alcohol) hydrogels and hybrids for rMPB70 protein adsorption,” *Mater. Res.*, vol. 9, pp. 185–191, 2006.

[12] M. B. Mohamed and M. H. Abdel-Kader, “Effect of excess oxygen content within different nano-oxide additives on the structural and optical properties of PVA/PEG blend,” *Appl. Phys. A*, vol. 125, no. 3, pp. 1–11, 2019.

[13] B. Ben Doudou, A. Vivet, J. Chen, A. Laachachi, T. Falher, and C. Poilâne, “Hybrid carbon nanotube—silica/polyvinyl alcohol nanocomposites films: preparation and characterisation,” *J. Polym. Res.*, vol. 21, pp. 1–9, 2014.

[14] B. Sasi, K. G. Gopchandran, P. K. Manoj, P. Koshy, P. P. Rao, and V. K. Vaidyan, “Preparation of transparent and semiconducting NiO films,” *Vacuum*, vol. 68, no. 2, pp. 149–154, 2002.

[15] F. Paquin, J. Rivnay, A. Salleo, N. Stingelin, and C. Silva, “Multi-phase semicrystalline microstructures drive exciton dissociation in neat plastic semiconductors,” *arXiv Prepr. arXiv1310.8002*, 2013.

[16] M. S. Kolathodi, M. Palei, and T. S. Natarajan, “Electrospun NiO nanofibers as cathode materials for high performance asymmetric supercapacitors,” *J. Mater. Chem. A*, vol. 3, no. 14, pp. 7513–7522, 2015.

[17] N. A. Hussein and N. A. Ali, “Synthesis and Characterization of Ni2O3 as a Phase of Nickel Oxide Nanomaterial,” *Iraqi J. Sci.*, pp. 4733–4739, 2022.

[18] K. Jouini, A. Raouafi, W. Dridi, M. Daoudi, B. Mustapha, R. Chtourou and F. Hosni “Investigation of gamma-ray irradiation induced phase change from NiO to Ni2O3 for enhancing photocatalytic performance,” *Optik (Stuttg).*, vol. 195, p. 163109, 2019.

[19] M. Sirait, S. Gea, and E. Marlianto, "Effect of mixed nanoparticles ZnS and polyvinyl alcohol (PVA) against nanocomposite mechanical properties of PVA/ZnS," *Am. J. Phys. Chem.*, vol. 3, no. 1, pp. 5–8, 2014.

[20] V. B. Sadhu, "Creation of crosslinkable interphases in polymer blends by means of novel coupling agents," 2004.

[21] M. Si, T. Araki, H. Ade, A. L. D. Kilcoyne, R. Fisher, J. Sokolov and M. H. Rafailovich, M "Compatibilizing bulk polymer blends by using organoclays," *Macromolecules*, vol. 39, no. 14, pp. 4793–4801, 2006.

[22] R. Sadri, M. Hosseini, S. N. Kazi,S. Bagheri, A. H. Abdelrazek, G. Ahmadi and N. I. Z. Abidin "A facile, bio-based, novel approach for synthesis of covalently functionalized graphene nanoplatelet nano-coolants toward improved thermo-physical and heat transfer properties," *J. Colloid Interface Sci.*, vol. 509, pp. 140–152, 2018.

[23] A. W. Hübler and O. Osuagwu, "Digital quantum batteries: Energy and information storage in nanovacuum tube arrays," *Complexity*, vol. 15, no. 5, pp. 48–55, 2010.

[24] C. M. Portela, A. Vidyasagar, S. Krödel, T. Weissenbach, D. W. Y Greer, and D. M. Kochmann "Extreme mechanical resilience of self-assembled nanolabyrinthine materials," *Proc. Natl. Acad. Sci.*, vol. 117, no. 11, pp. 5686–5693, 2020.

[25] T. Eldridge, "Achieving industry integration with nanomaterials through financial markets," *Nanotechnol. Now*, 2014.

[26] V. Pokropivny, R. Lohmus, I. Hussainova, A. Pokropivny, and S. Vlassov, *Introduction to nanomaterials and nanotechnology*, vol. 1. Tartu University Press Ukraine, 2007.

[27] R. C. Jaeger, "Film Deposition: Introduction to Microelectronic Fabrication," *Up. Saddle Rivers Prentice Hall*, vol. 83, 2002.

[28] C. Sun, "Controlling the rheology of polymer/silica nanocomposites."

Eindhoven University of Technology Eindhoven, The Netherlands, 2010.

[29] M. Arifitekhar, “Introduction to composite materials.” BMEn, 1999.

[30] R. Kochetov, “Thermal and electrical properties of nanocomposites, including material properties,” 2012.

[31] C. C. DeMerlis and D. R. Schoneker, “Review of the oral toxicity of polyvinyl alcohol (PVA),” *Food Chem. Toxicol.*, vol. 41, no. 3, pp. 319–326, 2003.

[32] C. Ravindra, M. Sarswati, G. Sukanya, P. Shivalila, Y. Soumya, and K. Deepak, “Tensile and thermal properties of poly (vinyl pyrrolidone)/vanillin incorporated poly (vinyl alcohol) films,” *Res. J. Phys.Sci.ISSN*, vol. 2320, p. 4796, 2015.

[33] K. Choo, Y. C. Ching, C. H. Chuah, S. Julai, and N.-S. Liou, “Preparation and characterization of polyvinyl alcohol-chitosan composite films reinforced with cellulose nanofiber,” *Materials (Basel).*, vol. 9, no. 8, p. 644, 2016.

[34] I. Sakurada, *Polyvinyl alcohol fibers*, vol. 6. CRC Press, 1985.

[35] R. De Jaeger and M. Gleria, “Poly (organophosphazene) s and related compounds: synthesis, properties and applications,” *Prog. Polym. Sci.*, vol. 23, no. 2, pp. 179–276, 1998.

[36] S. S. Chiad, S. F. Oboudi, K. H. Abass, and N. F. Habubi, “characterization of Silver/Poly (Vinyl Alcohol)(Ag/PVA) Films prepared by casting Technique,” *Iraqi J. Polym.*, vol. 16, no. 2, pp. 10–18, 2012.

[37] A. Gautam and S. Ram, “Preparation and thermomechanical properties of Ag-PVA nanocomposite films,” *Mater. Chem. Phys.*, vol. 119, no. 1–2, pp. 266–271, 2010.

[38] K. Ramamohan, V. B. S. Achari, A. K. Sharma, and L. Xiuyang, “Electrical and structural characterization of PVA/PEG polymer blend

electrolyte films doped with NaClO4," *Ionics (Kiel).*, vol. 21, no. 5, pp. 1333–1340, 2015.

[39] G. K. Prajapati and P. N. Gupta, "Comparative study of the electrical and dielectric properties of PVA–PEG–Al2O3–MI (M= Na, K, Ag) complex polymer electrolytes," *Phys. B Condens. Matter*, vol. 406, no. 15–16, pp. 3108–3113, 2011.

[40] K. Deshmukh, M. B. Ahamed, K. K. Sadasivuni, D. Ponnamma, R. P. Deshmukh, S. K. Pasha, and K. Chidambaram "Graphene oxide reinforced polyvinyl alcohol/polyethylene glycol blend composites as high-performance dielectric material," *J. Polym. Res.*, vol. 23, pp. 1–13, 2016.

[41] N.-J. Hempel, T. Dao, M. M. Knopp, R. Berthelsen, and K. Löbmann, "The influence of temperature and viscosity of polyethylene glycol on the rate of microwave-induced in situ amorphization of celecoxib," *Molecules*, vol. 26, no. 1, p. 110, 2020.

[42] L. Wu, Y. Wu, H. Wei, Y. Shi, and C. Hu, "Synthesis and characteristics of NiO nanowire by a solution method," *Mater. Lett.*, vol. 58, no. 21, pp. 2700–2703, 2004.

[43] A. A. Mariam, M. Kashif, S. Arokiyaraj, M, Bououdina, M. Sankaracharyulu, M. Jayachandran, and U. Hashim "Bio-synthesis of NiO and Ni nanoparticles and their characterization," *Dig. J. Nanomater. Biostructures*, vol. 9, No. 3, pp. 1007–1019, 2014.

[44] C. J. Pandian, R. Palanivel, and S. Dhananasekaran, "Green synthesis of nickel nanoparticles using Ocimum sanctum and their application in dye and pollutant adsorption," *Chinese J. Chem. Eng.*, vol. 23, no. 8, pp. 1307–1315, 2015.

[45] C. J. Pandian, R. Palanivel, and S. Dhananasekaran, "Green synthesis of NiO nanoparticles using Aegle marmelos leaf extract for the evaluation of in-vitro cytotoxicity, antibacterial and photocatalytic

properties," *J. Photochem. Photobiol. B Biol.*, vol. 180, pp. 39–50, 2018.

[46] M. Mohammadijoo, Z. N. Khorshidi, S. K. Sadrnezhaad, and V. Mazinani, "Synthesis and characterization of nickel oxide nanoparticle with wide band gap energy prepared via thermochemical processing," *Nanosci. Nanotechnol. Int. J*, vol. 4, no. 1, pp. 6–9, 2014.

[47] L. Ai, G. Fang, L. Yuan, N. Liu, M. Wang, C. Li and X. Zhao "Influence of substrate temperature on electrical and optical properties of p-type semitransparent conductive nickel oxide thin films deposited by radio frequency sputtering," *Appl. Surf. Sci.*, vol. 254, no. 8, pp. 2401–2405, 2008.

[48] D. S. Bai, R. P. Suvarna, and B. M. Nagabhushana, "Synthesis, characterization and electrical properties of PANI-Ni2O3 nanocomposites," *Mater. Today Proc.*, vol. 5, no. 10, pp. 20793–20802, 2018.

[49] K. S. Khashan, G. M. Sulaiman, A. H. Hamad, F. A. Abdulameer, and A. Hadi, "Generation of NiO nanoparticles via pulsed laser ablation in deionised water and their antibacterial activity," *Appl. Phys. A*, vol. 123, pp. 1–10, 2017.

[50] M. Irfan, S. R. Banu, R. S. Kumari, B. M. Veena, B. J. Madhu, and A. Manjunath, "Preparation, structural characterization and electrical studies on NiO doped PVA films," *Mater. Today Proc.*, vol. 5, no. 4, pp. 10839–10844, 2018.

[51] S. Ningaraju, A. P. G. Prakash, and H. B. Ravikumar, "Studies on free volume controlled electrical properties of PVA/NiO and PVA/TiO2 polymer nanocomposites," *Solid State Ionics*, vol. 320, pp. 132–147, 2018.

[52] K. O. Ukoba, A. C. Eloka-Eboka, and F. L. Inambao, "Review of nanostructured NiO thin film deposition using the spray pyrolysis

technique," *Renew. Sustain. Energy Rev.*, vol. 82, pp. 2900–2915, 2018.

[53] P. Liu, W. Chen, C. Liu, M. Tian, and P. Liu, "A novel poly (vinyl alcohol)/poly (ethylene glycol) scaffold for tissue engineering with a unique bimodal open-celled structure fabricated using supercritical fluid foaming," *Sci. Rep.*, vol. 9, no. 1, p. 9534, 2019.

[54] S. A. Bhat, F. Zafar, A. U. Mirza, A. H., A. H. Mondal, A. Kareem, Q. M. Haq and N. Nishat "NiO nanoparticle doped-PVA-MF polymer nanocomposites: Preparation, Congo red dye adsorption and antibacterial activity," *Arab. J. Chem.*, vol. 13, no. 6, pp. 5724–5739, 2020.

[55] N. M. Shaalan, T. A. Hanafy, and M. Rashad, "Dual optical properties of NiO-doped PVA nanocomposite films," *Opt. Mater. (Amst).*, vol. 119, p. 111325, 2021.

[56] H. Ali, T. M. Tiama, and A. M. Ismail, "New and efficient NiO/chitosan/polyvinyl alcohol nanocomposites as antibacterial and dye adsorptive films," *Int. J. Biol. Macromol.*, vol. 186, pp. 278–288, 2021.

[57] T. Alrebdi, H. A. Ahmed, S. H. Alrefaee, R. A. Pashameah, A. Toghan, A. M. Mostafa and R. A. Rezk"Enhanced adsorption removal of phosphate from water by Ag-doped PVA-NiO nanocomposite prepared by pulsed laser ablation method," *J. Mater. Res. Technol.*, vol. 20, pp. 4356–4364, 2022.

[58] R. O. Bewele, "Polymer and Technology," *CRC Press. Raton-New York*, 2000.

[59] Y. I. Sirotin and M. P. Shaskolskaya, "Fundamentals of Crystal Physics, Mir Publ." Moscow, 1982.

[60] J. P. Davim, *Biomedical composites: materials, manufacturing and engineering*, vol. 2. Walter de Gruyter, 2013.

[61] L. S. Schadler, "Polymer-based and polymer-filled nanocomposites," *Nanocomposite Sci. Technol.*, pp. 77–153, 2003.

[62] C.-C. Diao, C.-Y. Huang, C.-F. Yang, and C.-C. Wu, "Morphological, optical, and electrical properties of p-type nickel oxide thin films by nonvacuum deposition," *Nanomaterials*, vol. 10, no. 4, p. 636, 2020.

[63] A. Di Gianfrancesco, *Materials for ultra-supercritical and advanced ultra-supercritical power plants*. woodhead Publishing, 2016.

[64] S. Ebnesajjad and C. Ebnesajjad, *Surface treatment of materials for adhesive bonding*. William Andrew, 2013.

[65] G. S. Kino and T. R. Corle, *Confocal scanning optical microscopy and related imaging systems*. Academic Press, 1996.

[66] M. S. A. Hussien, M. I. Mohammed, and I. S. Yahia, "Multifunctional applications of graphene-doped PMMA nanocomposite membranes for environmental photocatalytic," *J. Inorg. Organomet. Polym. Mater.*, vol. 30, pp. 2708–2719, 2020.

[67] M. P. Q. Rodriguez, "Fourier transform infrared (FTIR) technology for the identification of organisms," *Clin. Microbiol. Newsl.*, vol. 22, no. 8, pp. 57–61, 2000.

[68] C. Sacksteder and B. A. Barry, "Fourier transform infrared spectroscopy: a molecular approach to an organismal question," *J. Phycol.*, vol. 37, no. 2, pp. 197–199, 2001.

[69] M. Lee, *X-Ray diffraction for materials research: from fundamentals to applications*. CRC Press, 2017.

[70] S. M. Sze, Y. Li, and K. K. Ng, *Physics of semiconductor devices*. John wiley & sons, 2021.

[71] C. Gumus, O. M. Ozkendir, H. Kavak, and Y. Ufuktepe, "Structural and optical properties of zinc oxide thin films prepared by spray pyrolysis method," *J. Optoelectron. Adv. Mater.*, vol. 8, no. 1, p. 299, 2006.

[72] S.-N. Bai and T.-Y. Tseng, “Electrical and optical properties of ZnO: Al thin films grown by magnetron sputtering,” *J. Mater. Sci. Mater. Electron.*, vol. 20, pp. 253–256, 2009.

[73] R. C. H. Cik, C. T. Foo, and A. F. O. Nor, “Field Emission Scanning Electron Microscope (FESEM) Facility in BTI,” 2015.

[74] G. W. Bailey, R. L. Price, E. Voelkl, I. H. Musselman, P. Gnauck, V. Drexel and J. Greiser “A new high resolution field emission SEM with variable pressure capabilities,” *Microsc. Microanal.*, vol. 7, no. S2, pp. 880–881, 2001.

[75] D. C. Joy and J. B. Pawley, “High-resolution scanning electron microscopy,” *Ultramicroscopy*, vol. 47, no. 1–3, pp. 80–100, 1992.

[76] L. A. Prystaj, “Effect of carbon filler characteristics on the electrical properties of conductive polymer composites possessing segregated network microstructures.” Georgia Institute of Technology, 2008.

[77] C. Kittel and P. McEuen, *Introduction to solid state physics*. John Wiley & Sons, 2018.

[78] F. Yakuphanoglu and H. Erten, “Refractive index dispersion and analysis of the optical constants of an ionomer thin film.,” *Opt. Appl.*, vol. 35, no. 4, 2005.

[79] C. Kittel, "Introduction to solid state physics", 5th ed., Willy, New York, (1981).

[80] A. V Vannikov, V. K. Matveev, V. P. Sichkar, and A. P. Tiutnev, “Radiation effects in polymers. Electrical properties,” *Moscow Izd. Nauk.*, 1982.

[81] C. Kittle, *Introduction to Solid State Physics*. John Wiley and Sons Inc., 2005.

[82] K. H. Abass and D. M. Latif, “The urbach energy and dispersion parameters dependence of substrate temperature of CdO thin films

prepared by chemical spray pyrolysis," *Int. J. ChemTech Res.*, vol. 9, no. 9, pp. 332–338, 2016.

[83] R. Sreekumar, R. Jayakrishnan, C. Sudha Kartha, and K. P. Vijayakumar, "Anomalous photoconductivity in gamma In 2 Se 3," *J. Appl. Phys.*, vol. 100, no. 3, p. 33707, 2006.

[84] K. J. Daul, "Total Ionizing Dose Effects in MOSFET Devices at 77 K.," Air force inst of tech wright-patterson AFB OH school of enginerring, 1994.

[85] D. A. Neamen, *semiconductor Physics and Devices Basic Principles*. Tata McGraw Hill Publishing, 1992.

[86] R. Naik, C. Kumar, R. Ganesan, and K. S. Sangunni, "Effect of thickness on the optical properties change in Bi/As2S3 bilayer thin films," in *AIP Conference Proceedings*, vol. 1447, no. 1, pp. 623–624, 2012.

[87] V. N. Suryawanshi, A. S. Varpe, and M. D. Deshpande, "Band gap engineering in PbO nanostructured thin films by Mn doping," *Thin Solid Films*, vol. 645, pp. 87–92, 2018.

[88] O. K. Abdali and O. Abdulazeez, "Optical and dielectrical properties of (PEG-CMC) films prepared by Drop Casting Method," *World Sci. News*, no. 46, pp. 189–203, 2016.

[89] R. Tintu, K. Saurav, K. Sulakshna, V. P. N. Nampoori, P. Radhakrishnan, and S. Thomas, "Ge28Se60Sb12/PVA composite films for photonic applications," *J. Non-Oxide Glas.*, vol. 2, no. 4, pp. 167–174, 2010.

[90] M. H. Hassouni, K. A. Mishjil, S. S. Chiad, and N. F. Habubi, "Effect of gamma irradiation on the optical properties of Mg doped CdO Thin films deposited by Spray Pyrolysis," *Int. Lett. Chem. Phys. Astron.*, vol. 11, pp. 26–37, 2013.

[91] P. Barber, S. Balasubramanian, Y. Anguchamy, S. Gong, A. Wibowo,

, H. Gao and H. C. Zur Loye"Polymer composite and nanocomposite dielectric materials for pulse power energy storage," *Materials (Basel).*, vol. 2, no. 4, pp. 1697–1733, 2009.

[92] T. Putjuso and P. Sangarun, "Influence of annealing on the giant dielectric properties of cuo ceramics prepared by a simple pva sol-gel," *Asia-Pacific J. Sci. Technol.*, vol. 17, no. 2, pp. 203–210, 2012.

[93] M. Akram, A. Javed, and T. Z. Rizvi, "Dielectric properties of industrial polymer composite materials," *Turkish J. Phys.*, vol. 29, no. 6, pp. 355–362, 2005.

[94] R. A. Hule and D. J. Pochan, "Polymer nanocomposites for biomedical applications," *MRS Bull.*, vol. 32, no. 4, pp. 354–358, 2007.

[95] Fox M: Optical Properties of Solids: Oxford University Press. In.: Oxford; 2001.

[96] Z. M. Elimat, A. M. Zihlif, and G. Ragosta, "Study of ac electrical properties of aluminium–epoxy composites," *J. Phys. D. Appl. Phys.*, vol. 41, no. 16, p. 165408, 2008.

[97] T. Seghier and F. Benabed, "Dielectric proprieties determination of high density polyethylene (HDPE) by dielectric spectroscopy," *Int. J. Mater. Mech. Manuf.*, vol. 3, no. 2, pp. 121–124, 2015.

[98] S. Shekhar, V. Prasad, and S. V Subramanyam, "Structural and electrical properties of composites of polymer–iron carbide nanoparticles embedded in carbon," *Mater. Sci. Eng. B*, vol. 133, no. 1–3, pp. 108–112, 2006.

[99] T. Furukawa, "Electrical properties of polymers," *Reports Prog. Polym. Phys. Japan*, vol. 43, pp. 369–390, 2000.

[100] R. C. Dorf, *The Electrical Engineering Handbook-Six Volume Set*. CRC press, 2018.

[101] R. G. AL-Morshdy, M. A. Habeeb, and H. M. M. AL-Asadi, "Effect

of Nano silver Particles on the Optical and Structural Properties of (PVA-PVP) Films, Adv," *Phy. Theo. Appl*, vol. 34, pp. 30–39, 2014.

[102] N. A. Azahari, N. Othman, and H. Ismail, "Biodegradation studies of polyvinyl alcohol/corn starch blend films in solid and solution media," *J. Phys. Sci.*, vol. 22, no. 2, pp. 15–31, 2011.

[103] I. Yücedağ, A. Kaya, Ş. Altındal, and I. Uslu, "Frequency and voltage-dependent electrical and dielectric properties of Al/Co-doped PVA/p-Si structures at room temperature," *Chinese Phys. B*, vol. 23, no. 4, p. 47304, 2014.

[104] A. Azam, A. S. Ahmed, M. Oves, M. S. Khan, S. S. Habib, and A. Memic, "Antimicrobial activity of metal oxide nanoparticles against Gram-positive and Gram-negative bacteria: a comparative study," *Int. J. Nanomedicine*, pp. 6003–6009, 2012.

[105] S.-W. Zhao, C.-R. Guo, Y.-Z. Hu, Y.-R. Guo, and Q.-J. Pan, "The preparation and antibacterial activity of cellulose/ZnO composite: A review," *Open Chem.*, vol. 16, no. 1, pp. 9–20, 2018.

[106] N. Tran, A. Mir, D. Mallik, A. Sinha, S. Nayar, and T. J. Webster, "Bactericidal effect of iron oxide nanoparticles on Staphylococcus aureus," *Int. J. Nanomedicine*, pp. 277–283, 2010.

[107] A. Azam, A. S. Ahmed, M. Oves, M. S. Khan, and A. Memic, "Size-dependent antimicrobial properties of CuO nanoparticles against Gram-positive and-negative bacterial strains," *Int. J. Nanomedicine*, pp. 3527–3535, 2012.

[108] K. R. Raghupathi, R. T. Koodali, and A. C. Manna, "Size-dependent bacterial growth inhibition and mechanism of antibacterial activity of zinc oxide nanoparticles," *Langmuir*, vol. 27, no. 7, pp. 4020–4028, 2011.

[109] M. Singh, S. Singh, S. Prasad, and I. S. Gambhir, "Nanotechnology in medicine and antibacterial effect of silver nanoparticles," *Dig. J.*

Nanomater. Biostructures, vol. 3, no. 3, pp. 115–122, 2008.

[110] V. Monzillo, C. Dalla Valle, M. Corbella, E. Percivalle, D. Sassera, D. Scevola and P. Marone"Antibacterial activity and cytotoxic effect of SIAB-GV3," *New Microbiol*, vol. 37, pp. 535–541, 2014.

[111] M. A. Ansari, H. M. Khan, A. A. Khan, A. Sultan, A. Azam, M. Shahid and F. Shujatullah"Antibacterial activity of silver nanoparticles dispersion against MSSA and MRSA isolated from wounds in a tertiary care hospital of north India.," 2011.

[112] L. G. Harris, S. J. Foster, and R. G. Richards, "An introduction to Staphylococcus aureus, and techniques for identifying and quantifying S. aureus adhesins in relation to adhesion to biomaterials: review," *Eur Cell Mater*, vol. 4, no. 3, pp. 100–120, 2002.

[113] V. P. Kumar, N. S. Chauhan, H. Padh, and M. Rajani, "Search for antibacterial and antifungal agents from selected Indian medicinal plants," *J. Ethnopharmacol.*, vol. 107, no. 2, pp. 182–188, 2006.

[114] A. Y. Itah and J. P. Essien, "Growth profile and hydrocarbonoclastic potential of microorganisms isolated from tarballs in the Bight of Bonny, Nigeria," *World J. Microbiol. Biotechnol.*, vol. 21, pp. 1317–1322, 2005.

[115] Z. L. Wang, "Zinc oxide nanostructures: growth, properties and applications," *J. Phys. Condens. matter*, vol. 16, no. 25, p. R829, 2004.

[116] S. Rajendran, M. Sivakumar, R. Subadevi, and M. Nirmala, "Characterization of PVA–PVdF based solid polymer blend electrolytes," *Phys. B Condens. Matter*, vol. 348, no. 1–4, pp. 73–78, 2004.

[117] J. I. Pankove, "Optical processes in semiconductors Prentice-Hall," *New Jersey*, vol. 92, p. 36, 1971.

[118] R. A. Amoresi, R. C. de Oliveira, J. L. Cichetto, P. M. Desimone, C. M. Aldao, M. A. Ponce and A. Z. Simoes "Pure and Ni2O3-decorated CeO2 nanoparticles applied as CO gas sensor: Experimental and theoretical insights," *Ceram. Int.*, vol. 48, no. 10, pp. 14014–14025, 2022.

[119] N. M. Vuong, N. M. Hieu, H. N. Hieu, H. Yi, D. Kim, Y. S. Han Aand M. Kim"Ni2O3-decorated SnO2 particulate films for methane gas sensors," *Sensors Actuators B Chem.*, vol. 192, pp. 327–333, 2014.

[120] H. H. Jassim and F. S. Hashim, "Synthesis of (PVA/PEG: ZnO and Co3O4) Nanocomposites: Characterization and Gamma Ray Studies," *NeuroQuantology*, vol. 19, no. 4, p. 47, 2021.

[121] A. M. Dumitrescu, G. Lisa, A. R. ordan, F. Tudorache, I. Petrila, A. I. Borhan, and C. Munteanu, C "Ni ferrite highly organized as humidity sensors," *Mater. Chem. Phys.*, vol. 156, pp. 170–179, 2015.

[122] J. Gong, J. Liu, D. Wan, X. Chen, X. Wen, E. Mijowska, and T. Tang, "Catalytic carbonization of polypropylene by the combined catalysis of activated carbon with Ni2O3 into carbon nanotubes and its mechanism," *Appl. Catal. A Gen.*, vol. 449, pp. 112–120, 2012.

[123] I. D. Likasari, R. W. Astuti, A. Yahya, N. Isnaini,G. Purwiandono, H. Hidayat, H. and I. Fatimah "NiO nanoparticles synthesized by using Tagetes erecta L leaf extract and their activities for photocatalysis, electrochemical sensing, and antibacterial features," *Chem. Phys. Lett.*, vol. 780, p. 138914, 2021.

[124] Z. Sabouri, A. Akbari, H. A. Hosseini, A. Hashemzadeh, and M. Darroudi, "Eco-friendly biosynthesis of nickel oxide nanoparticles mediated by okra plant extract and investigation of their photocatalytic, magnetic, cytotoxicity, and antibacterial properties," *J. Clust. Sci.*, vol. 30, pp. 1425–1434, 2019.

[125] W. Ariyawiriyanan, T. Meekaew, M. Yamphang, P., Tuenpusa, J. Boonwan, N. Euaphantasate and S. Chungpaibulpatana,"Thermal efficiency of solar collector made from thermoplastics," *Energy Procedia*, vol. 34, pp. 500–505, 2013.

[126] S. A. Mahmoud, A. A. Akl, H. Kamal, and K. Abdel-Hady, "Opto-structural, electrical and electrochromic properties of crystalline nickel oxide thin films prepared by spray pyrolysis," *Phys. B Condens. Matter*, vol. 311, no. 3–4, pp. 366–375, 2002.

[127] M. Anwar and C. A. Hogarth, "Structural investigations and colour centres in MoO3 films deposited by vacuum evaporation," *Int. J. Electron. Theor. Exp.*, vol. 67, no. 4, pp. 567–576, 1989.

[128] J. I. Pankove, *Optical processes in semiconductors*. Courier Corporation, 1975.

[129] M. Aftab, M. Z. Butt, D. Ali, M. U. Tanveer, and A. Hussnain, "Effect of Molarity on the Structure, Optical Properties, and Surface Morphology of (002)-Oriented Ni2O3 Thin Films Deposited via Spray Pyrolysis: Effect of Molarity on the Properties of Ni2O3 Thin Films," *Proc. Pakistan Acad. Sci. A. Phys. Comput. Sci.*, vol. 57, no. 2, pp. 51–74, 2020.

[130] Y. Xie, C. Wang, and D. Xue, "Research on Refractive Index and Polarization Direction of light in Crystal," in *2017 International Conference Advanced Engineering and Technology Research (AETR 2017)*, 2018, pp. 249–253.

[131] S. A. Mahmoud, A. Shereen, and A. T. Mou'ad, "Structural and optical dispersion characterisation of sprayed nickel oxide thin films," *J. Mod. Phys.*, vol. 2011, 2011.

[132] H. Yamamoto, S. Tanaka, and K. Hirao, "Nanostructure and optical nonlinearity of Cobalt oxide thin films," in *Journal of the Ceramic Society of Japan, Supplement Journal of the Ceramic Society of*

Japan, Supplement 112-1, PacRim5 Special Issue, pp. S876–S880, 2004

[133] K. S. Usha, R. Sivakumar, and C. Sanjeeviraja, "Optical constants and dispersion energy parameters of NiO thin films prepared by radio frequency magnetron sputtering technique," *J. Appl. Phys.*, vol. 114, no. 12, p. 123501, 2013.

[134] A. Qureshi, A. Mergen, and B. Aktaş, "Dielectric and magnetic properties of YIG/PMMA nanocomposites," in *Journal of Physics: Conference Series*, 2009, vol. 153, no. 1, p. 12061.

[135] B Abd-Alkareem, "Effect of Nano-Copper Oxide on the Electrical and Optical Properties of (PMMA) Polymer." M. Sc. thesis, College of Education for pure sciences, University of Babylon, 2016.

[136] A. M. El Sayed and S. El-Gamal, "Synthesis and investigation of the electrical and dielectric properties of Co_3O_4/(CMC+PVA) nanocomposite films," *J. Polym. Res.*, vol. 22, pp. 1–12, 2015.

[137] L. R. Yadav, B. Archana, K. Lingaraju, C. Kavitha, D. Suresh, H. Nagabhushana and G. Nagaraju "Electrochemical sensing, photocatalytic and biological activities of ZnO nanoparticles: synthesis via green chemistry route," *Int. J. Nanosci.*, vol. 15, no. 04, p. 1650013, 2016.

الخلاصة

المتراكب النانوي المبني على خليط من بولي (كحول فينيل) (PVA) وبولي (إيثيلين كلايكول) (PEG) مع 90:10 بالوزن٪ PEG في PVA و Ni_2O_3 عند خمسة أوزان مختلفة مثل 0.03, 0.045, 0.06, 0.075 و 0.09 غم تم تصنيعه باستخدام طريقة الصب. تشمل الخصائص الطيفية حيود الأشعة السينية (XRD)، والمجهر البصري (OM)، ومجهر الماسح الإلكتروني للانبعاث المجال (FESEM) وتحويلات فورير للأشعة تحت الحمراء (FTIR). وفقا لتحليل XRD، يظهر أن المزيج البوليمري له طبيعة شبه بلورية تكون ذروتها متوافقة مع انعكاس المستوى (101)، كما أن جسيمات نانوية NiO و Ni_2O_3 المدمجة في البوليمرات الممزوجة تعمل على تغيير ملحوظ في تبلور أفلام. تشير صور المجهر الضوئي إلى التوزيع الجيد لـ NiO وتشكل شبكة من مسارات نقل الشحنة داخل المزيج البوليمري. أظهرت صور FESEM زيادة في عدد التجمعات على سطح المصفوفة البوليمرية نتيجة إضافة كمية مختلفة من جسيمات النانوية NiO و Ni_2O_3. يؤكد تحليل أطياف FTIR وجود مجموعات وظيفية تنتمي إلى أنظمة البوليمر. من الخواص البصرية، الامتصاصية، معامل الامتصاص, معامل الانكسار, الاستقطابية , ثابت العزل الحقيقي والخيالي والتوصيلية البصرية تزداد مع زيادة تركيز الجسيمات النانوية NiO و Ni_2O_3، على التوالي. بينما النفاذية وفجوة الطاقة الغير مباشرة تقل مع زيادة تركيز الجسيمات النانوية NiO و Ni_2O_3، على التوالي مما يجعلها ملائمة للتطبيقات المختلفة ، مثل مجمعات الطاقة الشمسية ، وحماية الأشعة فوق البنفسجية والغلاف لتخزين الأدوية. تظهر الخواص الكهربائية للتيار المتردد أن ثابت العزل وفقدان العزل الكهربائي لأغشية (PVA-PEG/NiO) و (PVA-PEG/Ni_2O_3) يزداد مع زيادة كمية المواد المضافة النانوية ويتناقص مع زيادة تردد المجال الكهربائي المطبق، من ناحية أخرى ، زادت الموصلية الكهربائية للتيار المتردد مع زيادة كمية إضافات النانو وتناقص مع زيادة المجال الكهربائي المطبق. تم فحص الحساسية المضادة للبكتيريا لأغشية (PVA-PEG/9wt.%NiO) و (PVA-PEG/9wt.% Ni2O3) باستخدام طريقة قرص أجار ضد عزلتين من البكتيريا: البكتيريا سالبة الجرام المعوية القولونية والبكتيريا موجبة الجرام المكورات العنقودية الذهبية، وأظهرت أن أفضل منطقة تثبيط للنمو لوحظت بنسبة 9 % بالوزن من Ni_2O_3 (24 mm) ضد المكورات العنقودية الذهبية.

وزارة التعليم العالي والبحث العلمي
جامعة بابل - كلية التربية للعلوم الصرفة
قسم الفيزياء

تأثير جسيمات أوكسيد النيكل الأخضر والأسود النانوية على الخصائص التركيبية وبعض الخصائص الفيزيائية لمزيج البوليمر بولي (كحول فينيل) - بولي (إيثيلين جلايكول).

رسالة مقدمة إلى

مجلس كلية التربية للعلوم الصرفة / جامعة بابل وهي جزء من متطلبات

نيل درجة الماجستير في التربية / فيزياء

من قبل

مروة مازن نعيم عبد الامير

بكالوريوس تربية فيزياء 2009 م

جامعة بابل

بإشراف

أ.د. فؤاد شاكر هاشم **أ.د. شروق صباح عبد العباس**

1445 هـ **2023 م**